STEDIN.NET TU Delft

Energy Hubs within the Built Environment

Exploring opportunities and challenges for the low-voltage grid

E.J. Groene

Energy Hubs within the Built Environment

Exploring opportunities and challenges for the low-voltage grid

by

E.J. Groene

to obtain the degree of Master of Science in Sustainable Energy Technology,
at the Delft University of Technology,
to be defended publicly on Tuesday December 16, 2025 at 10:30.

Thesis Committee:	Dr. ir. M. Cvetkovic – *TU Delft*, ir. D. Georgiadi – *TU Delft*, Dr. ir. J.A. Groen – *TU Delft*, Dr. ir. S. Rivera Iunnissi – *TU Delft*, Dr. ir. A.M. van Voorden – *Stedin*
Project Duration:	April, 2025 - December, 2025
Faculty:	Electrical Engineering, Mathematics & Computer Science, Delft
Studentnumber:	4933257

TU Delft

Acknowledgments

This thesis was written as the final assignment of the MSc Sustainable Energy Technology at TU Delft. Before diving into the research itself, I would like to take the opportunity to thank a few people who helped during this process.

First, I would like to thank the TU Delft team, Milos Cvetkovic, Despoina Georgiadi, and Jort Groen. Thank you for your guidance, feedback, and for positive mindset. It was a pleasure to learn new concepts, and work with The Illuminator. Despoina and Jort, I hope I did not stalk you too often on Teams, but thank you for always being available and willing to help, it is extremely appreciated.

I also want to thank Arjan van Voorden and Emma Gerritse. I always felt very welcome at Stedin, and it was inspiring to experience the work environment there. Arjan, thank you for supervising me despite your busy schedule, your time and advice meant a lot. It was very valuable to have a supervisor from a company with that much experience in guiding students throughout their thesis! Emma, thank you for helping me in the early stages of the thesis and helping me with shaping a direction of the thesis, which was quite a challenge.

Additionally, I would like to thank The Green Village for their warm welcome and support. In particular, Roby van Praag, for helping me to get around at The Green Village and giving me background knowledge about the 24/7 Energy Hub. Thanks also to Marijn Leeuwenberg and Joep van der Weijen for sharing data and insights about the project.

Last but not least, I want to thank my parents for their support throughout both my bachelor's and master's studies. With this thesis, your last child officially graduates. And thank you for letting me stay at your house during the final two weeks before submission, probably the worst possible moment to decide to move..

E.J. Groene
Delft, January 2026

Summary

A scalable model was developed based on the 24/7 Energy Hub at The Green Village. The system includes short-term balancing through a battery, hydrogen production through an electrolyzer, and winter supply from a fuel cell. The validated component models were applied to a representative Dutch neighborhood consisting of 155 households (archetype 3) with an 250 kVA transformer, under projected 2050 demand and generation conditions. A set of 320 configurations was evaluated across multiple transformer capacities and hydrogen production sources. Feasible configurations were defined as those eliminating transformer violations while maintaining a positive annual hydrogen balance.

The 2050 baseline exhibited 67.9 MWh/year of congestion. Of the 320 evaluated configurations, 56 met the feasibility criteria, all requiring a transformer upgrade from 250 kVA to 400 kVA. Two lowest-cost feasible designs were identified: a PV-only hydrogen configuration and a configuration that explicitly used the grid to produce hydrogen in off-peak winter periods. Both eliminated congestion while maintaining hydrogen self-sufficiency. However, total system investment ranged between €0.7–€4.6 M, significantly higher than traditional transformer reinforcement (€34k).

The results from the case study show that decentralized hydrogen storage can technically resolve transformer congestion, but only when combined with moderate reinforcement and at substantially higher cost than conventional upgrading. Under current cost and efficiency assumptions, energy hubs has as a flexibility purpose rather than an economic substitute for grid reinforcement.

Contents

Nomenclature

Abrreviations, symbols and units are described below.

Abbreviations

Abbreviation	Definition
AC	Alternating Current
AEM	Anion-Exchange Membrane
ASHP	Air-Source Heat Pump
BESS	Battery Energy Storage System
BoP	Balance of Plant
CAPEX	Capital Expenditure
COP	Coefficient of Performance
DC	Direct Current
DEC	Decentrale Initiatieven
DER	Distributed Energy Resource
DHW	Domestic Hot water
DSO	Distribution System Operator
ECMWF	European Centre for Medium-Range Weather Forecasts
EMS	Energy Management System
EV	Electric Vehicle
FC	Fuel Cell
GO-e	Gebouwde Omgeving Elektrificatie
GTI	Global Tilted Irradiance
H_2	Hydrogen
HP	Heat Pump
HV	High-Voltage
KPI	Key Performance Indicator
LAN	Landelijk Actieplan Netcongestie
LHV	Lower Heating Value
LV	Low-Voltage
MILP	Mixed-Integer Linear Programming
MPPT	Maximum Power Point Tracking
MV	Medium-Voltage
NOCT	Nominal Operating Cell Temperature
OPEX	Operational Expenditure
PEM	Proton Exchange Membrane
$P2H_2$	Power-to-Hydrogen-to-Power
P2H	Power-to-Heat
P2G	Power-to-Gas
PV	Photovoltaics / Solar Panels
SAPM	Sandia PV Array Performance Model
STC	Standard Test Conditions
SSS	Seasonal Storage System
SOC	State of Charge
SVF	Sky View Factor
TSO	Transmission System Operator

Symbols

Symbol	Definition	Unit
General and Simulation		
Δt	Simulation time step	min
A_z	Solar azimuth angle	°
h_s	Solar elevation angle	°
θ	PV module tilt angle (from horizontal)	°
α	PV module azimuth angle (clockwise from north)	°
Load and Grid Connection		
P_{load}	Household AC power demand	kW
P_{grid}	Net grid power exchange (positive = import, negative = export)	kW
$P_{\text{trafo,limit}}$	Transformer rating / congestion threshold	kVA
$P_{\text{bat,ch}}$	Battery charging power (from grid/system)	kW
$P_{\text{bat,dis}}$	Battery discharging power (to grid/system)	kW
P_{el}	Electrolyser electrical power consumption	kW
P_{com}	Compressor electrical power	kW
PV System		
GTI	Global Tilted Irradiance on the PV plane	W/m^2
G_{dir}	Direct irradiance on the tilted plane	W/m^2
G_{diff}	Diffuse irradiance on the tilted plane	W/m^2
G_{ref}	Reflected irradiance on the tilted plane	W/m^2
G_{Bn}	Beam normal irradiance	W/m^2
G_{Dh}	Diffuse horizontal irradiance	W/m^2
G_{Gh}	Global horizontal irradiance	W/m^2
γ	Angle of incidence between beam and panel normal	°
SVF	Sky View Factor	–
ρ	Ground albedo	–
T_a	Ambient temperature	°C
T_m	PV module temperature	°C
G_{NOCT}	Irradiance at NOCT conditions	W/m^2
NOCT	Nominal Operating Cell Temperature	°C
η_{STC}	PV efficiency at standard test conditions	–
η	Temperature-corrected PV module efficiency	–
C	Installed PV capacity	kW
P_{AC}	AC power output of the PV system	kW
η_{inv}	PV inverter efficiency	–
η_{MPPT}	Maximum Power Point Tracking efficiency	–
η_{loss}	Additional PV system loss factor	–
FF	Wind-speed related factor in NOCT model	–
Battery Storage System		
SOC_{bat}	Battery state of charge	%
$SOC_{\text{bat,min}}$	Minimum allowable battery SOC	%
$SOC_{\text{bat,max}}$	Maximum allowable battery SOC	%
$E_{\max}$	Nominal battery energy capacity	kWh
$P_{\max}$	Maximum battery (dis)charge power	kW
$P_{\min}$	Minimum charging power (negative limit)	kW
P_{bat}	Net battery balance power (before limits)	kW
P_{flow2b}	Actual power exchanged with the battery	kW

η_{ch}	Battery charging efficiency	–
η_{dis}	Battery discharging efficiency	–
$\eta_{\text{inv,ch}}$	Inverter efficiency during charging	–
$\eta_{\text{inv,dis}}$	Inverter efficiency during discharging	–
Electrolyser System		
P_{in}	Electrolyser input electrical power	kW
P_{max}	Rated electrolyser power	kW
r_{prod}	Relative hydrogen production rate $(0.6–1)$	–
η_{el}	Electrolyser efficiency	–
$\dot{m}_{\text{H}_2}$	Hydrogen mass flow from electrolyser	kg/s
LHV_{H_2}	Lower heating value of hydrogen	kWh/kg
Compressor		
p_{in}	Inlet hydrogen pressure	bar
p_{out}	Outlet hydrogen pressure	bar
r	Pressure ratio ($p_{\text{out}}/p_{\text{in}}$)	–
γ	Heat capacity ratio of hydrogen	–
R	Universal gas constant	J/(mol·K)
T	Gas temperature	K
M	Hydrogen molar mass	g/mol
w_{is}	Isentropic compression work	J/mol
w_{real}	Real compression work (incl. efficiency)	J/mol
η_{mech}	Mechanical compressor efficiency	–
η_{ec}	Electrochemical compressor efficiency	–
E_{spec}	Specific energy consumption for compression	kWh/kg
$\dot{n}$	Molar hydrogen flow rate	mol/s
P_{comp}	Compressor power consumption	kW
Hydrogen Storage		
SOC_{H_2}	Hydrogen storage state of charge	%
m_{tot}	Maximum hydrogen mass stored	kg
Fuel Cell System		
P_{FC}	Fuel cell AC electrical power output	kW
$\dot{m}_{\text{H}_2,\text{in}}$	Hydrogen mass flow to the fuel cell	kg/s
η_{FC}	Fuel cell system efficiency (H_2 to AC)	–
Energy Management System (EMS)		
$P_{\text{PV,signal}}$	Available PV power signal to EMS	kW
$SOC_{\text{bat,el,start}}$	Battery SOC threshold for electrolyser start	%
$SOC_{\text{bat,el,stop}}$	Battery SOC threshold for electrolyser stop	%
$SOC_{\text{bat,fc,emergency}}$	Emergency SOC threshold for fuel cell start	%
$SOC_{\text{bat,fc,stop}}$	Battery SOC threshold for fuel cell stop	%
$SOC_{\text{H}_2,\max}$	Maximum allowable hydrogen SOC	%

Units

Unit	Name
€	Euro
€/kWh/year	Euro per kilowatt-hour per year
€/kg H_2/year	Euro per kilogram of hydrogen per year
%	Percentage
h	Hour
kg	Kilogram

kW	Kilowatt
kWh	Kilowatt-hour
kVA	Kilovolt-ampere
kV	Kilovolt
min	Minute
MW	Megawatt
MWh	Megawatt-hour
NL	Normal liter (gas volume at standard conditions)
s	Second
V	Volt

1

Introduction

Grid congestion has become one of the most urgent obstacles in the Dutch electricity system. Power peaks are increasingly pushing transformers and distribution cables toward their operational limits, restricting the connection of new consumers and producers and posing a growing challenge for grid operators. This congestion issue is triggered by the accelerating energy transition. To meet national climate policy and the Paris Agreement target of net-zero emissions by 2050, renewable electricity must replace fossil fuels[36]. As a result, the adoption of electric technologies such as heat pumps (HPs) and electric vehicles (EVs) has increased rapidly, driving up residential electricity demand and thereby putting pressure on the low-voltage (LV) network. At the same time, the Dutch electricity system is experiencing a rapid shift in generation patterns. A five-fold increase in installed rooftop photovoltaic (PV) capacity between 2018 and 2023 illustrates the fast-paced growth of distributed energy resources (DERs) [16]. While these resources contribute to de-carbonization, the LV grid managed by Distribution System Operators (DSOs), was not originally designed to accommodate bidirectional and highly intermittent power flows. The combination of higher electricity demand and fluctuating rooftop PV generation produces power peaks that can lead to unwanted voltage fluctuations, transformer overloading and increased strain on distribution cables [31]. Together, these developments indicate that, even if sufficient renewable resources are available, the current LV grid forms the bottleneck to achieving a fully renewable electricity system by 2050.

In December 2022, the Dutch government introduced the National Grid Congestion Action Program (Landelijk Actieplan Netcongestie, LAN), aimed at addressing the growing pressure on the electricity network. The newest LAN report shows that the demand for transport capacity is growing faster than the grid can be expanded, making netcongestion a structural and increasing national problem [17]. Grid reinforcement is the most direct solution to this issue. However, even though network operators have doubled investment levels and large infrastructure expansions are underway, the pace of grid expansion remains significantly slower than the speed at which congestion is developing. This means that physical expansion alone will not be sufficient to safeguard the reliability of the electricity system.

For this reason, the LAN prioritizes not only **network expansion** but also **better utilization of existing grid capacity** through *flexibility*, *storage*, and *collective coordination between energy users*. Within this strategy, stimulating *energy hubs* is listed as a national measure to reduce grid congestion by locally aligning electricity production, consumption, and storage. In parallel, the Dutch government launched the *Stimuleringsprogramma Energiehubs*, allocating €166 million to accelerate the development of regional and local energy hubs [1]. Its objective is to promote a more decentralized energy system in which coordination between local supply, demand, storage, and conversion contributes to an energy system that is *affordable*, *sustainable*, and *flexible*.

Consistent with the LAN, Dutch grid operators developed the *Integrale Energiesysteemverkenning 2030–2050* (II3050), a national scenario study exploring pathways towards a climate-neutral energy system by 2050, with 2030 as an intermediate step. These scenarios inform long-term infrastructure planning and highlight flexibility, electrification, and local system coordination as key requirements for

a reliable future grid. Within II3050, *Decentrale Initiatieven* (DEC), including renewable generation and local energy systems such as energy hubs, are assigned a central role in enabling this transition [64].

According to both the LAN program and the II3050 scenarios, energy hubs could therefore serve as a promising approach to improve the utilization of the electricity grid while also enabling the local generation, storage and consumption of renewable electricity. Based on public datasets, an analysis has shown that 1,183 potential energy hubs across the Netherlands could jointly contribute approximately 3.2 GW in peak load reduction on the electricity grid by 2030 [15]. Given that both LAN and II3050 designate 2030 and 2050 as key milestones toward a renewable electricity system aligned with the Paris Agreement, these years are used as baseline horizons to assess the potential role of energy hubs in the 2050 energy landscape.

As the parties responsible for operating and reinforcing the DSOs are directly confronted with the impacts of congestion and are crucial in enabling such decentralized solutions. One such DSO is Stedin, which oversees the LV and MV networks in South Holland, Utrecht and Zeeland, supplying electricity to more than 2.3 million customers [61]. Stedin and other DSOs must therefore not only invest in physical grid reinforcement, but also explore decentralized alternatives, including energy hubs, to alleviate pressure at the local level.

The *Energieagenda* [8] emphasizes that newly constructed buildings contribute only marginally to national sustainability targets; the primary challenge lies within the existing built environment. Many neighborhoods were built with limited electrical connection capacity and struggle to accommodate rising demand from electrification. For such areas, decentralized solutions that reduce grid dependency, such as local energy hubs, are therefore relevant to explore.

Given this context, this thesis focuses on the role of energy hubs within the existing built environment to structurally reduce grid congestion both in the short term and in the electricity system by 2050.

In renewable energy systems, short-term fluctuations (hours to days) can be covered by battery storage, but the seasonal mismatch between supply and demand requires a different approach. In the Dutch context, solar generation peaks in spring and summer, whereas residential electricity demand, driven largely by heating, reaches its highest levels in autumn and winter. Without long-duration storage, this gap would require high winter grid imports or extreme over sizing of PV capacity in the built environment.

Seasonal storage technologies such as Power-to-Gas (P2G), Power-to-Heat (P2H) and Power-to-Hydrogen (P2H2) can bridge this gap by converting surplus renewable electricity into storable thermal or chemical energy forms [52]. For residential LV grids, these technologies offer the potential to reduce winter peak imports and alleviate transformer congestion by using a seasonal storage technology in an energy hub.

This leads to the specific energy hub concept explored: rooftop PV, batteries and hydrogen storage integrated to shift energy not only within the day, but across seasons. This system stores surplus solar energy in batteries and partly converts it into hydrogen. During the day, the batteries supply electricity when demand exceeds production, while in winter the stored hydrogen is converted back into electricity to compensate for lower solar generation. This integrated configuration is referred to as the 24/7 Energy Hub. The concept was launched at The Green Village in June 2020 and is currently deployed at a single-person household [27], forming the basis for the scaled-up modeling in this thesis. A key objective of this research is to create a scalable 24/7 Energy Hub model that can be expanded from household level to neighborhood level while preserving its operational logic.

1.1. Problem Statement and Research Questions

As outlined in the introduction, grid congestion is a key bottleneck for the Dutch energy transition, driven by rapid electrification and growing rooftop PV adoption. While national strategy promotes both grid reinforcement and improved utilization of existing infrastructure, the role that neighborhood-scale energy hubs could play in this approach is still uncertain.

Figure 1.1 summarizes this context by illustrating how climate targets lead to grid congestion challenges, and how energy hubs are positioned as a potential solution under national strategies such as LAN and II3050.

Building on this background, this thesis investigates whether the 24/7 Energy Hub can reduce grid congestion within the existing built environment by 2050. To answer this question, it is necessary to assess the system's technical interaction with the LV network at transformer level. Specifically, the analysis examines how integrating PV, battery storage, and a Seasonal Storage System (SSS) based on hydrogen affects transformer loading, peak demand, and annual power flow patterns.

The core study is whether such a system can limit peak loads without exceeding transformer capacity, thereby enabling neighborhood-scale deployment of the 24/7 Energy Hub as a congestion mitigation measure. Although voltage effects and the spatial placement of storage assets also influence feasibility, these lie beyond the scope of this thesis and are considered logical future research directions if transformer-level performance proves promising.

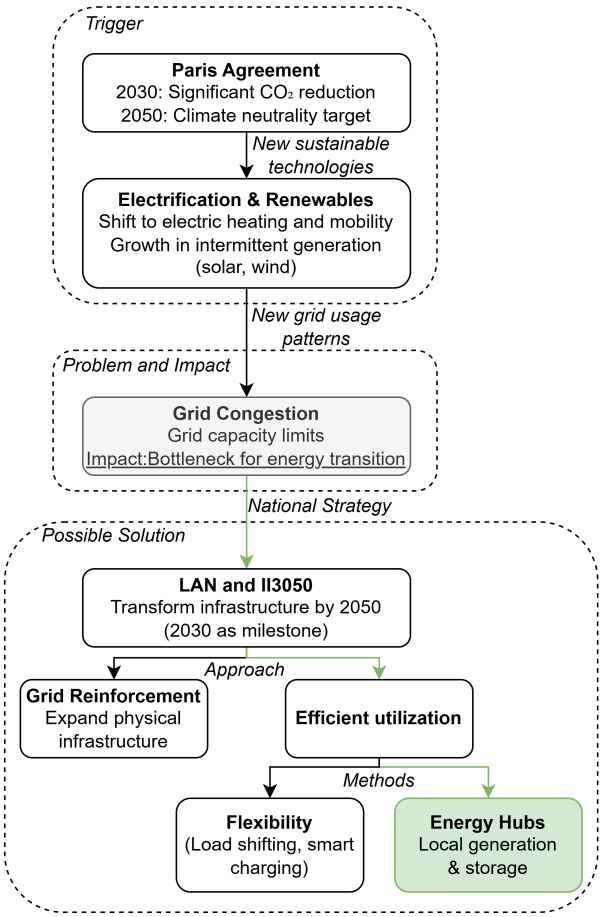

Figure 1.1: Problem context and motivation for energy hubs: from climate targets to grid congestion and national strategies.

1.1.1. Research Question

Given the challenges described in the problem statement, this thesis aims to answer the following research question:

> *To what extent can decentralized hydrogen storage mitigate grid congestion at low-voltage distribution transformers within the existing built environment by 2050?*

1.1.2. Sub-questions

To answer the main research question, this thesis is structured around three objectives. Each objective is related to one or more sub-questions (SQ):

- **Objective 1 — Assessment of the Future Energy Landscape**
  To evaluate how projected developments toward 2050 influence the suitability of the energy hub for grid congestion mitigation.

  - **SQ1:** Which built environment archetype is suitable for implementing the energy hub concept, and how transferable is the approach?
  - **SQ2:** How do projected changes in consumption and generation affect the potential of the energy hub to mitigate congestion by 2050?
- **Objective 2 — Case-study Evaluation and Techno-Economic Feasibility**
  To test the energy hubs in a neighborhood case study and its technical and economic performance.
  - **SQ3:** How does the existing Energy Management System (EMS) interact with the energy hub?
  - **SQ4:** How should the battery, electrolyzer and fuel cell be dimensioned to operate within transformer capacity limits?
  - **SQ5:** Under what production and grid conditions is seasonal hydrogen storage feasible for congestion mitigation?
  - **SQ6:** What are the investment and operational costs of the energy hub compared with grid reinforcement?
- **Objective 3 — Model Development: Validation and Applicability**
  To develop a model that recreates the operation of the 24/7 Energy Hub in a scalable form suitable for neighborhood-level use.
  - **SQ7:** How can the 24/7 Energy Hub be modeled as a reliable plug-and-play concept suitable for large-scale implementation in residential areas to mitigate grid congestion?

1.2. Outline of the Thesis

Chapter 1 introduced the motivation, research problem and scope of the work.

Chapter 2 provides the theoretical background by outlining the operation of LV grids and the principles of the 24/7 Energy Hub, while the State-of-the-Art review identifies relevant literature and highlights the knowledge gaps that motivate this research.

Chapter 3 details the methodological framework, which consists of four keystones. It begins with the description of the LV grid used in **the case study** and outlines the future electrification **time horizons**. It then introduces the set of **energy hub scenarios**, each characterized by a control strategies and component sizing, where **configurations** refer to the different component combinations tested based on different key performance indicators within each scenario. Building on this, the development of the small-scale **24/7 Energy Hub model** is presented.

Chapter 4 evaluates the reliability of the model through **validation** against measured data from The Green Village, after which the **baseline time horizons** without an energy hub are analyzed to understand how the grid would evolve without mitigating action. Thereafter, the different energy hub **configurations and their performance** are compared in terms of congestion mitigation and overall system effectiveness.

Chapter 5 reflects on the insights, outlines limitations of the study, answers the research questions and provides recommendations for future research.

Finally, Chapter 6 summarizes the main findings and contributions of this thesis.

2

Background Knowledge

This chapter provides the crucial background knowledge for this thesis, organized around two core themes. The first, described in section 2.1, focuses on the LV distribution network, pointing out its relevant characteristics. The second, covered in section 2.2, outlines the existing small-scale 24/7 Energy Hub, with its key components and the applied energy management system. Followed by the State-of-the-Art section 2.3, which researches prior work, highlights the knowledge gap. The methodological approach is outlined in section 2.4.

2.1. Low-voltage Grid

The LV grid provides consumers with electricity, primarily households and small businesses. Together with the medium-voltage (MV) grid, it forms the distribution network, organized and regulated by the DSO. The distribution network receives electricity from the transmission network, which consists of the high-voltage (HV) grid, the intermediate voltage network, and a transmission-functioning medium-voltage grid. Additionally, the transmission network can obtain electricity from other countries through interconnection networks, which is regulated by a Transmission System Operator (TSO). A schematic overview of the electricity network in the Netherlands is illustrated in Figure 2.1 [42].

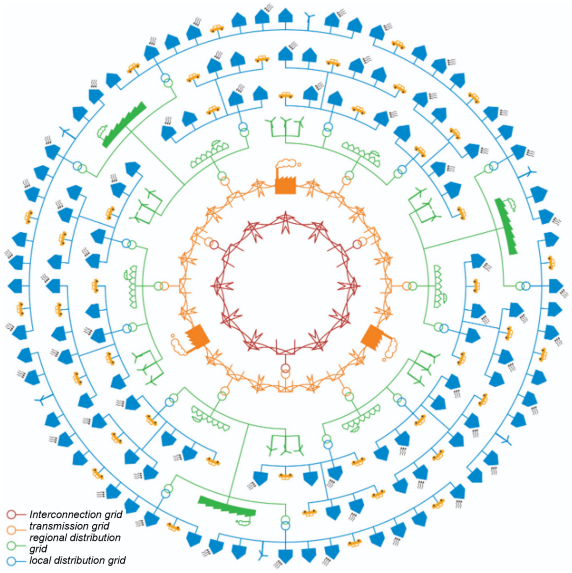

Figure 2.1: Schematic of the electricity network by voltage level [42]. From center outward: **Interconnection** (red, ∼300–400 kV), **Transmission** (orange, ∼110–220 kV), **Regional distribution** (green, ∼10–33 kV), and **Local distribution** (blue, 400/230 V). Ring transitions indicate transformer steps.

The LV grid is designed to handle voltage levels up to 1 kV, but the standard operating voltage is 400 V, with a phase voltage of 230 V, and a frequency of 50 Hertz.

The MV grid feeds electricity to the LV grid through a distribution substation, containing a transformer that transforms MV to LV for distribution. A typical transformer connects up to twelve LV feeders, each supplying electricity to households [42].

For the selection of MV/LV transformers, standardized transformer ratings are applied. Common nominal capacities include 50, 100, 160, 250, 400, 630, 1000 and 1600 kVA, depending on the neighborhood type and the number of connected households.[1]

From the substation, electricity is distributed through the LV cables to the grid connection points of customers, which are households or small businesses, where 3 x 25 A is the standard household connection [43].

2.1.1. Archetypes

Understanding the structure and layout of LV grids also requires recognizing the diversity of neighborhoods that are part of it. The Gebouwde Omgeving Elektrificatie (GO-e) project, which examines the flexibility potential of the built environment, has identified eight archetypical neighborhoods in the Netherlands. Factors such as the energy label, building type, and density of addresses are relevant for LV considerations, since they portray their different needs. These archetypes, which reflect common residential and commercial areas, are described below in Table 2.1.

Archetype	Year	Type	Address Density	Energy Label
1. Pre-housing bill homes	1874-1920	Apts.	High	Mostly C/D
2. Pre-war residences	1920-1946	Apts.	High	Mostly A/B
3. Post-war terraced houses	1970-2010	Row houses/apts.	Low	Mixed
4. Post-war tenements	1970-2010	Mostly apts.	Low-med	Mixed
5. Corporation residences	1920-2010	Multi-family	Med	Mostly C-D-E
6. Detached houses	1946-1960 / 1874-1920	Detached	Low	Mostly F/G
7. Rural area	1946-1960 / 1874-1920	Row houses/apts.	Med	Mostly C/D/E
8. Industry / few residents	1970-2010	Commercial	Low	N/A

Table 2.1: The eight neighborhood archetypes established by the Gebouwde Omgeving Elektrificatie (GO-e) Project, representing the dominant types of existing built environments in the Netherlands. These archetypes are widely used to describe residential areas in energy-system research due to their distinct structural and energy-use characteristics [14].

As established in Chapter 1, the existing built environment forms the greatest challenge in relation to both grid congestion and sustainability goals. For this reason, the case study in this thesis focuses on a representative neighborhood topology within the existing built environment rather than on new developments, which can be designed to accommodate higher electricity demand, and are often way more energy-efficient. Among these, post-war terraced houses (archetype 3) are particularly relevant for studying the integration of energy hubs. First, they constitute the largest share of the Dutch residential area, representing approximately 26% of all neighborhoods, and therefore have high impact. Second, the GO-e project indicates that archetype 3 has a high quality of fit, meaning that its architectural and electrical characteristics are relatively consistent across the country [14]. In contrast to archetypes such as rural areas or detached houses, where local conditions vary strongly and would lead to location-specific conclusions rather than broadly applicable insights.

Archetype 3 also aligns well with the technical focus of this thesis. Post-war terraced houses typically have row-house layouts with medium to high roof availability for rooftop PV, creating the potential for high PV penetration and associated power peaks on the LV grid. At the same time, the existing grid

[1] These values reflect standard design conventions for MV/LV transformer substation at Stedin.

connection capacity in these neighborhoods is often insufficient to handle the increased demand from electrification.
Together, these factors make archetype 3 an good reference case for evaluating energy hub integration.

2.1.2. Grid Operational Limits and Congestion

To understand the congestion problem on the Dutch LV grid, it is essential to first consider the operational boundaries within which DSOs must operate. The Netcode and EN 50160 define the quality requirements for LV grids, including limits on voltage behavior and thermal loading of cables and transformers [53]. The most relevant monitored indicators are:

- **Slow voltage variations:** The voltage at a LV connection point must remain within 10% of the nominal voltage ($U_{\mathrm{nom}} = 230\ V$), i.e., $U \in [207\ V, 253\ V]$. Long-term deviations outside this range may lead to improper or unsafe device operation, especially in cases of high rooftop-PV feed-in.
- **Rapid voltage variations (flicker):** Short-term fluctuations caused by switching high-power appliances, experienced as visible light-intensity variations.
- **Voltage unbalance:** Uneven distribution of single-phase loads or generators over the three phases cause voltage unbalance.
- **Harmonic distortion:** Introduced by non-linear devices such as power electronics and LED lighting, resulting in waveform distortion and additional thermal stress.
- **Voltage dips:** Short-term decreases in voltage due to faults or abrupt load changes.

These limits are essential for maintaining the reliability and safety of the LV grid. Congestion emerges when power flows push network components beyond their operational boundaries, causing the thermal limits of cables or transformers to be exceeded [20]. Voltage and transformer constraints are closely linked, both originating from the same underlying mechanism: high import or export currents caused by power peaks. High electricity demand results in high import currents, leading to transformer loading and voltage drops, while high rooftop-PV feed-in results in reverse power flows, causing transformer loading and voltage rises.

In recent literature, congestion-mitigation strategies in LV networks are predominantly explored from a voltage-control perspective. Numerous studies demonstrate that battery storage can mitigate voltage fluctuations [29, 60, 3, 55, 63]. These works highlight the contribution of storage to improving voltage quality and increasing hosting capacity. In addition, a community battery project in Rijsenhout connects 35 homes with rooftop PV panels to a shared battery system. Supported by grid operator Liander, the project has shown that such systems manage voltage regulation effectively [9].

However, these approaches mainly target local voltage behavior within LV feeders, whereas this thesis focuses on congestion at the MV/LV transformer level. Transformer loading is not only a constraint for congestion, but it also reflects the degree of dependency on the external grid. This makes it a particularly relevant indicator for assessing the potential of the energy hub concept, whose objective is to mitigate grid congestion by increasing local self-consumption and reducing reliance on the external grid, since transformer loading reflects the aggregated effect of all consumption and generation within the serviced LV area.

After examining congestion mechanisms at the LV level, the situation can be evaluated at a national scale. Figure 2.2 illustrates the regional capacity maps published by Dutch grid operators. Figure 2.2a presents MV capacity limitations for electricity consumption (imports), and Figure 2.2b presents capacity limitations for electricity feed-in (exports). Yellow areas indicate limited availability, while red areas represent full congestion. The maps clearly show that both rising electricity demand and increasing renewable generation contribute to capacity shortages.

Although Figure 2.2 reflects congestion at the MV level, capacity shortages at different voltage levels are closely interconnected. LV, MV and HV grids do not operate in isolation: high PV feed-in or electrification at the LV level can increase power flows toward the MV network, while capacity limitations in the MV or HV network can restrict the amount of power that LV substations are permitted to import or export. As a result, congestion at one voltage level can cause congestion at another, and the bottleneck may shift over time depending on demand and generation patterns. The MV/LV transformer

is important because everything that happens in the LV grid, local demand and rooftop-PV generation, becomes visible here as power going to or from the MV network.

Electrification and new sustainability regulations are expected to intensify the congestion in the coming decades. From 2050 onward, residential heating and cooking using natural gas will no longer be allowed [65], meaning that households will increasingly adopt heat pumps and electric cooking. In addition, from 2035 all newly sold passenger cars must be zero-emission, and by 2050 the entire car fleet must meet this standard [8], resulting in a rapidly growing demand for charging infrastructure. Another regulation introduced on 1 February 2022 requires that major building renovations meet a minimum renewable energy threshold, typically through rooftop solar or heat pumps [21].

These developments are essential for reaching climate targets but significantly increase electricity demand and solar feed-in on the LV grid, making the need for smart congestion-relief solutions increasingly urgent.

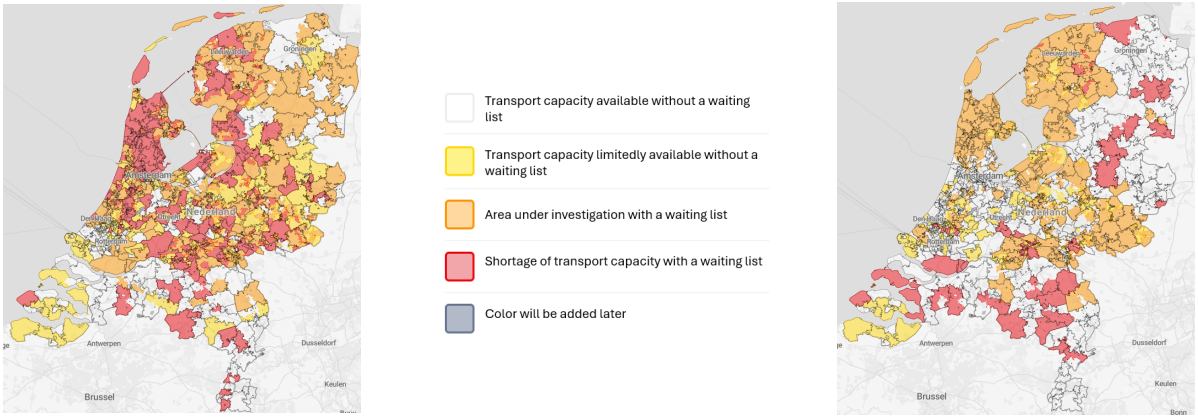

(a) Consumption (import) capacity.

(b) Feed-in (export) capacity.

Figure 2.2: Regional **medium-voltage (MV) transport capacity** in the Netherlands for new or expanded connections (Version 2024). (a) Capacity for electricity consumption (imports). (b) Capacity for electricity feed-in (exports) [6].

2.2. Energy Hubs

With the structure and challenges of the LV grid established, the focus now shifts to the energy hub perspective. The purpose of energy hubs is to organize local electricity production, consumption and storage in a way that relieves pressure on the grid and increases the use of renewable energy.

The impact of grid congestion differs across stakeholder groups and shapes the feasibility of any solution. Residents depend on affordable and reliable energy and increasingly value sustainability. DSOs must maintain grid reliability but operate within investment and grid constraints. Municipalities aim to accelerate sustainable neighborhood development, while delays in housing and electrification projects can occur when grid capacity is insufficient. Any solution for relieving congestion, including energy hubs, must therefore be compatible with these partly overlapping and partly competing interests.

In response to this challenge, the LAN sets three main objectives: enabling the energy transition, maintaining reliability and available capacity on the existing grid, and safeguarding affordability by preventing excessive long-term reinforcement [17]. Energy hubs align with these goals because they reduce stress on the electricity grid by organizing renewable generation and flexible storage locally rather than relying solely on upstream infrastructure expansion.

Energy hubs can also bring direct benefits to residents. Adoption of rooftop PV continues to increase, but the gradual phase-out of the net-metering scheme and the appearance of lower or even negative export tariffs reduce the financial benefit of exporting electricity to the grid [66]. As a result, households are increasingly motivated to increase self-consumption. By allowing renewable electricity to be shared or stored within the neighborhood, energy hubs make residents less dependent on fluctuating electricity prices, while supporting the affordability objective of the LAN.

Storage systems play a central role in this development. Local batteries can reduce congestion by

absorbing surplus solar energy that would otherwise be exported during peak periods. At the same time, if batteries operate solely on electricity market incentives, they may charge during low-price hours that coincide with high grid loading, which can unintentionally worsen congestion. Within the LAN program, grid operators, market parties and the Ministry of Climate and Green Growth therefore work toward voluntary coordination to ensure that storage behavior does not worsen congestion [17].

In line with that ambition, this thesis does not consider market participation or financially optimized battery control. The scope is limited to the technical effect of local storage on grid congestion, with a specific focus on how the energy hub interacts with transformer loading.

According to research, four distinct *families* of energy hubs can be identified, described below.

- **Built Environment Hub:** These hubs are situated in residential areas and often include small to medium-sized businesses. They combine living, working, and mobility functions within urban environments and typically operate at the LV level.
- **Mobility Hub:** These hubs are centered around transportation infrastructure such as road, rail, and charging systems. They focus on integrating transport-related energy demands with storage to support sustainable mobility but generally do not act as generation or storage sources themselves.
- **Business Park Hub:** Located in industrial or commercial zones, these hubs may exchange energy with nearby residential areas and often absorb or generate excess renewable energy, such as from solar or wind power. They typically operate on the MV grid.
- **Cluster 6 Industry Hub:** This type includes large-scale energy-intensive industries. These hubs typically operate as grid-connected installations at MV or HV level, serving primarily as energy sinks that flexibly absorb surplus renewable generation.

Based on these definitions, this thesis falls within the category of *Built Environment Hubs*. Accordingly, the next section introduces the 24/7 Energy Hub at The Green Village.

2.2.1. The 24/7 Energy Hub

To address the lack of real-world initiatives on seasonal energy storage in the built environment, the TU Delft Faculty of Electrical Engineering, Mathematics & Computer Science together with the field lab The Green Village launched the *Seasonal Storage System* project in June 2020. The objective of this initiative was to develop and evaluate local energy hub concepts under realistic operating conditions. Within this project, the 24/7 Energy Hub was realized as a living laboratory that integrates PV generation, short-term battery storage and long-term hydrogen storage to enable year-round renewable energy supply at the household level [27]. The system is connected to a single fully electric household, as shown in Figure 2.3.

Figure 2.3: The outdoor, fenced compound of the 24/7 Energy Hub pilot at The Green Village. The orange cylinder racks are the high-pressure hydrogen storage tanks; a control/power cabinet stands to the right [27].

The 24/7 Energy Hub can be described as a household-scale energy system that aims to operate on locally generated renewable electricity throughout the entire year by combining daily battery storage with seasonal hydrogen storage.

The 24/7 Energy Hub couples a one-person household with rooftop PV, a lithium iron phosphate

($LiFePO_4$) battery and a hydrogen storage system. Solar energy is generated by PV panels and converted from direct current (DC) to alternating current (AC) using a PV inverter. Surplus electricity is first stored in the battery for short-term daily cycling. Once the battery approaches its maximum state-of-charge (SOC), the remaining excess PV power is diverted to an anion-exchange membrane (AEM) electrolyzer, which produces hydrogen from water. The hydrogen is then compressed using a solid-state electrochemical compressor and stored in high-pressure tanks. During winter periods of low PV production, the stored hydrogen is converted back into electricity via a fuel cell, whose DC output is routed to the household and the battery through a dedicated fuel cell inverter. In combination, the battery and hydrogen storage system allow continuous operation throughout the year, with the battery absorbing short-term fluctuations and hydrogen providing seasonal balancing.

A schematic overview of the system and its main components is presented in Figure 2.4a, while Figure 2.4b illustrates the AC and DC power flows. The technical specifications of all components are summarized in Table 2.2.

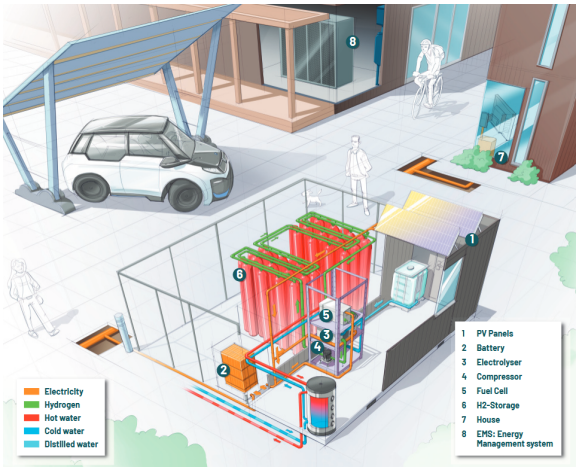

(a) Schematic overview of the 24/7 Energy Hub [27].

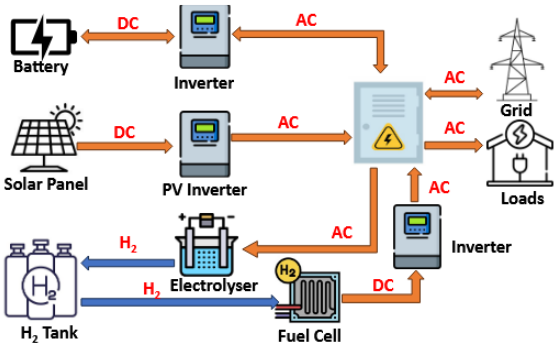

(b) System components and power paths [11].

Figure 2.4: 24/7 Energy Hub visuals: (a) schematic overview; (b) component-level layout.

Energy Management System

The Energy Management System (EMS) is designed around seasonal behavior, the winter period is from 15 October to 15 March, where battery SOC, PV generation, and time of day to organize the hydrogen system. The battery is the primary electricity supplier for the user [45].

The fuel cell is activated only during the winter period and based on the battery's SOC & the time of day. The fuel cell is turned off when the battery SOC reaches 90%, ensuring it's only used when truly needed [45]. Since $LiFePO_4$ batteries are sized for short-term balancing: they deliver near-instant power with a round-trip efficiency of $\sim$90–95% and are well suited to frequent cycling. In contrast, the electricity$\rightarrow$hydrogen$\rightarrow$electricity chain has a much lower electrical round-trip efficiency ($\sim$25–40%; electrolyzer $\sim$60–70% and fuel cell $\sim$45–60%, plus Balance-of-Plant, BoP, losses), but H_2 stores energy with negligible self-discharge over long periods, making it suitable for seasonal deficits.

For this reason, the control strategy is *battery-first, hydrogen-second*: the fuel cell is enabled only in winter and only when the battery SOC is low, and it is turned off once SOC reaches 90%. This minimizes conversion losses and preserves hydrogen for long-term shortages, while the battery covers routine evening/overnight demand.

The electrolyzer typically operates during the summer period (16 March to 14 October), when there is surplus solar generation. It operates only when PV output exceeds 1 kW and the battery is sufficiently charged (SOC $\geq$ 80%), and is limited to the morning ($time < 12{:}00$) to reserve afternoon PV for charging the battery for evening/overnight demand. The system turns off the electrolyzer when PV generation is under 50 W or the battery SOC drops below 65% [45].

The detailed control scheme of the system is discussed later in Section 3.4.5 (Figure 3.16), while the

Component	Function and Main Specifications
Household (1-person, fully electric)	Represents the residential electricity demand supplied by the hub. Annual consumption: **2,200 kWh/year**.
PV Panels	Primary source of renewable electricity. Installed capacity: **5.28 kWp**. DC output converted to AC via a PV inverter.
Lithium Battery (short-term storage)	Captures surplus PV energy for daily cycling and supplies the household or electrolyzer. Capacity: **15 kWh**; power: **5 kW**. Bidirectional conversion via a battery inverter.
Electrolyzer (Enapter)	Converts excess solar power to hydrogen via AEM electrolysis. Input power: **2.4 kW**; hydrogen production: **1 kg/24 h**.
Compressor (HyEt)	Compresses hydrogen for storage using a solid-state electrochemical cell. Input power: **600 W**; maximum throughput: **2 kg H_2/24 h**.
Hydrogen Storage (long-term storage)	Seasonal storage of compressed hydrogen. Total capacity: **47 kg (≈ 1,565 kWh)** in **53 tanks of 50 L**; storage pressure: **272 bar**.
Fuel Cell (Nedstack)	Converts stored hydrogen back to electricity and heat. Electrical power: **2.3 kW**; electrical capacity: **13.3 kWh/kg H_2**; thermal capacity: **14.5 kWh/kg H_2**. AC conversion through a fuel-cell inverter.

Table 2.2: Overview of the 24/7 Energy Hub components, including their functions and technical specifications [27].

technology behind the individual components is explained in the other sections of Chapter 3.

The 24/7 Energy Hub demonstrates that PV, battery and hydrogen can be integrated at household scale. To position this within the broader field, Table 2.3 summarizes real-world residential pilots using similar technologies. Existing implementations remain mostly small-scale and primarily target self-sufficiency rather than grid congestion mitigation.

Project	Country	Scale	Technologies	Building Type	Main Objective	Relevance / Missing Aspect for This Thesis
House of the Future (Zurich) [2]	Switzerland	9 households	PV, battery, hydrogen (electrolyzer + fuel cell)	New-build, high-efficiency	Full off-grid autonomy	Demonstrates technical feasibility of autonomy, but not scalable to existing neighborhoods; no assessment of grid interaction.
InnovaHub (Stad aan 't Haringvliet) [24, 13]	Netherlands	17 homes	70 kW electrolyzer, 30 kW fuel cell, 140 kWh battery, 3 MWh H_2 storage, heat/-cooling network	New-build	High self-sufficiency using EMS optimization	Large-scale and multi-vector, but not representative of retrofits; EMS driven by price and demand forecasts rather than grid congestion.
Open Hofkerk (Wolfheze) [47, 48]	Netherlands	8 homes	PV, electrolyzer, hydrogen storage, fuel cell, heat pump, thermal storage	Retrofit (church + timber homes)	Reducing grid pressure	Small scale and not analyzed for transformer loading or LV congestion.
FlexEh$_2$ome (Schöneiche) [12]	Germany	Single home	PV, 20 kWh battery, hydrogen storage (electricity + heating)	Single-family home	Autonomous building demonstration	Shows technical viability for one home but not applicable to neighborhoods; no grid interaction study.
SoCalGas Hydrogen Home [51]	USA	Single home	PV, battery, hydrogen production and storage for power + heating	Single-family home	Zero-emission demonstration building	Demonstration project; no analysis of transformer loading or congestion.

Table 2.3: Overview of real-world energy-hub demonstrations integrating solar, battery and hydrogen storage. Most projects focus on small-scale or new-build developments and do not analyze grid congestion or transformer loading when deployed in existing residential neighborhoods.

2.3. State-of-the-Art

This section presents a brief literature review to discover the knowledge gaps. Section 2.3.1 reviews previous research related to the 24/7 Energy Hub at The Green Village, which forms the core concept of this thesis and is the foundation of what is researched about the system and if it can be put it in different perspective. Next, Section 2.3.2 addresses existing research and has as goal to gain knowledge of the sizing strategy (in combination with section 2.3.1). Finally, section 2.3.3 examines the societal impact of energy hubs by considering the perspectives of different stakeholders: residents, municipalities, and DSOs in order to establish relevant key performance indicators. Together, these different aspects form the basis for identifying the knowledge gap in Section 2.3.4.

2.3.1. 24/7 Energy Hub Prior Research

Earlier work on the 24/7 Energy Hub includes the study by Maselli [33], which scaled the concept from a single household to community level using a multi-objective genetic optimization. Component sizes and energy dispatch were optimized by resolving the PV–load mismatch at each timestep and evaluating annualized cost, self-sufficiency and reliability. The results show that hydrogen storage is crucial for maintaining supply during winter shortages and that relying only on PV and batteries leads to high grid import peaks. Full autonomy is technically achievable, but requires large hydrogen storage capacity and high fuel cell power, which substantially increases investment cost.

Li et al. [30] examined scale-up to four student apartments and three family homes using a systematic, **power-based sizing method** rather than an optimization. Component sizes were selected such that the power difference between PV generation and demand could always be balanced by the battery, electrolyzer and fuel cell within their power limits, where the battery smooths short-term fluctuations and stabilizes electrolyzer operation. The resulting system achieves full annual self-sufficiency, but exhibits a structural seasonal imbalance: the electrolyzer, hydrogen storage and fuel cell must be sized large enough to cover peak winter deficits. Their results show that autonomy can be achieved with a relatively small battery for short-term balancing and a large hydrogen system for seasonal balancing. This thesis also deploys a form of power-based sizing method, but applies it from a grid-technical perspective at the MV/LV transformer when deployed at large-scale scale in the future.

Using operational data from The Green Village, [40] calibrated a Simulink model of the existing PV–battery–hydrogen energy hub and evaluated alternative EMS parameter settings by comparing grid exchange, efficiency and hydrogen production and consumption. The study provides valuable insight into the real system's behavior and control sensitivities at household scale. In this thesis, the small-scale 24/7 Energy Hub serves as a reference for developing a model that can be applied at neighborhood level, addressing the need for an easy scalable model and the relevance of transformer congestion rather than improving EMS parameters, thus a more zoomed out view.

Taken together, these studies provide strong evidence that hydrogen plays a crucial role in enabling autonomy and give insights on the 24/7 Energy Hub working principles. However, all three focus primarily at household or small-community scale and do not analyze how different sizing choices affect peak power exchange with the grid. This is essential, because rated peak power determines whether an energy hub can actually reduce congestion at the MV/LV transformer, needed for large-scale deployment in the built environment.

2.3.2. System Sizing

In general, the literature distinguishes two main approaches to system sizing:

- **Energy-based sizing**: determines component capacities based on cumulative energy balances over daily or seasonal timescales. Commonly applied in off-grid or autonomous systems, especially when PV capacity is a fixed design input, and often combined with optimization methods to minimize costs or maximize self-sufficiency [32], [50], [35]. While useful for autonomy, these methods often overlook grid constraints and peak power flows.
- **Power-based sizing**: selects components to handle power mismatches at each timestep. This method is more relevant for grid-connected neighborhoods where transformer capacity and peak demand are critical. It is used by [30] to size a residential hub without optimization, and by [28] to assess dispatch performance under varying peak conditions.

Sizing strategies for PV–battery–hydrogen systems vary depending on the design objective. Many studies integrate system sizing with dispatch optimization, typically using Mixed-Integer Linear Programming (MILP) or genetic algorithms, to optimize investment and operation without explicitly modeling an EMS [32], [35].

By contrast, this thesis adopts a *power-based, non-optimized* sizing approach, in which components are dimensioned to balance mismatches between generation and demand at each timestep. This method prioritizes grid-technical performance. Under and over sizing is used to evaluate robustness, and dynamic simulation captures the interaction between component operation and local grid constraints.

2.3.3. Stakeholder Considerations

Studies consistently show that energy hubs are viewed positively by residents, municipalities and DSOs, but the incentives and concerns of these actors differ substantially. Homeowners and tenants generally perceive energy hubs as useful, yet not economically attractive, due to high upfront investment and regulatory complexity [68]. Many residents are motivated by sustainability and energy independence, but prefer that external organizations initiate and manage such systems rather than taking responsibility themselves. Similar findings are reported in research on community energy systems [25], which shows that willingness to participate often conflicts with practical barriers such as limited time, financial capacity and technical expertise.

Investment motivations further vary by community type. In “communities of place”, social and environmental motives tend to dominate, whereas in “communities of interest” economic returns are the primary driver [4]. Municipalities and collective actors are also driven by environmental and social goals, yet face regulatory uncertainty and grid-interaction challenges that complicate implementation [18]. DSOs, in turn, prioritize grid reliability and affordability at system level and are cautious about concepts that could increase operational complexity or introduce new peak loads.

Taken together, the literature highlights that residents, municipalities and DSOs share similar high-level goals, affordable, reliable and sustainable energy, but implement them differently. Residents mainly want the electricity generated on their rooftops to benefit them rather than being exported at low or negative tariffs. Municipalities and DSOs emphasize the reliability of the system and expect new decentralized initiatives to not overload MV/LV transformers or worsen congestion. Across stakeholders, affordability remains a recurring condition, meaning that system costs must be proportional to the value delivered.

These interests closely align with the LAN action agenda, which aims to better utilize the existing grid, improve reliability and maintain affordability without relying solely on grid reinforcement. Meeting these objectives first requires clear technical evidence that residential energy hubs can reduce transformer loading rather than intensify it.

For this reason, this thesis focuses on the technical feasibility of residential energy hubs from a grid perspective. The analysis does not yet determine participation models or stakeholder roles, but their incentives are reflected in the selection of the Key Performance Indicators (KPIs): reduction of peak import and export power at the transformer - *reliability*, total system cost including Capital Expenditure (CAPEX) and Operational Expenditure (OPEX) - *affordability*. In addition, the ratio between hydrogen produced and consumed is included as an indicator of the *efficient utilization* of long-term storage, supporting the LAN ambition of smarter use of existing infrastructure rather than maximal expansion.

2.3.4. Summary of Knowledge Gaps

The literature shows insights in modeling energy hubs at small scale, understanding their technical operation and identifying the stakeholders. However, several important knowledge gaps remain:

1. **Scale gap**: Prior studies on the 24/7 Energy Hub, and other energy hub researches, investigate pilot-scale systems. There is limited research on how such concepts perform when deployed at *neighborhood scale* and evaluated from a grid-technical perspective.
2. **Future horizon gap**: Most existing research use historical load profiles. They do not explore *forward-looking energy horizons* (for 2030 and 2050) that account for rising electrification, widespread PV adoption, and HP or EV uptake.

3. **Performance evaluation gap**: While the motivations of residents, municipalities and DSOs are well studied, they should translate into *scenarios and KPIs* that allow for evaluation of the system configuration based on (shared) stakeholder goals: reliability, affordability, and better utilization.
4. **System integration gap**: Many optimization-based sizing studies do not include a control strategy through an EMS, and implementation of detailed technologies of each component. This makes it difficult to assess their true grid impact under dynamic control, and therefore recreating real-life implementation.

2.4. Methodology Overview

To address the research questions and close the identified knowledge gaps, this thesis develops an integrated modeling and simulation framework, described in Chapter 3, built on the following steps:

1. **Neighborhood-scale case study**: Define a *neighborhood-scale* test grid (archetype 3) to evaluate the energy hub performance under LV grid conditions, beyond the pilot-scale system.
2. **Time horizon definition**: Construct *the representative test grid* to simulate baseline energy conditions for the *years 2023, 2030 and 2050*. These horizons incorporate evolving demand patterns and electrification trends, using available policy and infrastructure forecasts.
3. **Hub integration and sizing**: Design the energy hub to neighborhood level using a *non-optimized, power-based sizing strategy* aligned with grid constraints. Including the effect of under and over sizing to gain insight on the sizing, while testing with a rule-based EMS. Finally assess the performance using KPIs linked to stakeholder incentives.
4. **Reference model development**: Model the existing 24/7 Energy Hub at *The Green Village*. This ensures that system behavior, including electrolyzer, fuel cell, and battery interactions, can be validated and thus reflects real-world dynamics.

Besides, most research either zooms in on system control without considering grid interaction, or zooms out at a conceptual level without detailing the technical operation of components. This thesis explicitly bridges that gap by applying realistic component behavior to the future grid by 2050, allowing for robust assessment of energy hub feasibility.

The identified gaps motivate the research objectives and sub-questions, which structure the methodology. This link is summarized in Table 2.4. By addressing these gaps systematically, the thesis generates insights needed to answer the main research question: *"To what extent can decentralized hydrogen storage mitigate grid congestion at low-voltage distribution transformers within the existing built environment by 2050?"*

Table 2.4: Alignment between knowledge gaps, research objectives, and methodological response

Knowledge Gap	*Research Objective and Questions Addressing It*	*Methodological Response & Relevant Section*
1. Scale gap	• Objective 1 — Energy landscape toward 2050: **RQ1**	• Neighborhood-scale case study – *section 3.1*
2. Future horizon gap	• Objective 1 — Energy landscape toward 2050: **RQ2**	• Time horizon definition – *section 3.2*
3. Performance evaluation gap	• Objective 2 — Case-study evaluation and techno-economic feasibility: **RQ3,4,5,6**	• Hub integration and sizing – *section 3.3*
4. System integration gap	• Objective 3 — Model development: validation and applicability: **RQ7**	• Reference model development – *section 3.4*

3

Methodology

This chapter presents the methodology. Section 3.1 first describes the residential LV grid selected as the case study. Section 3.2 introduces the projected time horizons that reflect future electrification trends. Section 3.3 then explains the design of the energy hub configurations implemented within this case study. Finally, Section 3.4 details the development of the models, which represents the integrated operation of the grid and the energy hub. The methodology is structured in a top-down manner, starting from the high-level system context and narrowing the focus to the detailed development of the simulation model.

3.1. Low-Voltage Grid: Case Study

This section defines the LV case study grid corresponding to archetype 3. The grid consists of 155 households (1- to 5-person households) distributed across five LV feeders, also used in research [39] and [38]. As mentioned and motivated in section 2.1.1, this is an archetype 3 area. A visual lay-out is shown in Figure 3.1.

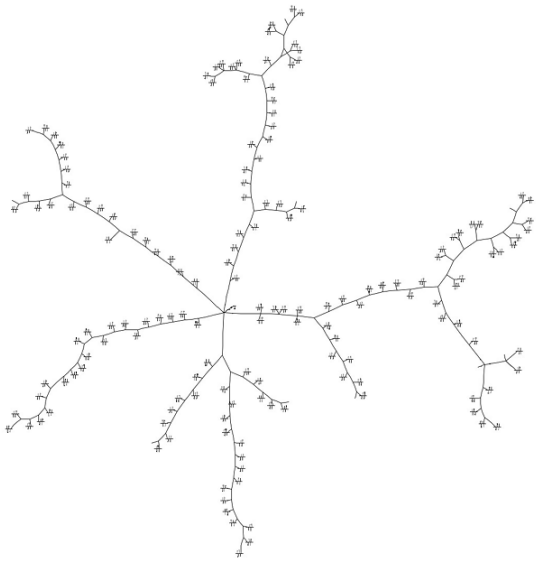

Figure 3.1: Topological layout of the low-voltage grid (archetype 3), consisting of 155 households, used in the case study. *Source: PowerFactory*

In the modeled LV grid, household electricity demand is assumed to be non-flexible. It is assumed that the increase in electricity use over time is balanced by improved device efficiency, so the non-flexible household load profiles remain unchanged and do not include additional heating or charging schedules.

Load profiles for five household categories were used, corresponding to annual electricity consumptions of 1,500, 2,500, 3,500, 4, 00 and 4,500 kWh, occurring in archetype 3. These profiles, available at 15-minute resolution, were derived from real anonymized residential neighborhoods and were previously applied in the GO-e project for power flow simulations and calculations ([14], [59]).

The household load profiles categories are distributed across all five feeders in the proportions shown in Table 3.1, which together represent the full composition of the 155-household grid. As previously noted, the modeled grid consists of 155 households, with over 70% belonging to the lower consumption categories (1,500 and 2,500 kWh). This distribution is noticeable in the aggregated group demand shown in Figure 3.2, where these groups contribute the most to total electricity use. Conversely, the average per-household demand is highest for the 4,500 kWh group, as shown in Figure 7.1 in Appendix 7.1.

Table 3.1: Households per annual electricity consumption ban and feeder (N = 155).

Annual consumption (kWh)	Feeder 1	Feeder 2	Feeder 3	Feeder 4	Feeder 5	Total
1,500 (1-person)	14	9	9	11	17	60
2,500 (2-person)	11	7	7	9	16	50
3,500 (3-person)	4	2	2	4	7	19
4,000 (4-person)	4	3	3	3	5	18
4,500 (5-person)	2	1	1	1	3	8
Total Households	**35**	**22**	**22**	**28**	**48**	**155**
(%)	(22.6%)	(14.2%)	(14.2%)	(18.1%)	(31.9%)	(100%)

To confirm their suitability for Dutch conditions, reference data from Nibud, CBS, and Milieu Centraal [26] were consulted. These sources report average household electricity consumption in 2023 ranging from approximately 1,600 kWh for single-person households to nearly 4,000 kWh for larger households, aligning well with the annual consumption used in this test grid.

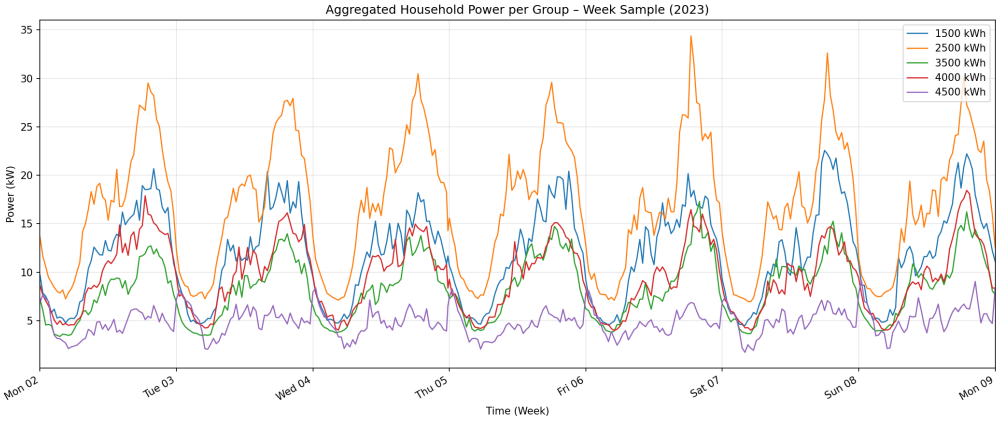

Figure 3.2: Aggregated electricity demand across household groups over a representative week. Each curve represents the total load from all households in a specific consumption category (1,500–4,500 kWh/year).

3.2. Baseline Time Horizons

The goal of this section is to assess how rising electrification and solar adoption affect the LV grid, and to establish baseline scenarios that reveal potential grid congestion risks and highlight the need for mitigation strategies by 2050. With the characteristics of the test grid and its household loads established, this section outlines the three time horizons used in the analysis: **2023 as the baseline, and 2030 and 2050 as projected future projections.** These follow the II3050 framework developed by Dutch grid operators and reflect national planning milestones set by the LAN, both of which aim for a climate-neutral electricity system, as discussed in Chapter 1. Year-specific penetration rates, based on projections provided by Stedin, of EVs, HPs, and rooftop PV are summarized in Table 3.2. This process results in a feeder-level distribution of these assets for each time horizon, as

presented in Table 3.4 (2023), Table 3.5 (2030), and Table 3.6 (2050).

Table 3.2: Penetration rates per time horizon (N = 155 households) [39].

Penetration rate	2023	2030	2050
PV [%]	30	45[1]	85[1]
EV home chargers [%]	2.7	5.7[1]	15.6[1]
EV public chargers [count]	7	14	31
Heat pumps [%]	16	24[1]	100[1]
Max Peak Import [kW]	186	237	536
Max Peak Export [kW]	126	174	301
Av. Summer Peak Export [kW]	60	87	152

[1] Rates determined by the Stedin Energietransitie Impact Assessment Model (SETIAM).

The remainder of this section zooms in on the profiles of the distributed assets (PV, EV charging, and HPs), which together determine the evolution of the test grid for 2023, 2030 and 2050.

3.2.1. Electric Vehicle Charging Points

The EV charging points consist of both public and private charging profiles (for distribution over the feeders see Table 3.4, 3.5, 3.6), reflecting real neighborhood conditions. Public charging profiles are generated using the Charging Profile Generator developed by ElaadNL, a tool widely used by municipalities, provinces, and grid operators to support the roll out of EV charging infrastructure under the National Charging Infrastructure Agenda. This tool estimates the load resulting from EV charging [49].

For public charging points, dual-socket chargers are assumed, with an available power of 11 kW per socket, resulting in 17.25 kW per charging point. The datasets for 2023, 2030, and 2050 represent forecast charging demand under non-dynamic conditions and are provided with a 15-minute resolution. Dynamic prices were excluded to isolate the congestion-mitigating effect of the energy hub, since flexibility markets are themselves a congestion-mitigation strategy. Moreover, assessing the energy hub without price incentives first clarifies to what extent households can become less dependent on external electricity prices

Private charging profiles are based on real-world data from the GO-e project [14] (2018). Although the data originates from 2018, it is assumed to remain representative for the 2023, 2030, and 2050 horizons due to the lack of more recent measurements. These profiles capture typical home-charging behavior, often occurring in the evening and with less overlap in usage compared to public charging. The private charging time series are also provided at 15-minute resolution and scaled to reflect the projected EV adoption for 2030 and 2050 (Table 3.2).

A visual comparison of representative private and public EV charging patterns is shown in Figure 3.3, highlighting differences in timing and peak power demand between both charging types.

3.2.2. Heat Pumps

As gas heating is phasing out in the Netherlands, described in section 2.1.2, electric HPs are evolving as the primary technology for residential heating. This study models an all-electric air-source heat pump (ASHP), the most widely adopted type in the Netherlands, with a market share of 76% [39].

Each ASHP supplies both space heating and domestic hot water (DHW). DHW demand is based on household profiles generated using the open-source model *pySIMDEUM* [41], which produces realistic 15-minute time-resolution hot water usage patterns derived from Dutch statistical data. These are distributed across single-person, two-person, and family households according to national demographics.

Both the DHW and space heating demands are processed by an adapted version of the thermal model developed by None [39], which simulates the building's heat losses (through conduction, infiltration, and ventilation), thermal mass, and indoor temperature control. Outdoor temperature data from KNMI is used as input. The ASHP responds to a setpoint of 20 °C and dynamically adjusts its coefficient of

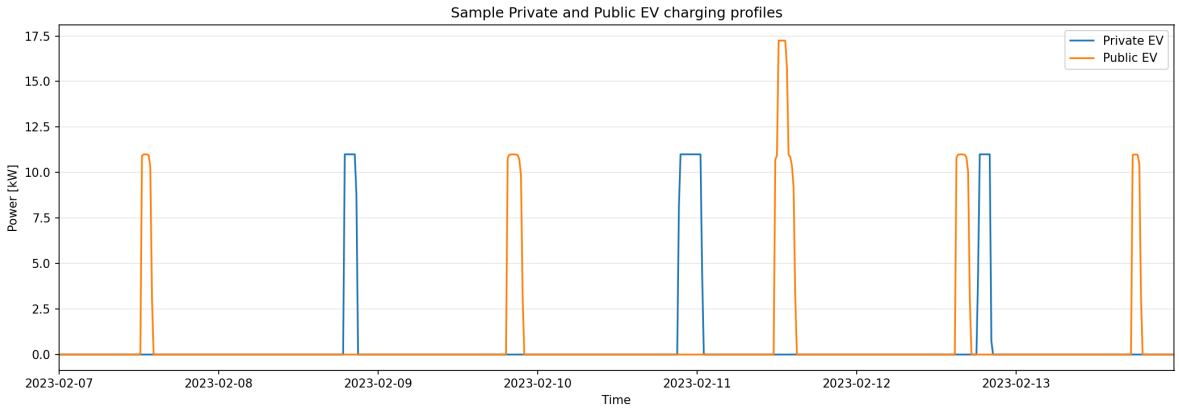

Figure 3.3: Sample 15-minute resolution power profiles for private and public EV charging. Public chargers show higher and more uniform peak loads, while private charging happens at different times and is less likely to occur all at once compared to public charging.

performance (COP) depending on outdoor conditions.

The resulting 15-minute electrical consumption profiles for all 155 households are used for the grid impact assessment. A sample power profile of one ASHP is shown in Figure 3.4, illustrating its characteristic cycling behavior over a winter week. A complete description of the thermal model is provided in Appendix 7.2.

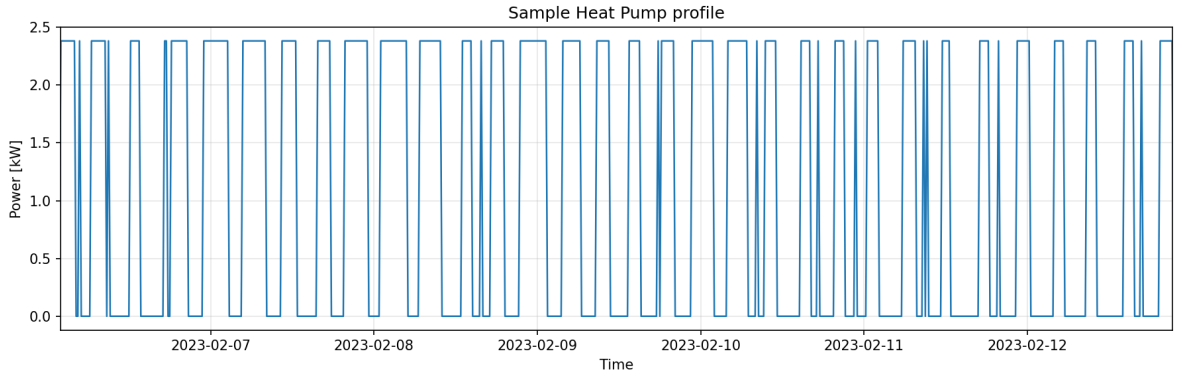

Figure 3.4: Sample 15-minute resolution power profile of a single air-source heat pump (ASHP) over a winter week in 2023, illustrating typical on/off cycling behavior in response to heating demand.

3.2.3. PV Panels

For the rooftop PV panels, it is assumed that all panels are oriented towards the south, as this orientation provides the highest annual solar energy yield. An east–west orientation could also be applied, allowing panels to be placed closer together without shading each other. However, since the PV model in section 3.4.3 used in this study does not account for shading effects, a south-facing orientation was selected.

An additional advantage of an east–west configuration is that it distributes the energy production more evenly throughout the day, with peaks in the morning and afternoon rather than a single midday maximum. Although this results in a lower total annual energy yield, it provides a flatter generation profile. In contrast, the purpose of the energy hub in this study is to store excess solar energy for use at desired moments; therefore, maximizing the total yearly production is preferred over a temporally balanced output.

Furthermore, an optimal tilt angle of 35° is assumed for all rooftop panels. This value represents a typical optimal angle for the Netherlands and simplifies the modeling process. In practice roof tilts generally vary between 15° and 55°, depending on building geometry and roof design [7].

The installed PV capacity per household category is scaled to annual electricity demand, taking into account that lower-consumption households (e.g., 1-person households) typically also have less available roof area than higher-consumption households such as 5-person households. The peak power of a single PV module is set to 440 Wp, consistent with the panels used in the 24/7 Energy Hub project.

To account for non-ideal conditions such as suboptimal orientation, shading, and system losses, a performance factor of 0.85 is applied. The required number of panelsN_{panels} is then calculated as follows [67]:

$$N_{\text{panels}} = \frac{E_{\text{annual}}}{\eta_{\text{loss}} \cdot P_{\text{panel}}}, \tag{3.1}$$

where E_{annual} is the annual household electricity consumption in kWh, $\eta_{\text{loss}} = 0.85$ is the system efficiency factor, and $P_{\text{panel}} = 0.44$ kW_p is the rated peak power of a single PV module.

Table 3.3 summarizes the estimated PV system sizing per household category. Smaller households are assigned fewer panels, while larger households have greater installed PV capacity due to higher energy demand.

Table 3.3: Estimated PV sizing per household consumption category; amount of panels and the installed capacity (assumes 440 Wp modules).

Annual consumption (kWh)	Required PV capacity (Wp)	Panels (rounded)	Installed capacity (Wp)
1,500	1,765	4	1,760
2,500	2,941	7	3,080
3,500	4,118	9	3,960
4,000	4,706	11	4,840
4,500	5,294	12	5,280

Figure 3.5 shows the corresponding per-household PV generation profiles on a clear summer day (June 21), where the impact of system size on peak generation becomes evident. These profiles form the basis for assessing realistic generation potential and grid injection patterns in later sections.

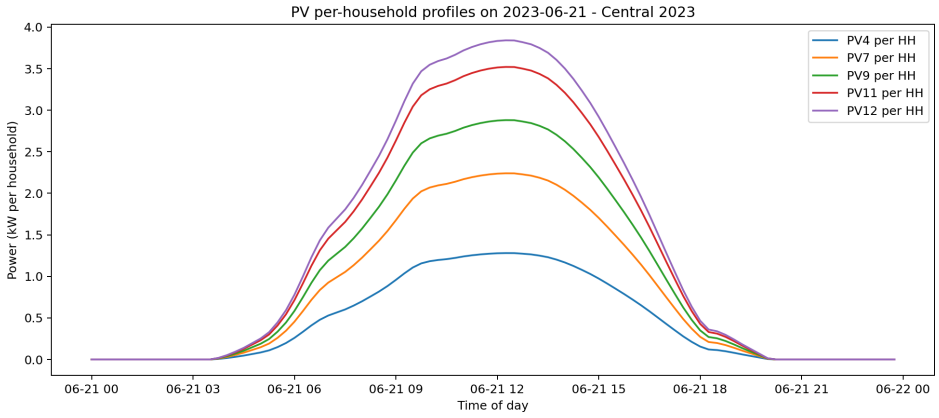

Figure 3.5: Simulated PV generation profiles per household on June 21, 2023, for different system sizes. Larger households show higher midday peaks due to greater installed capacity (HH=Household).

Table 3.4: Distribution of PV systems, EV chargers and heat pumps across household consumption categories and feeders in 2023.

	Feeder 1			Feeder 2			Feeder 3			Feeder 4			Feeder 5		
Annual consumption (kWh)	**PV**	**EV**	**HP**	**PV**	**EV**	**HP**	**PV**	**EV**	**HP**	**PV**	**EV**	**HP**	**PV**	**EV**	**HP**
1,500	2	0	0	3	0	0	2	0	0	2	0	0	0	0	0
2,500	1	0	0	2	0	0	3	0	0	1	0	0	1	0	0
3,500	2	2	5	1	0	0	2	0	0	2	0	0	1	0	0
4,000	3	0	1	3	0	0	3	0	1	2	0	0	4	1	1
4,500	2	0	1	1	0	0	1	0	0	1	0	0	3	0	0
Totals (by feeder)	**10**	**2**	**7**	**10**	**0**	**0**	**11**	**0**	**1**	**8**	**0**	**0**	**9**	**1**	**1**
Public EV chargers		**2**			**2**			**2**			**2**			**3**	

Table 3.5: Distribution of PV systems, EV chargers and heat pumps across household consumption categories and feeders in 2030.

	Feeder 1			Feeder 2			Feeder 3			Feeder 4			Feeder 5		
Annual consumption (kWh)	**PV**	**EV**	**HP**	**PV**	**EV**	**HP**	**PV**	**EV**	**HP**	**PV**	**EV**	**HP**	**PV**	**EV**	**HP**
1,500	4	0	1	3	0	4	4	0	0	4	0	0	5	0	0
2,500	3	0	5	3	0	1	3	0	4	2	0	3	6	0	8
3,500	3	0	0	2	0	0	2	0	3	2	0	0	3	0	0
4,000	3	2	0	2	0	2	3	2	0	3	1	2	3	1	0
4,500	2	1	1	1	0	0	1	0	0	1	0	1	2	2	2
Totals (by feeder)	**15**	**3**	**7**	**11**	**0**	**7**	**13**	**2**	**7**	**12**	**1**	**6**	**19**	**3**	**10**
Public EV chargers		**4**			**2**			**2**			**4**			**4**	

Table 3.6: Distribution of PV systems, EV chargers and heat pumps across household consumption categories and feeders in 2050.

	Feeder 1			Feeder 2			Feeder 3			Feeder 4			Feeder 5		
Annual consumption (kWh)	**PV**	**EV**	**HP**	**PV**	**EV**	**HP**	**PV**	**EV**	**HP**	**PV**	**EV**	**HP**	**PV**	**EV**	**HP**
1,500	9	0	14	9	0	9	8	0	9	11	0	11	13	0	17
2,500	10	0	11	5	0	7	6	0	7	7	0	9	12	0	16
3,500	3	0	4	2	0	2	2	0	2	3	0	4	6	0	7
4,000	4	4	4	3	3	3	3	3	3	3	2	3	5	5	5
4,500	2	2	2	1	1	1	1	1	1	1	1	1	3	2	3
Totals (by feeder)	**28**	**6**	**35**	**20**	**4**	**22**	**20**	**4**	**22**	**25**	**3**	**28**	**39**	**7**	**48**
Public EV chargers		**8**			**5**			**5**			**5**			**8**	

3.3. Energy Hub Scenarios & Configurations

This aim of this section is to outline how multiple energy hub scenarios and configurations are developed and implemented in the LV grid case study to evaluate the feasibility and performance of the energy hub concept under the 2050 time horizon. The scenario framework is built in two steps: (i) conceptual development of the scenarios (section 3.3.1) and (ii) component dimensioning for scenario configurations (section 7.8.2). The first step defines the **energy hub scenarios**, while the second states the **energy hub configurations**. Section 3.3.3 concludes by introducing the KPIs used for evaluation.

3.3.1. Conceptual Development of Scenarios

Figure 3.6 illustrates the conceptual process used to define technically viable and operationally flexible energy hub scenarios. The starting point was the autonomous 24/7 Energy Hub operated at The Green Village, which aims for minimum grid reliance by using battery and hydrogen storage to balance local electricity generation and demand.

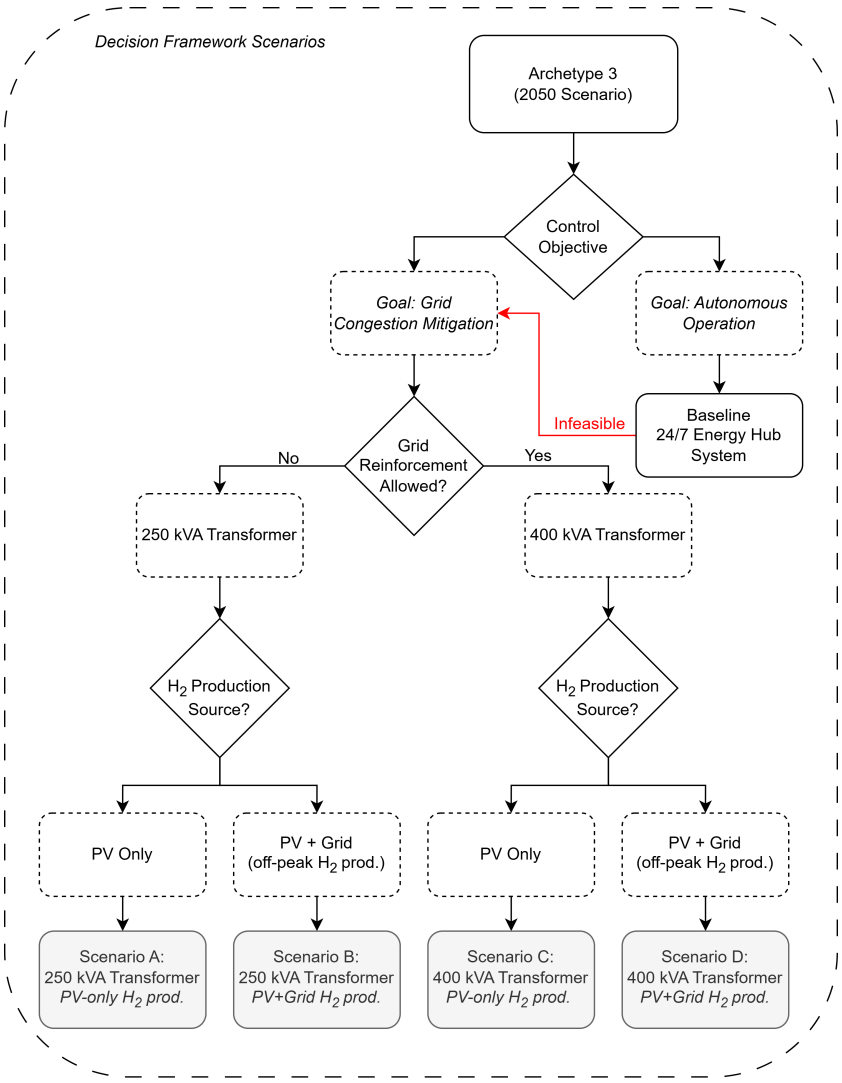

Figure 3.6: Decision-making framework for defining energy hub scenarios.

To test whether this concept could scale to a full neighborhood, the original control logic and sizing philosophy is initially applied without modification under 2050 conditions as a reference point. As reflected by the red *"infeasible"* branch in Figure 3.6, this screening step showed that a fully autonomous configuration is not feasible, which is described later in section 4.3. The autonomous assessment revealed two key barriers to large-scale deployment: (i) disproportionate fuel cell over dimensioning to indepen-

dently serve all winter peak demand, and (ii) persistent negative hydrogen balance when hydrogen production is limited to PV surplus.

This motivates a shift toward the grid-oriented interpretation of the energy hub, which is the focus of this thesis. Instead of targeting full autonomy, the energy hub is used for congestion mitigation by operating the fuel cell only when neighborhood demand exceeds the transformer rating. Two additional design factors were introduced to systematically explore feasibility:

1. **Transformer rating:** 250 kVA (existing) vs. 400 kVA (moderate reinforcement), allowing comparison between operation under current LV transformer limits and under expanded capacity.
2. **Hydrogen sourcing strategy:** PV-only vs. PV + grid summer production. Two EMS control variants were implemented across the scenarios regarding the **hydrogen sourcing strategy**. Figures 3.7 and 3.8 provide a visual representation of the EMS logic implemented in the model.
    - **PV-only control (Scenarios A & C):** Summer electrolyzer operation is triggered exclusively by PV surplus; the fuel cell activates only when SOC < 25 % and net demand exceeds transformer capacity (Figure 3.7).
    - **PV + grid control (Scenarios B & D):** The electrolyzer uses PV and grid electricity during low-load summer hours if SOC < 90 % and transformer headroom is available. Fuel cell behavior is similar to the PV-only control (Figure 3.8).

Combining these factors yields four scenarios shown in Table 3.7

These scenarios enable a controlled comparison of how reinforcement level and hydrogen sourcing influence congestion mitigation performance.

Table 3.7: Overview of energy hub scenarios

Scenario	Transformer capacity	Hydrogen production strategy
A	250 kVA	PV-only
B	250 kVA	PV + grid
C	400 kVA	PV-only
D	400 kVA	PV + grid

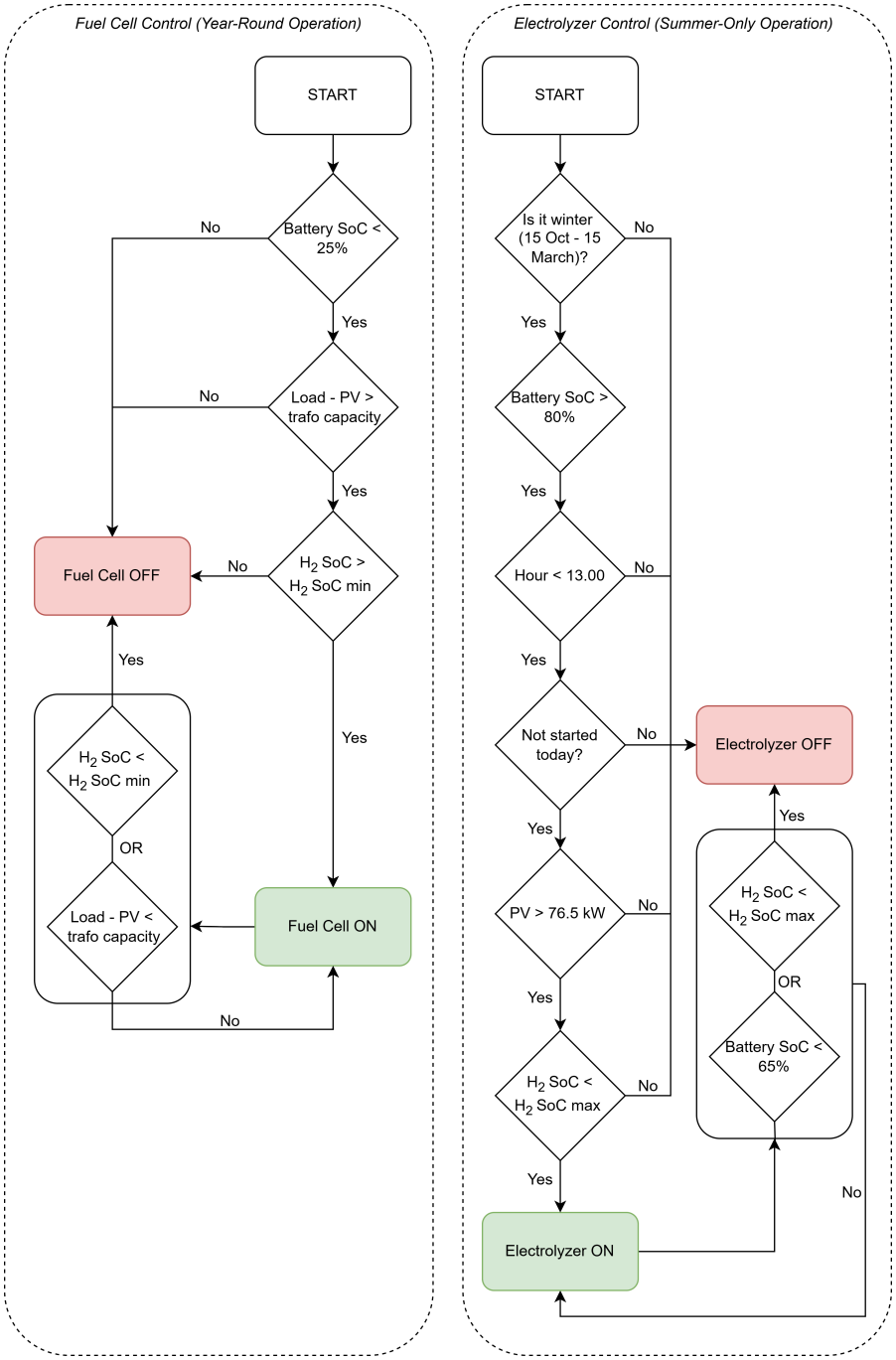

Figure 3.7: Control flowchart for PV-only operation (Scenario A & C): electrolyzer runs exclusively on PV surplus during summer; fuel cell activates only when SOC is low and transformer limits are exceeded.

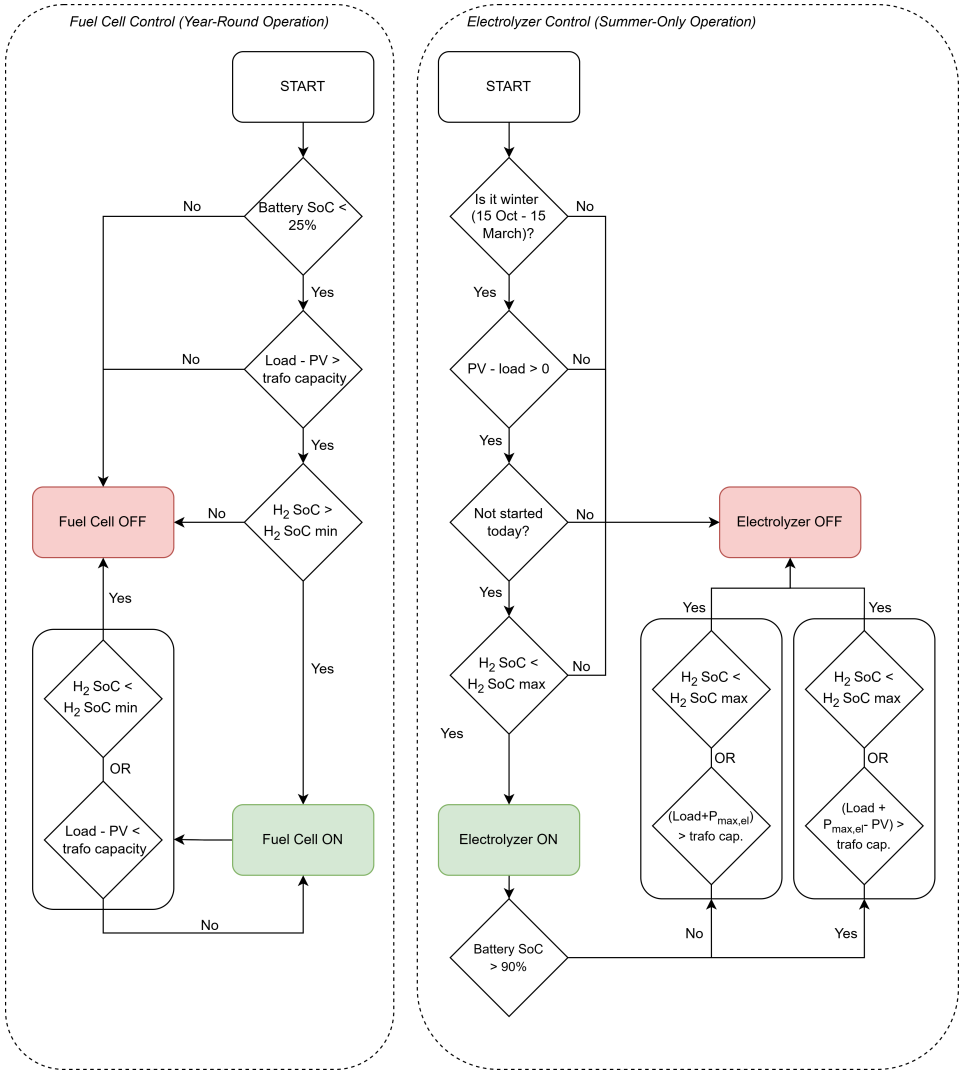

Figure 3.8: Control flowchart for PV+Grid operation (Scenario B & D): electrolyzer prioritizes PV but may additionally use grid electricity during low-load summer hours; fuel cell activation logic remains unchanged.

3.3.2. Component Dimensioning for Scenario Configurations

For every scenario, the battery, electrolyzer and fuel cell sizes are systematically varied to assess the trade-off between congestion mitigation and system costs. Table 3.8 summarizes the design logic and variation ranges.

The **battery capacity** is tested across five levels (400-2,000 kWh). Capacity is assigned per household as 5 kWh for 1,500 kWh/year, 10 kWh for 2,500-3,500 kWh/year and 15 kWh for 4,000-4,500 kWh/year, consistent with standard residential battery systems [62]. Summed over all PV-equipped households, this results in a **base-case capacity of 1200 kWh**.

The **fuel cell** is sized to shave import peaks exceeding the transformer rating. For the 250 kVA transformer, this requires a stack power of 420 kW, while the 400 kVA case results in 200 kW (stack-efficiency of 68.8%). Each over four (under sized) levels:

- **250 kVA (A & B):** 100, 200, 300, 420 kW
- **400 kVA (C & D):** 50, 100, 150, 200 kW

The **electrolyzer** size depends on the hydrogen sourcing strategy. In PV-only scenarios (A & C), sizing is based on available, average and max daily summer surplus, which differs from **150 kW (av.) to 300 kW (max.)**. For grid-assisted configurations (B & D), the range varies up to the full transformer headroom: **250 kW** (250 kVA) and **400 kW** (400 kVA), respectively.

Each scenario consists of **80 configurations**, resulting in a total of **320 configurations** across all four scenarios. Table 3.8 summarizes the logic and ranges.

Table 3.8: Sizing parameters for grid-oriented energy hub configurations

Component	Design Logic	Base	Under- and Oversize Range	Variants
Battery capacity	Energy buffer	1200 kWh	400, 800, 1,200, 1,600, 2,000 kWh	5
Fuel cell (250 kVA, **Scen. A & B**)	Peak shaving	420 kW	100, 200, 300, 420 kW	4
Fuel cell (400 kVA, **Scen. C & D**)	Peak shaving	200 kW	50, 100, 150, 200 kW	4
Electrolyzer (PV-only **Scen. A & C**)	Summer PV surplus	150 kW	50, 100, 150, 300 kW	4
Electrolyzer (Grid+PV, **Scen. B**)	250 kVA headroom	250 kW	100, 150, 200, 250 kW	4
Electrolyzer (Grid+PV, **Scen. D**)	400 kVA headroom	400 kW	100, 200, 300, 400 kW	4
			Total configurations per scenario:	**80**
			Total across all scenarios:	**320**

Figure 3.9 shows an overview of the case study evaluated across different time horizons, where the 2050 horizon is analyzed through multiple energy hub scenarios, each consisting of different configurations.

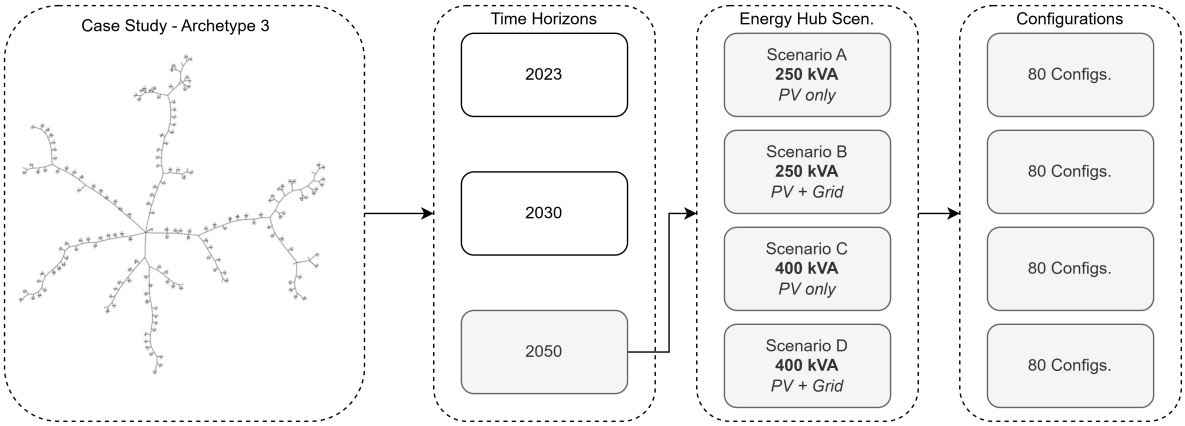

Figure 3.9: Overview of the different layers in the case study: Archetype 3 → Time horizons → energy hub scenarios → 80 configurations per scenario

3.3.3. Key Performance Indicators

As derived in section 2.3.3 from stakeholder considerations, the following KPIs serve to evaluate the system's technical feasibility and economic viability:

- **Transformer Violations:** A hard constraint, any configuration that results in import or export violations is deemed infeasible and excluded from further analysis.
- **Net Hydrogen Balance:** The difference between annual hydrogen production and consumption. A negative balance implies reliance on external hydrogen supply and is thus considered infeasible for autonomous operation.
- **Total System Cost:** The sum of CAPEX and annual OPEX for all energy hub components. While this study assumes the energy hub is a public infrastructure investment (not resident-owned), cost efficiency remains a priority for municipalities and DSOs. Cost components are detailed in Table 3.9.

Table 3.9: energy hub [5] and Grid Connection; Capital and Operational Expenditure

Component	CAPEX	OPEX
Energy Hub Components		
Battery Storage	150 €/kWh	5 €/kWh/year
Electrolyzer	700 €/kW	20 €/kW/year
Hydrogen Storage	500 €/kg H_2	1 €/kg H_2/year
Fuel Cell	1,000 €/kW	30 €/kW/year
Grid Connection		
Transformer Connection	34,002 € (one-time)	1,455,500 €/year

The configuration assessment follows a three-stage process aligned with the research objective of mitigating transformer congestion through the 24/7 Energy Hub. Starting from 320 technically possible system configurations (4 scenarios × 80 component combinations each), constraints were applied sequentially based on the KPIs. This filtering process consists of a feasibility screening followed by a cost-optimization step, as shown in Figure 3.10. The feasibility screening includes two stages: technical feasibility and energy feasibility, which are explained below. The final stage applies cost-optimization to identify the most economically attractive configurations.

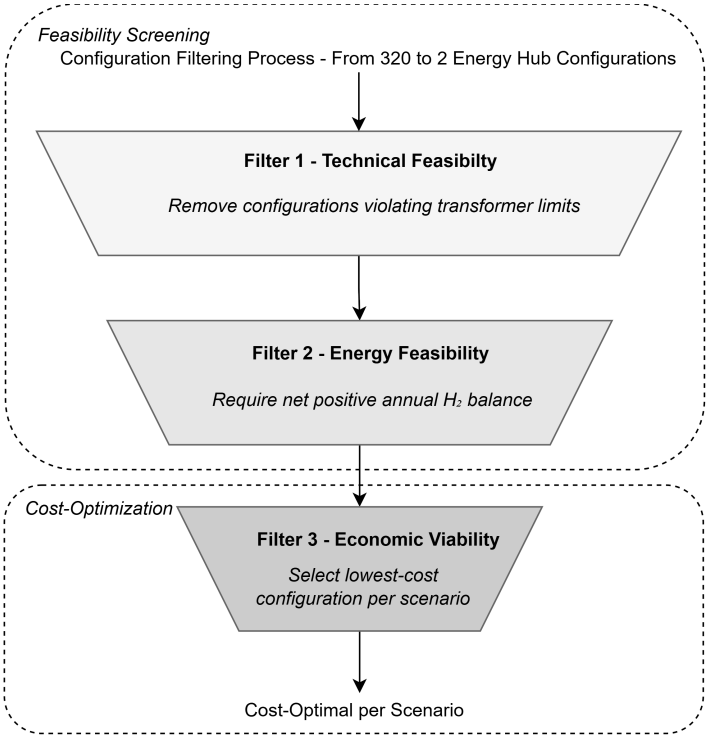

Figure 3.10: Configuration Filtering Process consisting of a Feasibility Screening and Cost-Optimization: From 320 Simulations to Cost-Optimal energy hub Configurations.

The first requirement is the elimination of **transformer violations** (technical). Any configuration exhibiting annual import or export limit violations is considered infeasible, as such behavior undermines the objective of mitigating grid congestion.

The second feasibility condition concerns the **net hydrogen balance** (energy). A configuration that consumes more hydrogen than it produces over a year would require external hydrogen supply and therefore cannot provide seasonal balancing.

Finally, this screening forms the foundation for the **cost-based** selection of the optimal configuration. From each scenario, the lowest-cost configuration was selected based on the CAPEX and OPEX values in Table 3.9. For each scenario, the single lowest-cost configuration was selected, so that trade-offs between scenarios can be made.

3.4. Simulation Models

The final phase of the methodology describes the development of the energy hub model, which will be deployed on the test grid. It replicates the real-life 24/7 Energy Hub setup, connected to a single household. **The goal of this approach, is to have a validated model to implement in the test grid.** The tool that is used is the Illuminator [23], which is a flexible simulation tool that lets users model and test how different energy technologies work together in real-world systems. The Illuminator uses Mosaik [56], which is a flexible Smart Grid co-simulation framework, with the eventual goal of simulating multiple large scale grid scenarios.

Each model in the Illuminator exists of a standard structure. First of all *Parameters* are defined, which are fixed configuration values set at initialization. Then *Inputs* which are dynamic values received from other models within the scenario. *States*, which are internal variables that persist between simulation steps, it can also be an input for other models within the scenario. Finally, the *Outputs*, the calculated values during the timestep, that form inputs again for the other models. The models and their connections are configured through a YAML file that defines each simulation's scenario. A visual representation of two models and their connections is shown in Figure 3.11.

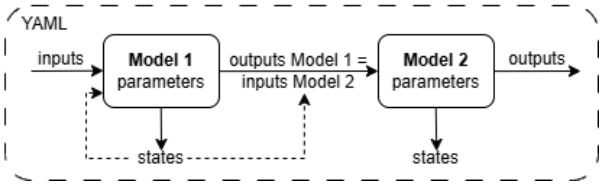

Figure 3.11: Example of model interaction in the Illuminator framework, showing how parameters, inputs, states, and outputs are defined and exchanged between models. The dashed arrows represent the mapping of states into input definitions.

3.4.1. System Architecture

The system consists of nine interconnected models that collectively manage generation, storage, and distribution shown in Table 3.10. All models are defined and connected through a YAML configuration file, the full system is illustrated in Figure 3.23, and more thoroughly explained in the following sections. While this chapter provides a concise overview of the model development, the complete implementation is detailed in the Appendix 7.3, Figure 7.2.

Data exchange between components occurs at each simulation timestep, with the YAML configuration file defining the connection topology. Each scenario corresponds to a YAML file. Different configurations are generated by changing the combinations of relevant model parameters. An overview of the 24/7 Energy Hub was earlier shown in Figure 2.4.

Model	Description
Load Profile (section 3.4.2)	Simulates electrical demand profiles
PV System (section 3.4.3)	Calculates solar power generation
Battery Storage System (section 3.4.4)	Models electrochemical energy storage
Controller (EMS) (section 3.4.5)	Implements the energy management strategy
Electrolyzer (section 3.4.6)	Simulates hydrogen production
Compressor (section 3.4.7)	Models hydrogen compression
Hydrogen Storage (section 3.4.8)	Tracks compressed hydrogen inventory
Fuel Cell (section 3.4.9)	Simulates hydrogen-to-electricity conversion
Grid Connection (section 3.4.10)	Manages grid interaction

Table 3.10: Overview of the nine interconnected models that form the system architecture, including generation, storage, control, and grid interaction components.

3.4.2. Load Profile

The load model evaluates the electrical demand. It is receiving the data from 15-minute interval time-series data, stored in CSV format, that specify the AC electric load demand. The output is AC power in kW, schematically shown in Figure 3.12.

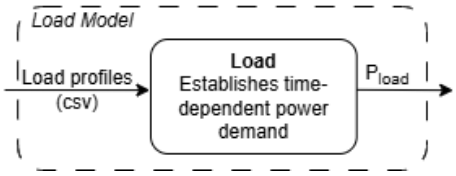

Figure 3.12: Schematic of the Load Model converting CSV demand profiles into simulation time-dependent AC power output P_{load}.

3.4.3. PV System

The PV system represents how solar panels convert solar radiation into electrical energy under varying environmental conditions. It provides a simplified implementation inspired by the Sandia PV Array Performance Model (SAPM) [34]. The model determines the AC electrical output of the PV array based on incident irradiance, temperature & wind effects, and system characteristics, while accounting for orientation and efficiency.

Data required for the simulation, *global, diffuse, and direct irradiance, ambient temperature, and wind speed*, are retrieved from the Open-Meteo API [10]. These data are based on ECMWF (European Centre for Medium-Range Weather Forecasts) reanalysis at 9 km resolution, incorporating satellite, ground station, and radar observations. The model used coordinates from The Green Village (latitude 52.00, longitude 4.38). Solar position parameters (azimuth A_z and elevation h_s) are obtained using the `pvlib` library from Sandia, based on the same location and time inputs. All data is provided to the model through a CSV reader.

Irradiance on the Tilted Plane

The model first determines the Global Tilted Irradiance (GTI) of the PV panel, which is the sum of direct, diffuse, and reflected components:

$$GTI = G_{\text{dir}} + G_{\text{diff}} + G_{\text{ref}}, \tag{3.2}$$

Where the direct beam irradiance is computed using the cosine of the angle of incidence γ:

$$G_{\text{dir}} = G_{\text{Bn}} \cdot \cos\gamma, \tag{3.3}$$

The angle of incidence depends on both solar geometry and panel orientation, and is expressed as:

$$\cos\gamma = \cos(90^\circ - \theta)\cos(h_s)\cos(\alpha - A_z) + \sin(90^\circ - \theta)\sin(h_s), \tag{3.4}$$

where θ [°] is the module tilt angle, measured from the horizontal plane, and α [°] is the module azimuth angle, measured clockwise from north.

The diffuse component represents scattered radiation from the sky and is proportional to the sky view factor (SVF), which defines the fraction of visible sky:

$$\text{SVF} = \frac{1 + \cos(\theta)}{2}, \tag{3.5}$$

Using the isotropic sky model, the diffuse irradiance G_{diff} is then given by:

$$G_{\text{diff}} = \text{SVF} \cdot G_{\text{Dh}}, \tag{3.6}$$

Reflected irradiance G_{ref} from the ground is estimated assuming a constant albedo $\rho = 0.2$, typical for built environments:

$$G_{\text{ref}} = \rho \cdot (1 - \text{SVF}) \cdot G_{\text{Gh}}, \tag{3.7}$$

Temperature Effects and Efficiency
PV module performance decreases with rising temperature. The module temperature T_m is estimated using the Nominal Operating Cell Temperature (NOCT) method [37]:

$$T_m = T_a + \frac{GTI}{G_{\text{NOCT}}} \cdot (\text{NOCT} - 20) \cdot \left(\frac{9.5}{5.7 + 3.8FF}\right) \cdot \left(1 - \frac{\eta_{\text{STC}}}{0.9}\right), \tag{3.8}$$

Here, η_{STC} is the efficiency at standard test conditions, and FF is the wind speed.

The temperature-corrected efficiency η is computed following the SAPM [46]:

$$\eta = \eta_{\text{STC}} \cdot [1 + 0.0031 \cdot (T_m - 25)], \tag{3.9}$$

Electrical Output
The AC P_{AC} power output of the system is calculated as:

$$P_{\text{AC}} = \eta \cdot C \cdot \eta_{\text{inv}} \cdot \eta_{\text{MPPT}} \cdot \eta_{\text{loss}}, \tag{3.10}$$

where C is the installed PV capacity in kW, $\eta_{\text{inv}} = 0.96$ is the inverter efficiency, $\eta_{\text{MPPT}} = 0.99$ is the Maximum Power Point Tracking (MPPT) efficiency, and $\eta_{\text{loss}} = 0.97$ accounts for additional system losses.

Figure 3.13 provides an overview of the PV model, illustrating the relationship between irradiance, temperature, and power output.

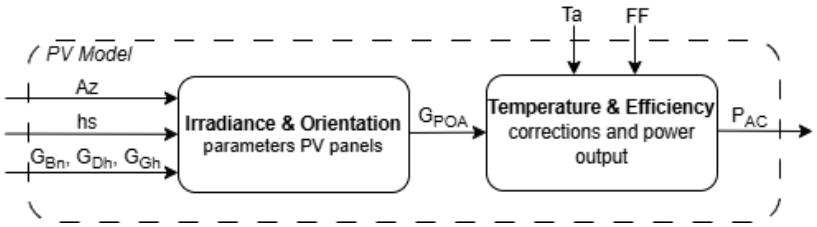

Figure 3.13: Overview of the PV system model showing irradiance, orientation, temperature, and efficiency interactions.

3.4.4. Battery Storage System

The battery model represents an electrochemical energy storage system that dynamically balances power flows between generation and demand. It charges when excess PV power is available and discharges when local demand exceeds generation, maintaining operation within predefined limits of power and battery SOC (SOC_{bat}). The model also includes conversion and inverter losses to reflect real-world round-trip efficiencies.

The system exchanges power with the PV system, load, electrolyzer, compressor and fuel cell. The resulting power imbalance P_{flow2b} determines whether the battery charges or discharges:

$$P_{\text{bat}} = (P_{\text{load}} + P_{\text{flow2e}} + P_{\text{comp}}) - (P_{\text{PV}} + P_{\text{FC}}), \tag{3.11}$$

When $P_{\text{bat}} > 0$, the battery discharges to supply power to the system. When $P_{\text{bat}} < 0$, it absorbs surplus power by charging. These operations are constrained by power limits and SOC_{bat} boundaries, defined by the minimum and maximum allowed charge levels.

State of Charge Dynamics
The SOC_{bat} evolves at each timestep Δt according to the power exchanged and the respective charging or discharging efficiencies. During discharging ($P_{\text{bat}} > 0$ and $SOC_{\text{bat}} \geq SOC_{\text{bat,min}}$), the power output P_{flow2b} is limited by both maximum discharge rate and available stored energy:

$$P_{\text{flow2b}} = \min\left(P_{\text{bat}}, P_{\max}, \frac{(SOC_{\text{bat}} - SOC_{\text{bat,min}}) \cdot E_{\max}}{\Delta t \cdot \eta_{\text{dis}} \cdot \eta_{\text{inv,dis}} \cdot 100\%}\right), \tag{3.12}$$

$$SOC_{\text{bat}} = SOC_{\text{bat}} - \frac{P_{\text{flow2b}} \cdot \Delta t}{E_{\max} \cdot \eta_{\text{dis}} \cdot \eta_{\text{inv,dis}}} \cdot 100\%, \tag{3.13}$$

Similarly, during charging ($P_{\text{bat}} < 0$ and $SOC_{\text{bat}} \leq SOC_{\text{bat,max}}$), the model ensures that energy input does not exceed capacity constraints:

$$P_{\text{flow2b}} = \max\left(P_{\text{bat}}, P_{\min}, -\frac{(SOC_{\text{bat,max}} - SOC_{\text{bat}}) \cdot E_{\max}}{\Delta t \cdot \eta_{\text{ch}} \cdot \eta_{\text{inv,ch}} \cdot 100\%}\right), \tag{3.14}$$

$$SOC_{\text{bat}} = SOC_{\text{bat}} + \frac{|P_{\text{flow2b}}| \cdot \Delta t \cdot \eta_{\text{ch}}}{E_{\max} \cdot \eta_{\text{inv,ch}}} \cdot 100\%, \tag{3.15}$$

If neither condition is met, the battery remains idle, maintaining its SOC_{bat}.

Model Parameters and Constraints
The model is defined by the nominal capacity $E_{\max}$ (kWh), the maximum and minimum power ratings $(P_{\max}, P_{\min})$, and the efficiency parameters for charging (η_{ch}) and discharging (η_{dis}), together with the corresponding inverter efficiencies $(\eta_{\text{inv,ch}}, \eta_{\text{inv,dis}})$. The allowable power is set by the selected C-rate, where $P_{\max}$ denotes the upper power limit and $P_{\min}$ is its negative counterpart. The C-rate stands for the ratio between battery power and stored capacity, which means a 1 C rate corresponds to charging or discharging the battery fully in one hour. SOC boundaries $(SOC_{\min}, SOC_{\max})$ ensure that the battery neither overcharges nor fully depletes during operation.

Output
The resulting output, P_{flow2b} in kW, represents the actual power exchanged between the battery and the rest of the system, positive during discharge and negative during charge. This value accounts for all losses and operational limits, ensuring realistic performance within the integrated energy system.

This approach is also shown in Figure 3.14.

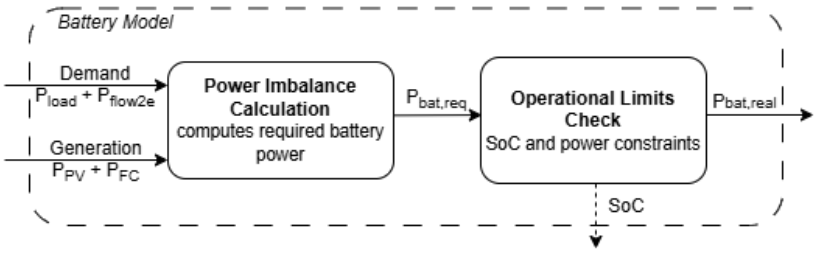

Figure 3.14: Schematic of the battery model showing power imbalance calculation and check of the battery's state of charge and power limits.

3.4.5. Controller (EMS)

Before describing the hydrogen-based subsystems in detail, the EMS is explained, which controls their operation through a rule-based control strategy. The EMS controls the electrolyzer, fuel cell, compressor, and hydrogen storage tanks. It aims to enable autonomous operation by coordinating power flows using a rule-based control strategy. This strategy is based on the SOC_{bat} and hydrogen storage, as well as seasonal solar availability.

The EMS receives: (i) available PV power $P_{\text{PV,signal}}$, (ii) SOC_{bat}, and (iii) hydrogen SOC (SOC_{H_2}). Parameters define operational thresholds, minimum and maximum SOC limits for the battery and hydrogen tank, and control triggers for the electrolyzer and fuel cell. The EMS uses simple deterministic logic for daily and seasonal operation, shown in Figure 3.15.

Electrolyzer Control The electrolyzer operates only in the summer period (March 16–October 14). It starts once per day if:

- $SOC_{\text{bat}} > SOC_{\text{bat,el,start}}$ (The electrolyzer becomes active when the SOC_{bat} exceeds 80%)
- $SOC_{\text{H}_2} < SOC_{\text{H}_2,max}$ (maximum SOC_{H_2}, which is set to 100%)

It stops if the SOC_{bat} drops below 65%, which is the $SOC_{\text{bat,el,stop}}$, or if the hydrogen tank is full.

Fuel Cell Control The fuel cell is activated under:

1. *Emergency Mode:* Activated when SOC_{bat} drops below the emergency threshold $SOC_{\text{bat,fc,emergency}}$ of 25% and hydrogen is available; the fuel cell supplies power to prevent battery depletion.
2. *Seasonal Mode:* In winter (October 15–March 15), a time-dependent trigger activates the fuel cell based on SOC_{bat} and the hour of the day (Figure 3.15a).

It deactivates when SOC_{bat} rises above the stop threshold $SOC_{\text{bat,fc,stop}}$ (e.g., 90%) or when the hydrogen storage level becomes insufficient to continue operation.

Compressor and Hydrogen Flow Control Hydrogen flow to the compressor and tanks is automatically managed according to the active operating state of the electrolyzer and fuel cell:

$$storage\_flow = \begin{cases} 1, & \text{electrolyzer active (storage)} \\ -1, & \text{fuel cell active (withdrawal)} \\ 0, & \text{idle} \end{cases} \qquad compressor = \begin{cases} 1, & \text{if } storage\_flow = 1 \\ 0, & \text{otherwise} \end{cases}$$

In summary, shown in Figure 3.16, the EMS ensures robust operation of the hybrid system without forecasting or optimization. It enables reliable and local use of renewable energy by applying fixed thresholds and seasonal constraints.

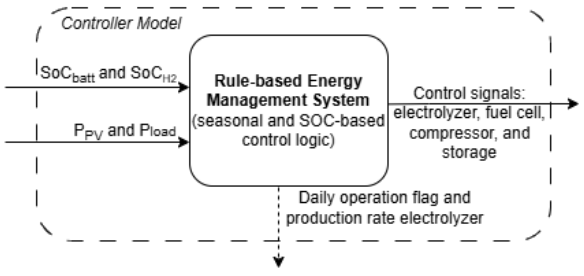

Figure 3.16: Rule-based Energy Management System (EMS) using SOC thresholds and seasonal logic to generate control signals for electrolyzer, fuel cell, compressor, and hydrogen storage.

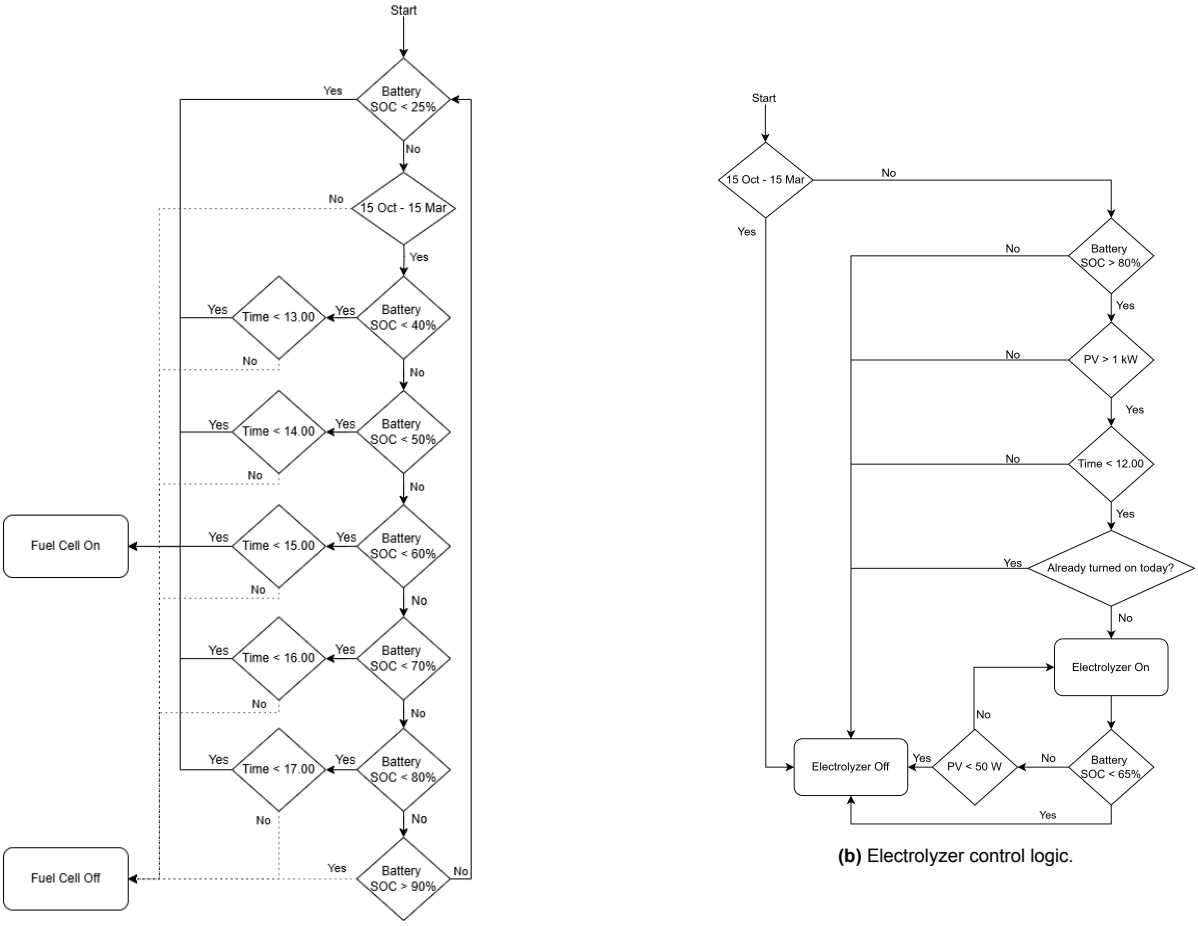

(a) Fuel cell control logic.

(b) Electrolyzer control logic.

Figure 3.15: Rule-based control logic of the Energy Management System (EMS), showing decision pathways for activating the electrolyzer and fuel cell based on time, battery state of charge, PV availability, and seasonal conditions.

3.4.6. Electrolyzer

The electrolyzer model represents the dynamic operation of an AEM electrolyzer, capturing warm-up, ramp-up, steady-state, ramp-down and hold behavior. It converts AC electrical input into hydrogen at a fixed efficiency while accounting for internal conversion and BoP losses. The model is operated through an on/off control signal derived from the controller logic described above, and a relative production rate ($r_{\text{prod}} \in [0.6, 1]$), which scales hydrogen output according to available energy.

Upon activation, the electrolyzer transitions through five sequential phases regulated by internal timers. In the *warm-up* phase, the electrolyzer draws a constant auxiliary power, about one-tenth of its nominal consumption, while no hydrogen is yet produced. Once ready, the input power *ramps-up* linearly to its nominal value P_{max} over a specified duration. In the *steady-state phase*, the consumed power P_{in} is defined as:

$$P_{\text{in}} = r_{\text{prod}} \cdot P_{\text{max}}, \tag{3.16}$$

and hydrogen generation m_{H_2} in kg per timestep is computed from the lower heating value of hydrogen (LHV_{H_2}):

$$\dot{m}_{\text{H}_2} = \frac{-P_{\text{in}} \cdot \eta_{\text{el}} \cdot \Delta t}{3600 \cdot LHV_{\text{H}_2}}, \tag{3.17}$$

where $LHV_{\text{H}_2} = 33.33$ kWh/kg. When switched off, the electrolyzer follows a controlled *ramp-down* to 60% of P_{max}, then holds this level briefly before complete shutdown, during the *hold-phase*. These sequential transitions ensure physically realistic dynamics. The phase steps are visualized in Figure 3.17.

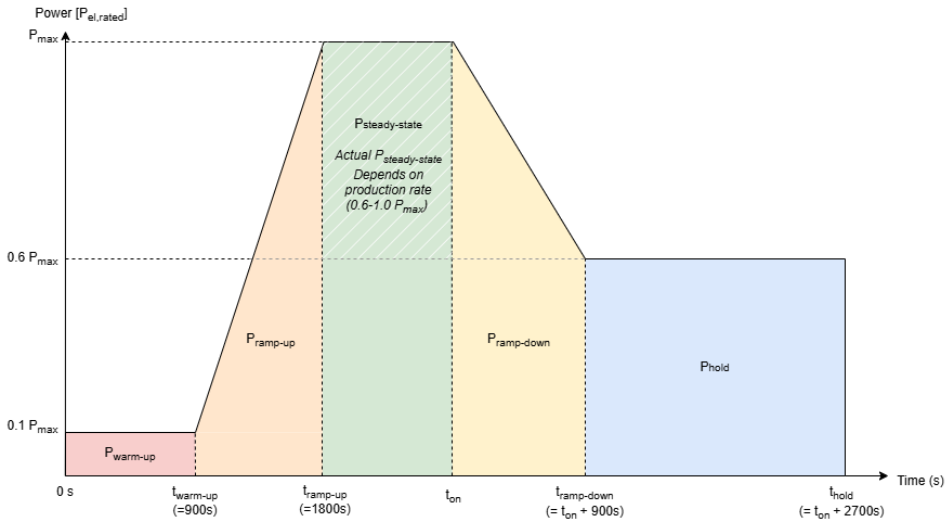

Figure 3.17: Operational profile of the electrolyzer, illustrating warm-up, ramp-up, steady-state, ramp-down, and hold phases. The actual steady-state power depends on the target production rate, ranging between 60–100% of the rated power.

The system efficiency η_{el} was derived from manufacturer test data of the 24/7 Energy Hub. An efficiency of 63.6% is applied for all production rated, representing the overall system efficiency including BoP and DC–AC conversion losses. See Appendix 7.4 for the derivation.

The model outputs the power consumption P_{max} and the hydrogen mass flow $\dot{m}_{\text{H}_2}$ directed to the compressor. Internal states track the current operating phase and manage phase transitions to maintain time-dependent behavior. Figure 3.18 illustrates this process in a simplified form.

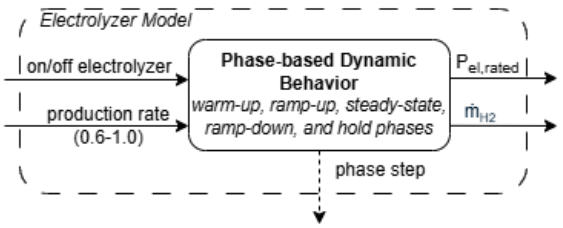

Figure 3.18: Schematic of the electrolyzer model implementing phase-based dynamic behavior, driven by on/off signals and production rate input. It outputs rated electrical power consumption and hydrogen production flow.

3.4.7. Compressor

The compressor model increases hydrogen pressure from the electrolyzer output level of $p_{\text{in}} \approx 35$ bar to $p_{\text{out}} \approx 272$ bar to enable storage. Two compression technologies are supported, *mechanical and electrochemical*, selectable via a model parameter. For the large-scale case study, *mechanical compression* is assumed due to its lower energy demand, whereas the 24/7 Energy Hub pilot relies on *electrochemical compression* consistent with the installed system. The compressor is activated whenever the electrolyzer is producing hydrogen.

Mechanical Compression (used for large-scale storage): Power demand is based on isentropic compression corrected by mechanical efficiency. Given pressure ratio $r = p_{\text{out}}/p_{\text{in}}$, heat capacity ratio $\gamma = 1.41$ for H_2, ambient temperature T, gas constant R, and molar mass M, the specific isentropic work w_{is} in J/mol is:

$$w_{\text{is}} = \frac{\gamma}{\gamma - 1} RT \left(r^{(\gamma-1)/\gamma} - 1 \right) \quad , \tag{3.18}$$

The actual work is adjusted by efficiency η_{mech}: $w_{\text{real}} = w_{\text{is}}/\eta_{\text{mech}}$. With molar flow $\dot{n} = \dot{m}_{\text{H}_2} \cdot (10^3/M)/\Delta t$, power consumption becomes:

$$P_{\text{comp}} = \frac{w_{\text{real}} \cdot \dot{n}}{10^3} \quad , \tag{3.19}$$

Electrochemical compression (used for 24/7 Energy Hub): The model uses a fixed specific energy for compression,

$$P_{\text{comp}} = \frac{\dot{m}_{\text{H}_2}^{(\text{kg/h})} \, E_{\text{spec}}}{\eta_{\text{ec}}}, \tag{3.20}$$

with E_{spec} the nominal compression energy (kWh/kg).

Figure 3.19 presents a simplified schematic of the compressor model.

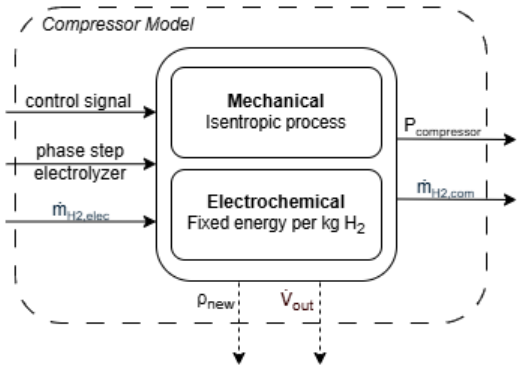

Figure 3.19: Compressor model overview. Depending on the selected mode, either a mechanical isentropic process or an electrochemical approach is used to compress hydrogen.

3.4.8. Hydrogen Storage

The hydrogen storage model represents compressed tanks that receives hydrogen from the compressor and supplies it to the fuel cell. The system tracks the hydrogen SOC_{H_2}, defined as the ratio between stored hydrogen mass and total storage capacity.

The model operates based on control signals from the controller earlier mentioned, indicating whether hydrogen should be stored (*charge*), withdrawn (*discharge*), or remain idle. At each timestep, hydrogen inflow and outflow are determined, and the tank SOC_{H_2} is updated.

The SOC_{H_2} evolves according to the signed net hydrogen mass flow per timestep $\dot{m}_{\text{H}_2}$ in kg:

$$SOC_{\text{H}_2} = SOC_{\text{H}_2} \pm \frac{\dot{m}_{\text{H}_2} \cdot \eta}{m_{\text{tot}}} \cdot 100\%, \tag{3.21}$$

where:

- $\dot{m}_{\text{H}_2} > 0$: charging (electrolyzer active), with $\eta = \eta_{\text{ch}}$
- $\dot{m}_{\text{H}_2} < 0$: discharging (fuel cell active), with $\eta = \eta_{\text{dis}}$

In idle operation, both in and out flow are zero, and the SOC_{H_2} remains constant.

A schematic overview of the hydrogen storage model is shown in Figure 3.20, summarizing the key flows and operating modes.

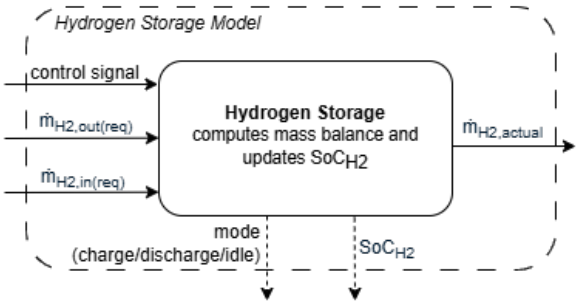

Figure 3.20: Overview of the hydrogen storage model. The system receives control signals indicating whether to charge, discharge, or remain idle, and updates the hydrogen state of charge (SOC) based on the resulting net hydrogen flow.

3.4.9. Fuel Cell System

The fuel cell system represents a low-temperature PEM fuel cell that converts stored hydrogen into electrical power. It operates under a control signal that dictates whether the unit is active or idle. When active, the model assumes steady-state operation at a fixed efficiency, converting hydrogen input to electrical output according to the $LHV_{\mathrm{H_2}}$. The dynamic ramp-up and ramp-down transitions are neglected in this implementation. This simplification is justified by the short duration of these transitions, typically a small fraction of a simulation timestep, and their negligible influence on the total "zoomed-out" operational period.

The model is a direct relation between the hydrogen input and the produced electrical power. The AC electrical output P_{FC} is determined by:

$$P_{\mathrm{FC}} = \dot{m}_{\mathrm{H_2,in}} \cdot 60 \cdot \eta_{\mathrm{FC}} \cdot \mathrm{LHV}_{\mathrm{H_2}}, \tag{3.22}$$

where η_{FC} represents the overall efficiency of the fuel cell system.

The applied efficiency accounts for all conversion stages and auxiliary components. A stack-to-grid efficiency analysis, detailed in Appendix 7.5, was conducted to quantify power output and identify losses throughout the energy conversion chain. The analysis yielded a hydrogen-to-electricity conversion efficiency of approximately 58%, and a DC-to-AC output efficiency (including BoP and conversion losses) of 68.8%. This results in a total system efficiency of 39.8%, which is used in the model to represent the effective fuel cell-to-grid conversion under standard operating conditions.

The model represents the main operating behavior of the fuel cell with a simplified, steady-state approach. It reflects the measured efficiency and power response of the real system and can be easily integrated into the hybrid energy hub (see Figure 3.21).

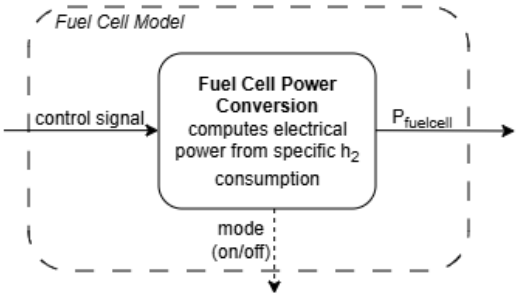

Figure 3.21: Fuel cell model representation showing control signal input, on/off operating mode, and power output computation based on hydrogen consumption.

3.4.10. Grid Connection

The grid connection model calculates the net power exchange between the energy system and the external grid. It compares total internal electricity consumption, including loads, electrolyzer, compressor,

and battery charging, with local generation from the PV system, fuel cell, and battery discharge. This balance determines whether the system imports or exports electricity. The model also evaluates grid exchange against defined power thresholds to detect potential overloads. *Ultimately, this is the key power flow used to identify potential overload conditions in the case study.*

The net grid power flow P_{grid} is given by:

$$P_{\text{grid}} = \underbrace{P_{\text{load}} + P_{\text{el}} + P_{\text{com}} + P_{\text{bat,ch}}}_{\text{Total consumption}} - \underbrace{(P_{\text{PV}} + P_{\text{FC}} + P_{\text{bat,dis}})}_{\text{Total generation}}, \tag{3.23}$$

where:

- $P_{\text{grid}} > 0$: the system imports electricity from the grid,
- $P_{\text{grid}} < 0$: the system exports surplus electricity to the grid.

If P_{grid} exceeds a specified upper or lower threshold, a warning flag is raised to indicate potential violation of grid capacity constraints.

This model provides the real-time grid interaction of the energy hub and identifies moments when grid exchange approaches or exceeds technical connection limits.

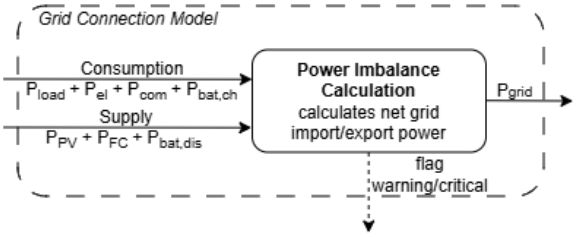

Figure 3.22: Grid connection model illustrating the calculation of net power flow between the energy hub and the external grid, raising warning flags when grid import/export exceeds predefined thresholds.

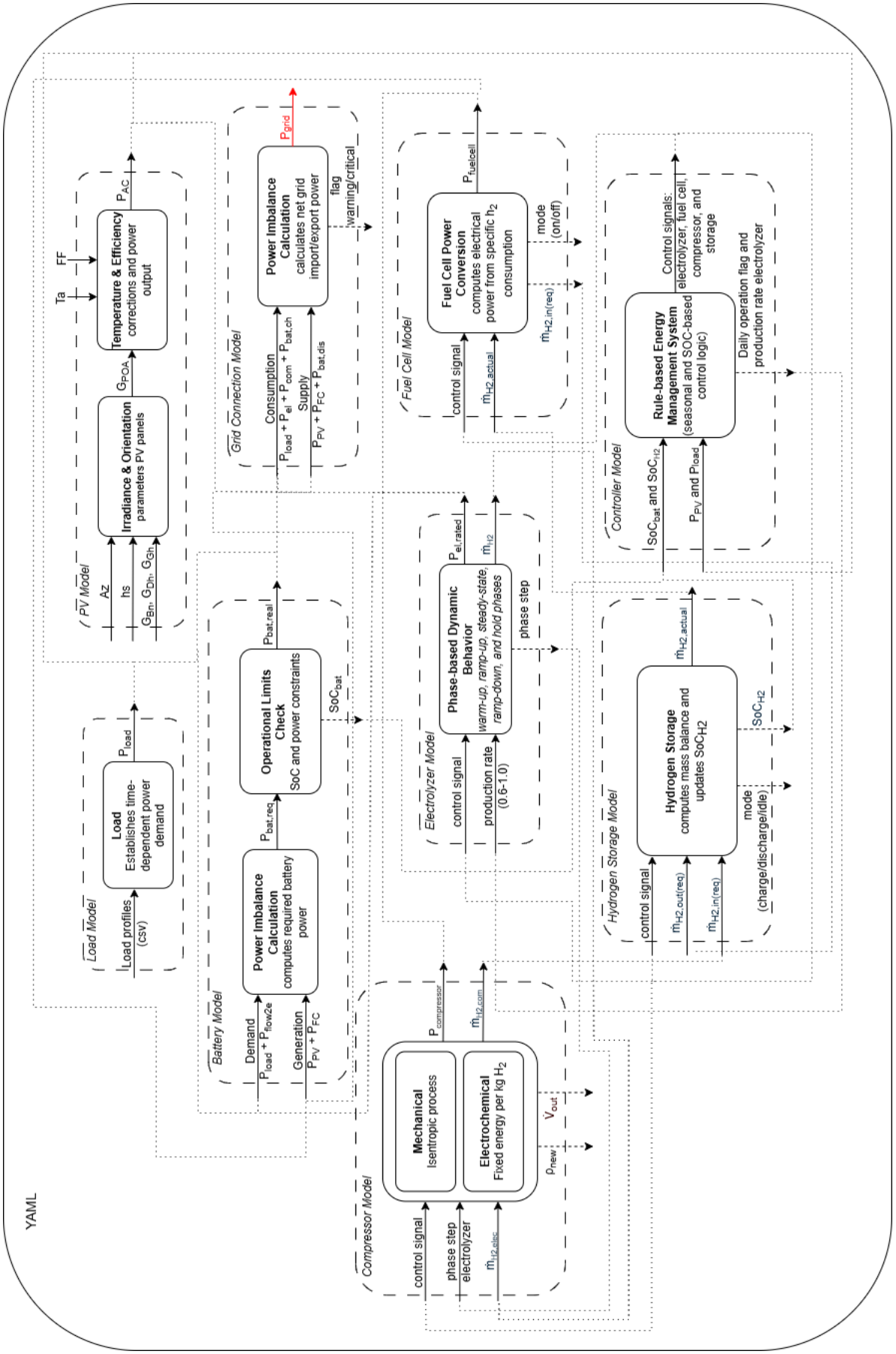

Figure 3.23: Schematic representation of the full energy hub model architecture defined through a YAML. It illustrates the interconnection of subsystem models—PV, load, battery, electrolyzer, fuel cell, compressor, hydrogen storage, controller, and grid, along with their key signals, control flows, and energy exchanges.

4

Results

This chapter presents the results derived from the methodology outlined in Chapter 3. It begins with a validation of the developed energy hub model in section 4.1, continues with the results of the baseline time horizons in section 4.2. Finally, it presents the simulation outcomes of the energy hub configurations, starting with the autonomous use case (section 4.3) as a reference and progresses to the grid-oriented configurations, whose performance is assessed against the key performance indicators in section 4.4.

4.1. Validation of the System

This section presents the validation of the developed model using measured data from the 24/7 Energy Hub at The Green Village. As these data formed the basis for the model's development, the first step of the results involves validating the 24/7 Energy Hub. This ensures the model's reliability before applying it to the test grid context.

4.1.1. PV System: From Irradiance to Power Output

The modeled GTI is compared against pyranometer measurements at the Office Lab roof (Figure 4.1a). The integrated irradiance over the five-day period results in an energy deviation of only -2.4%, meaning that the area under the modeled GTI curve is slightly lower than the measured profile. The maximum daily peak irradiance during these five days differed by merely -0.2%.

The validated GTI is passed through the PV model to compute AC output power, which is compared against 15-minute interval inverter data from the 24/7 Energy Hub (Figure 4.1b). Over the same five-day validation window, the modeled PV output differs from measured inverter energy by $+6.9\%$, and the maximum daily peak power error was $+3.0\%$. The model captures both the magnitude and timing of PV output with high fidelity. Additional validation results for two more summer weeks and one winter week are provided in the Appendix 7.6, Figure 7.3.

To ensure robustness, validation is extended beyond a single week, over 65 summer days (PV-dominant), the total active energy error is $+8.35\%$, and the daily peak power error has a mean of 10% and median of 6.0%.

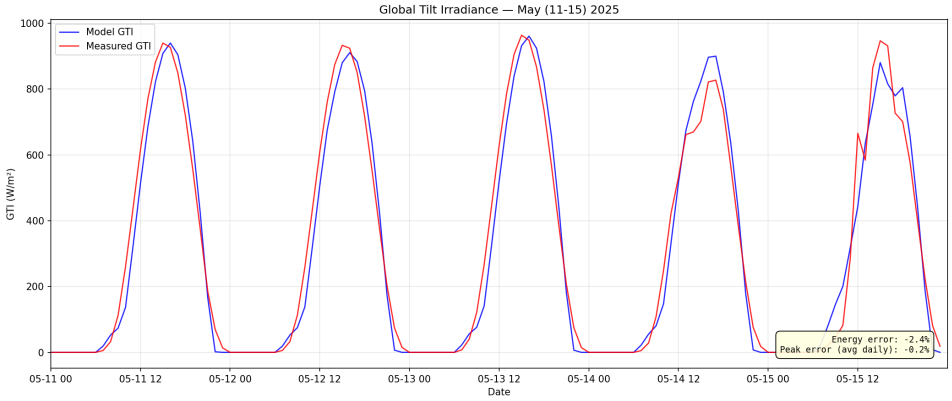

(a) Comparison of modeled and measured Global Tilted Irradiance (GTI).

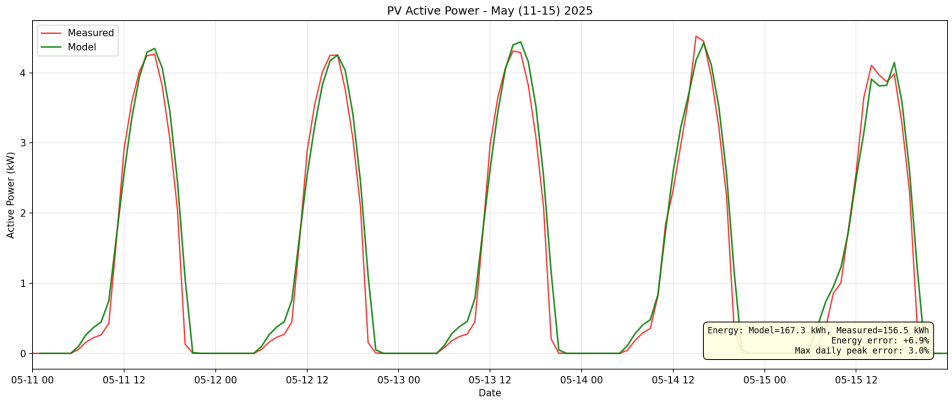

(b) Comparison of modeled and measured PV active power (kW).

Figure 4.1: Validation of the PV model: comparison of modeled and measured (a) GTI; (b) resulting PV active power output over a representative summer week (May 11–15, 2025).

4.1.2. Electrolyzer: Steady-state Power

Figure 4.2 shows the measured electrolyzer power consumption at production rates of 60%, 70%, 80%, 90%, and 100% over a 15-minute (900 s) interval. This corresponds to the steady-state phase, highlighted as the green area in Figure 3.17.

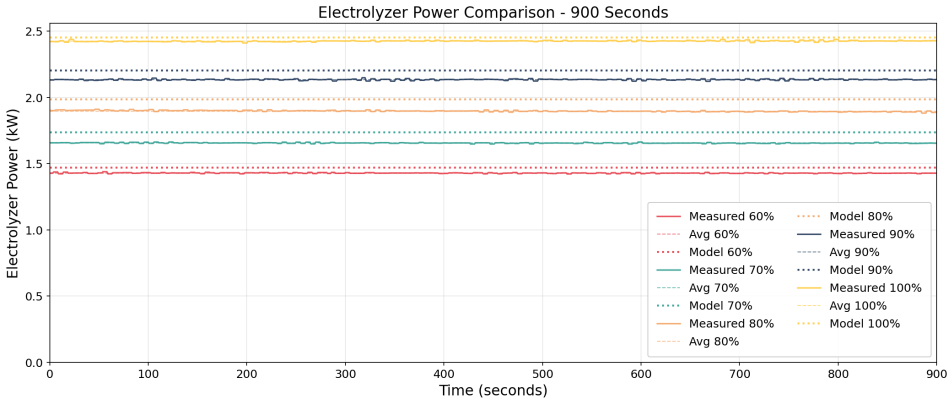

Figure 4.2: Comparison of measured and modeled electrolyzer power consumption at steady-state operation for production rates of 60%, 70%, 80%, 90%, and 100% over a 900-second interval. The close alignment confirms the model's accuracy during constant load conditions.

To quantify the alignment, the modeled and measured power profiles are integrated over time (900s) to compute total energy consumption per operating point. The resulting deviations range between $+1.1\%$

and $+4.8\%$ (model over-estimation), which means that the area under the modeled power curves is only slightly higher than the measured values. These errors remain below +5% across all production rates and are summarized in Figure 4.3.

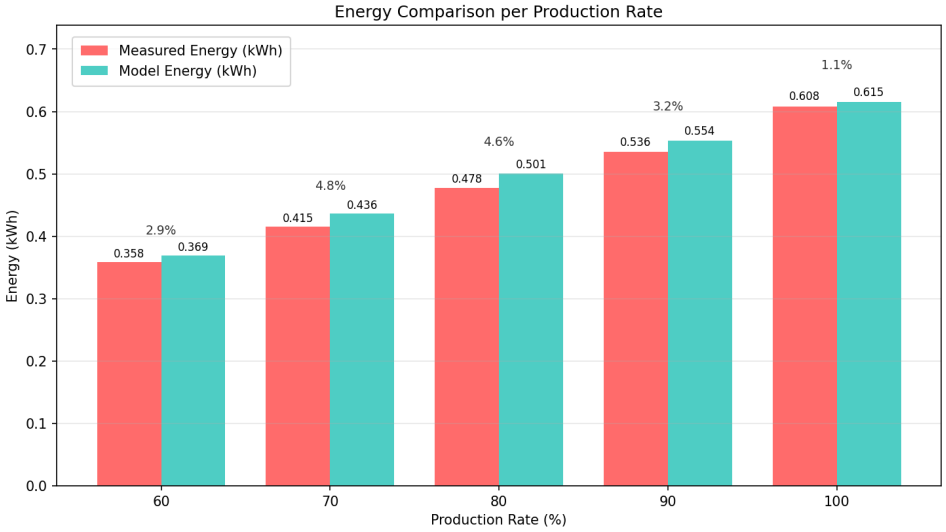

Figure 4.3: Electrolyzer model versus measured energy output across five production rate scenarios, showing consistent agreement (differences <5% at all rates).

4.1.3. Fuel Cell: Power output

Over a one-hour steady-state test period, the model predicts a hydrogen consumption of 1440.01 NL, compared to a measured value of 1498.02 NL. This corresponds to a relative deviation of -4%, which means that the modeled fuel use slightly underestimates the measured hydrogen demand.

Figure 4.4 presents the validation of the fuel cell model by comparing measured and simulated AC power output. The plot compares AC power output for three cases:

1. **Measured AC Power – before BoP:** raw output without BoP losses,
2. **Model AC Power – after BoP:** simulated output including BoP efficiency,
3. **Model AC Power – before BoP:** offset model output for direct comparison, shifted by the BoP efficiency (corresponding to an ≈ 0.138 kW correction).

Based on the integrated under the curves over the one-hour test period, the measured energy output (before BoP) is 1.82 kWh, while the simulated value is 1.85 kWh, yielding a deviation of $+1.8\%$. This shows that the model tracks both fuel consumption and delivered AC energy with high fidelity under steady-state operation.

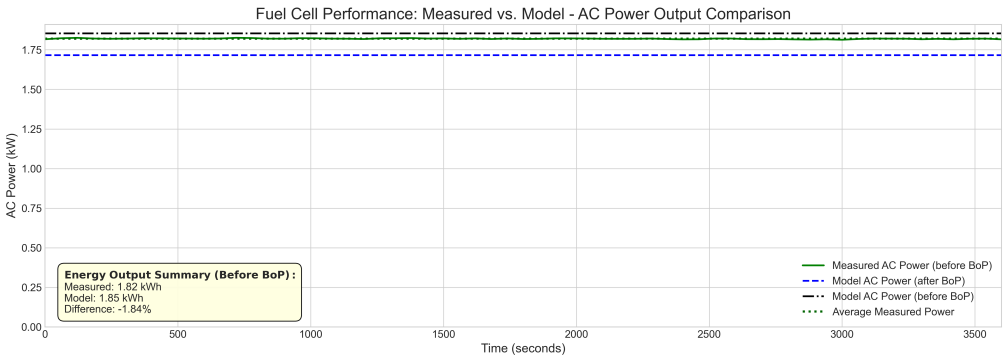

Figure 4.4: Fuel cell validation results: AC power output for a one-hour test period.

4.1.4. Hydrogen Storage: State of Charge

The hydrogen storage model is validated against measured data during two operational periods: January 2025 and August 2024. The winter period (Figure 4.5a) has low PV availability and continuous hydrogen depletion, with the modeled $SOC_{\mathrm{H_2}}$ closely following measured data. Full depletion occurs on January 23–24, aligning with the model prediction. The summer validation (Figure 4.5b) shows gradual charging. The model reproduces the upward trend in $SOC_{\mathrm{H_2}}$, while a sawtooth pattern is observed in measurements reflects, which are not present in the model.

Together, the seasonal validations demonstrate that the hydrogen storage model (and thus the controller) closely tracks both real depletion and charging behavior.

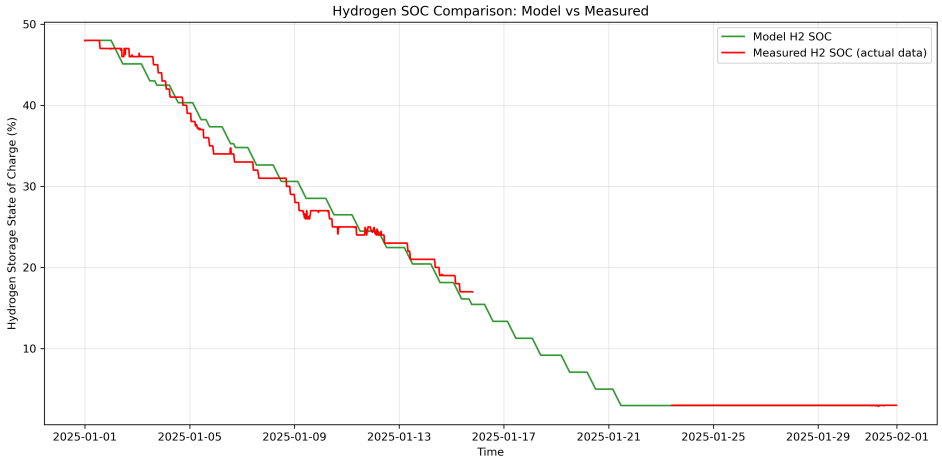

(a) Winter validation (January 2025) – $SOC_{\mathrm{H_2}}$ depletion over time under low PV generation conditions.

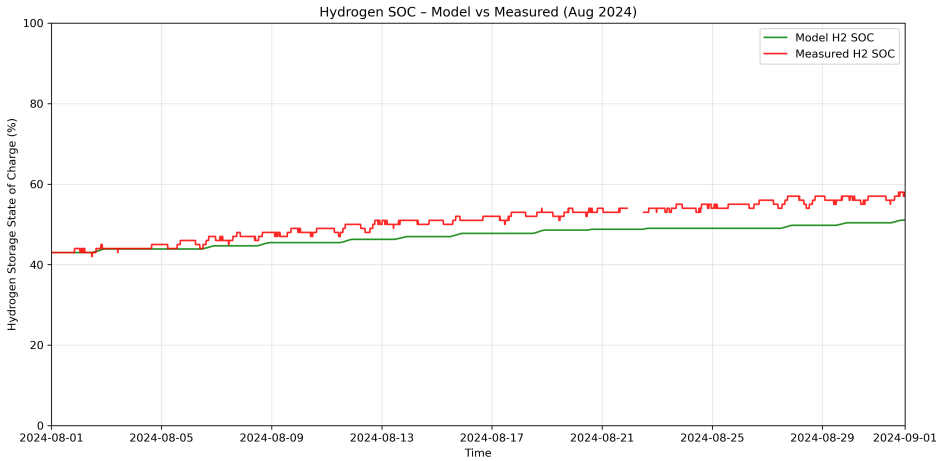

(b) Summer validation (August 2024) – $SOC_{\mathrm{H_2}}$ increases gradually with regular charging cycles. Sawtooth pattern in measured data reflects thermal transients not captured by the isothermal model.

Figure 4.5: Comparison of modeled and measured hydrogen storage state of charge ($SOC_{\mathrm{H_2}}$) over two seasonal periods: a) winter and b) summer.

4.1.5. Battery System

Figure 4.6 compares modeled and measured SOC_{bat} over a winter week (sub figure 4.6a) and a summer week (sub figure 4.6b). Some alignment is observed, for instance the overlapping trends at the end of the winter week and isolated cycles in summer.

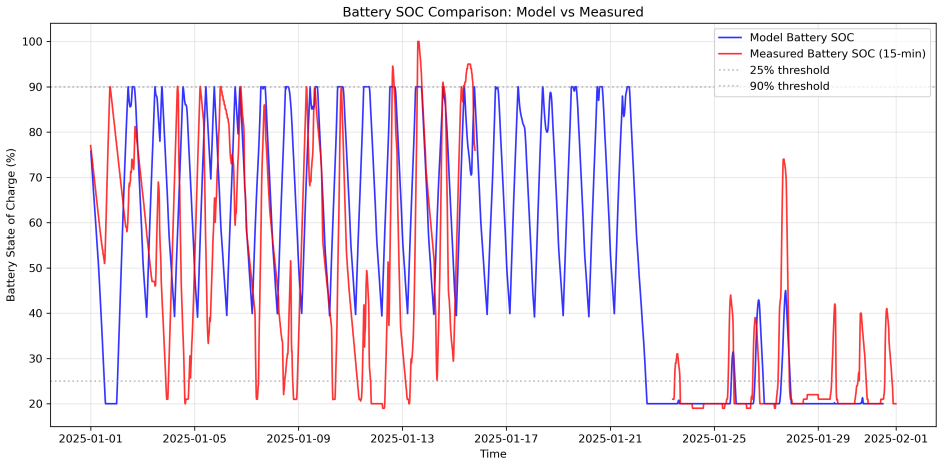

(a) Winter operation (January 2025): comparison of measured and modeled battery state of charge (SOC) showing (dis)charge cycles.

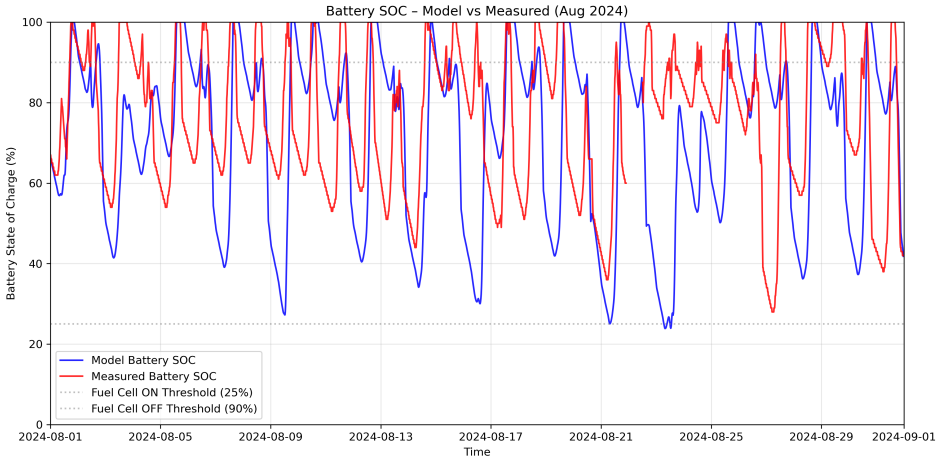

(b) Summer operation (August 2024): comparison of measured and modeled battery state of charge (SOC) showing (dis)charge cycles.

Figure 4.6: Validation of the battery state of charge (SOC) for the 24/7 Energy Hub: comparison between measured data and the simulation model under different seasonal conditions.

This section presented the validation of the models, comprising the PV system, electrolyzer, fuel cell, hydrogen tanks and the battery assets controlled by a rule-based EMS. The model is constructed to replicate the operational behavior of the physical 24/7 Energy Hub at The Green Village, and its performance is compared against real measured data, summarized in Table 4.1.

Subsystem	**Quantification of Validation**
PV Generation	GTI energy error: -2.4%; active power energy error over 65 days: 8.35%. Peak power error average and median:10.0% and 6.0%.
Electrolyzer	15-min steady-state intervals at production rates (60–100%). Energy error: $< +4.8\%$.
Fuel Cell	Hydrogen consumption: -4.03% error over 1-hour test. AC power modeled over 1-hour. Energy error: $< -1.8\%$.
Hydrogen Storage	January (winter): close alignment, including depletion timing. August (summer): reproduces the observed trend over time.
Battery Storage	Some overlap during summer and winter weeks.

Table 4.1: Summary of validation results across all system components. Each subsystem was tested using measurements from The Green Village.

4.2. Baseline Time Horizons

All individual profiles have been defined and their construction explained, they are applied according to the penetration levels outlined in Table 3.2. Given that this thesis focuses on impacts at the MV/LV transformer level, transformer loading is analyzed for the three time horizons (2023, 2030, and 2050) using both annual and seasonal perspectives.

Figure 4.10 shows the annual power flow across the transformer. The grid flow is expressed in kW, assuming equivalence with kVA for simplicity. Although a transformer's rated capacity is technically given in kVA, it is a common simplification to approximate 1 kVA as 1 kW under the assumption of a power factor close to 1 [22]. In the 2023 baseline case (Figure 4.10a), no violations are observed, indicating that the current 250 kVA transformer is sufficient for operation. In 2030 (Figure 4.10b), overall grid power flow increases due to greater electrification and PV penetration but remains within acceptable operational margins. By 2050, however (Figure 4.10c), the system experiences significant congestion, with **4,778** 15-minute import violations and **188** export violations. The peak import reaches 536 kW, more than twice the transformer rating, clearly exceeding technical limits on both import and export sides.

To further explain these results, Figure 4.7 compares grid import/export peaks by season (winter and summer) for each year. Figure 4.7a shows the evolution of average daily peaks, while Figure 4.7b captures maximum peak values to reflect both typical and extreme system conditions. Winter seasons are marked by high import demand, with the average daily peak rising from 141 kW in 2023 to 345 kW in 2050 (Figure 4.7a). Maximum winter peaks reach up to 536 kW (Figure 4.7b), primarily driven by increased heating demand and low solar generation. In contrast, summer months experience growing export flows due to PV surplus, with 2050 showing export peaks up to 301 kW. This trend reflects an asymmetric increase in grid flows: winter import peaks rise more steeply than summer export peaks, indicating that winter congestion becomes the dominant challenge under electrification, while in summer, a larger share of PV is self-consumed, limiting export growth.

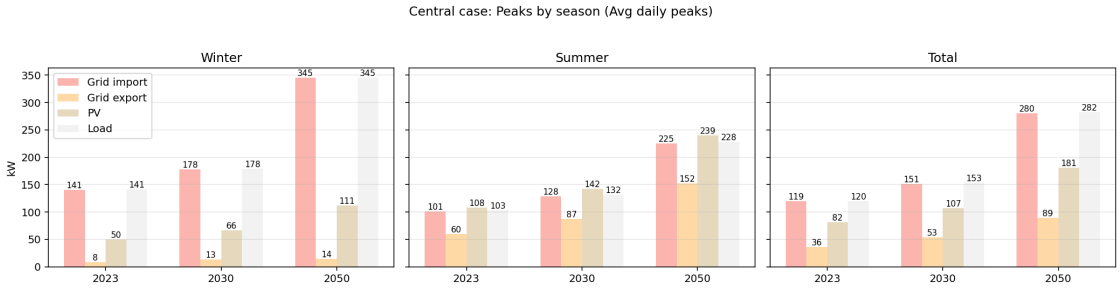

(a) Average daily peak power by season (winter, summer, total) for 2023, 2030, and 2050.

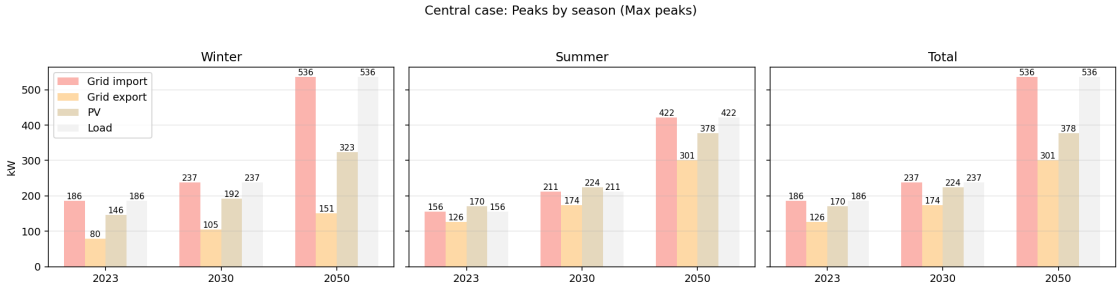

(b) Maximum instantaneous peak power by season for 2023, 2030, and 2050.

Figure 4.7: Seasonal comparison of grid import, export, PV generation, and household load for different temporal horizons. The results highlight the growing imbalance between import and export power flows toward 2050.

The characteristics of the 2050 grid violations are examined in more detail. Figure 4.8 visualizes all transformer power limit violations over the year as a function of their magnitude and duration. Each point represents a violation event, with color intensity indicating the duration of the event.

From Figure 4.8, it can be observed that the most severe violations occur during winter months, with both higher magnitudes and longer durations. These are primarily import violations, often persisting for several hours and exceeding the 250 kVA transformer limit by up to 286 kW. In contrast, the summer months show export violations resulting from PV overproduction. Although these export violations are fewer in number and shorter in duration, typically lasting less than four hours, they still indicate moments where local generation temporarily exceeds the connection capacity. The maximum export peak exceeds the transformer limit by approximately 51 kW. A more detailed monthly breakdown of transformer violations in 2050 is provided in Appendix 7.7, Figure 7.4. Figure 4.9 shows that most import violations are short, typically lasting between 15 minutes and 2 hours, though extend up to 8 hours or 16 hours. Export violations, in contrast, are less frequent and generally shorter in duration.

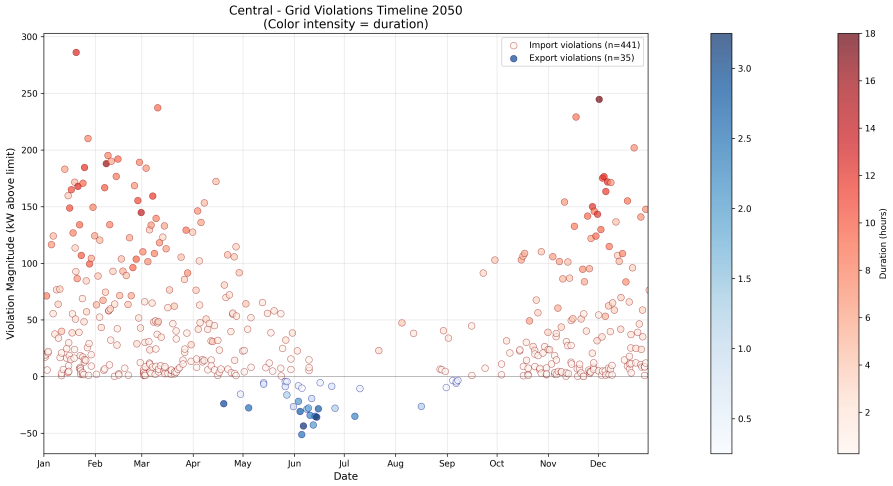

Figure 4.8: Timeline of transformer power violations in 2050. Each marker represents an individual violation, with color intensity indicating the duration. Import violations (red) dominate in winter, while export violations (blue) appear primarily in summer months.

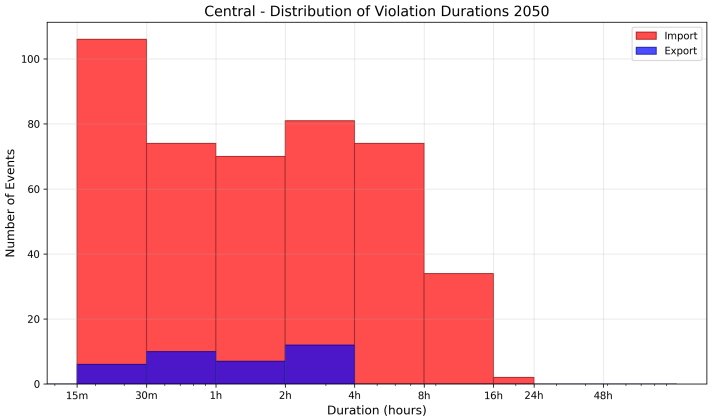

Figure 4.9: Distribution of violation durations in 2050, distinguishing between import (red) and export (blue) events. Short-duration import violations are most common, but longer events up to 8 hours also occur.

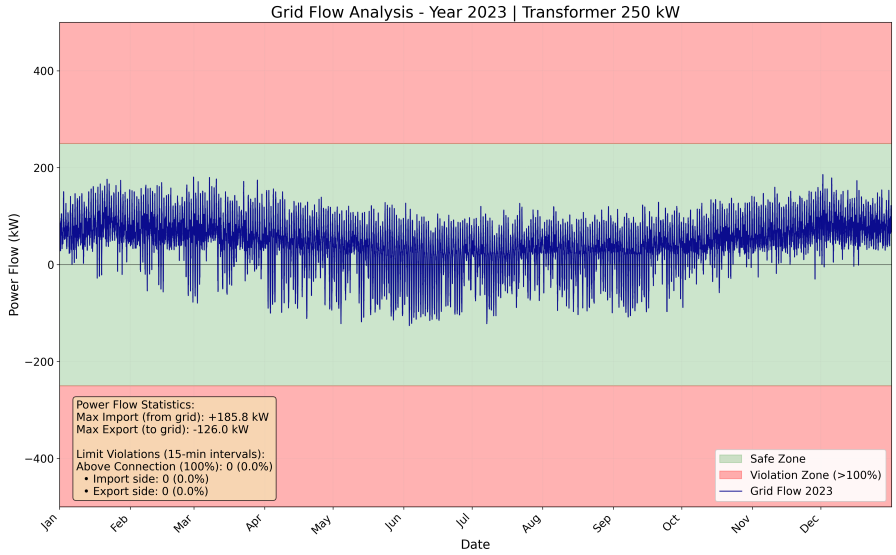

(a) Grid power flow in 2023 under a 250 kVA transformer: no violations observed, indicating sufficient capacity for the baseline year.

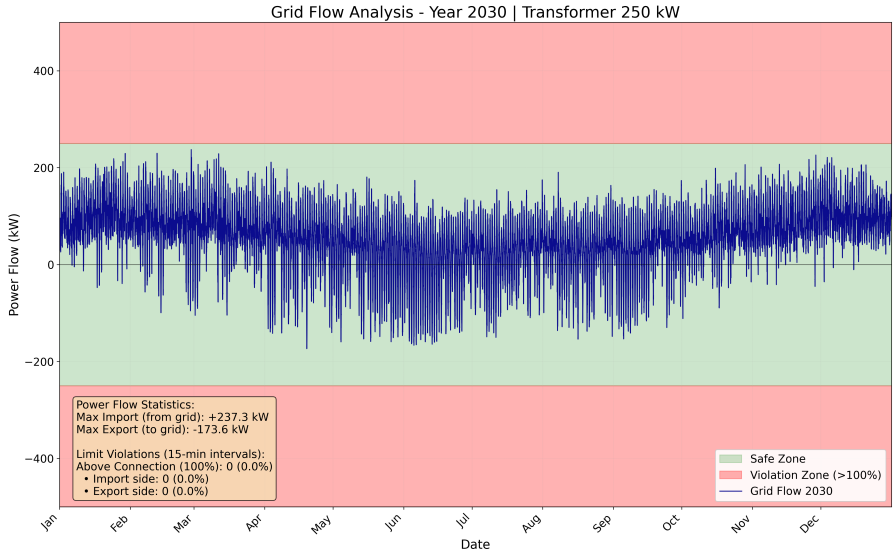

(b) Grid power flow in 2030 under a 250 kVA transformer: load and PV export increase but remain within connection limits.

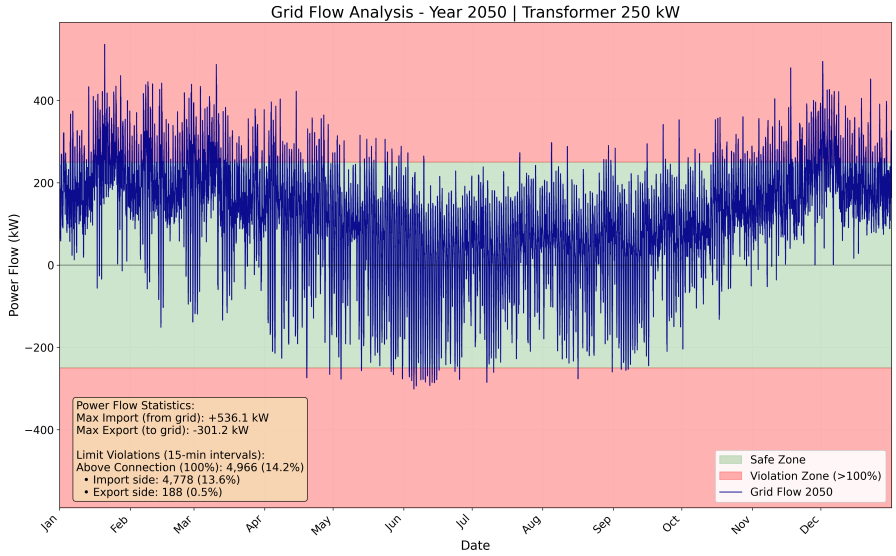

(c) Grid power flow in 2050 under a 250 kVA transformer: significant congestion occurs, with approximately 14% of intervals exceeding the connection limit.

Figure 4.10: Evolution of annual grid power flow for a 250 kVA transformer from 2023 to 2050. The green zone represents operation within transformer capacity, while the red zones indicate overload conditions. The increasing frequency of violations illustrates the growing grid congestion expected by 2050.

4.3. Autonomous Reference Case

Before analyzing the grid-oriented energy hub configurations, an autonomous reference case was evaluated to determine whether the original 24/7 Energy Hub operation, independently of the grid, using battery and hydrogen storage, can be transferred to a full neighborhood under 2050 demand conditions.

The autonomous reference case corresponds to the configuration (identified in the sizing analysis Appendix 7.8) as achieving the minimum annual grid dependency under 2050 demand conditions. This configuration reduces annual grid reliance to just 0.03%, importing 142.1 kWh and exporting 3,936.3 kWh of electricity. However, this requires large component sizes and results in a hydrogen deficit. Over one year the hub consumes 95,265 kg of hydrogen while producing only 2,314 kg, resulting in a deficit of 92,950 kg. Meaning the hub produces only 2.4% of the hydrogen it consumes annually. A detailed breakdown of the autonomous configurations is provided in Appendix 7.8, and the resulting transformer behavior is illustrated in Figure 7.5.

Table 4.2: Performance of the most grid-independent autonomous configuration (2050 horizon)

Component sizing	Battery: 2,000 kWh; Electrolyzer: 300 kW; Fuel cell: 600 kW
Annual grid imports	142.1 kWh (0.03% of demand)
Annual grid exports	3,936.3 kWh (0.9% of generation)
Hydrogen produced	2,314 kg
Hydrogen consumed	95,265 kg
Hydrogen deficit	92,950 kg (balance: -2.4%)

4.4. Configuration Results

This section reports the outcomes of the configuration procedure defined in section 3.3.3, which consists of a feasibility screening (section 4.4.1) followed by an economic selection (section 4.4.2). Finally section 4.4.3 contextualizes the feasible configurations by comparing them to the baseline and reinforcement cases.

4.4.1. Feasibility Screening

Applying the screening procedure described in Section 3.3.3 reduces the initial set of 320 configurations to **159 transformer-violation-free cases**. Of these, **56 configurations achieve a positive annual hydrogen balance**, in other words annual hydrogen production exceeds consumption. No configurations within Scenarios A or B satisfy this criterion. The filtering progression is shown in Figure 4.11.

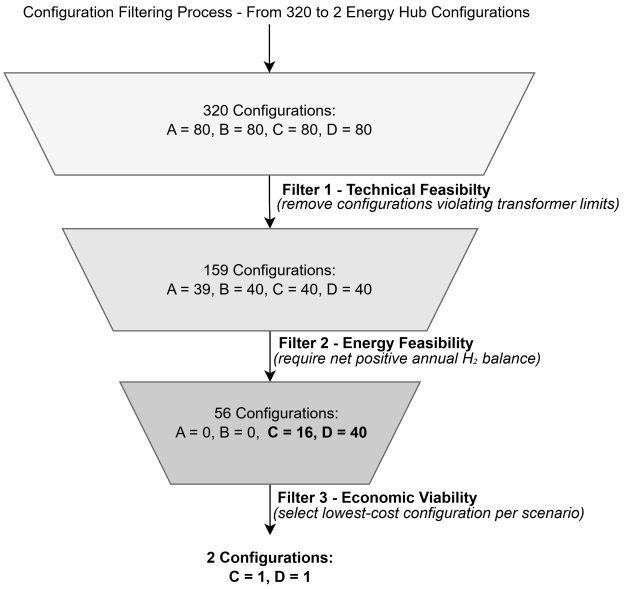

Figure 4.11: Configuration Filtering Process: From 320 Simulations to 2 Cost-Optimal Energy Hub Configurations

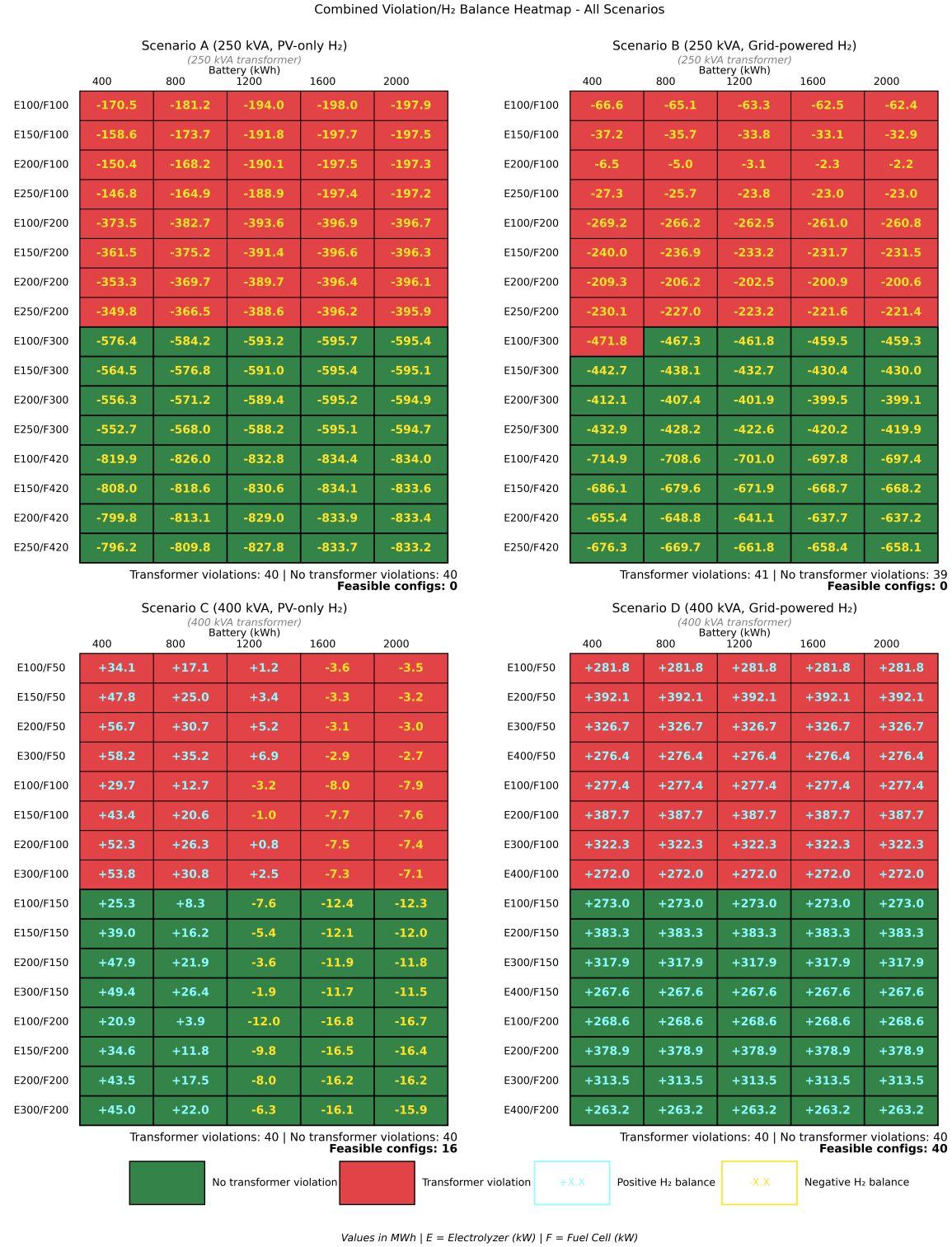

Figure 4.12: Feasibility heatmaps of scenarios, showing annual hydrogen balance (MWh) across the configuration space. Cell color indicates transformer constraint status (green = no violation, red = violation); text sign indicates hydrogen balance (positive = surplus, negative = deficit).

4.4.2. Economic Analysis

For each scenario, the lowest-cost configuration is selected based on the CAPEX and OPEX values in Table 3.9. Only Scenarios C and D passed the feasibility screening (transformer-violation-free and positive annual hydrogen balance). Therefore, only their lowest-system-cost configurations proceed to

the economic comparison stage, resulting in two candidates (Figure 4.11). Scenario C consists of a 400 kVA transformer upgrade, an 800 kWh battery, a 100 kW electrolyzer,a 150 kW fuel cell, and 644 kg hydrogen storage (21.5 MWh). Scenario D uses the same electrolyzer, fuel cell and transformer ratings but has a 400 kWh battery and a significantly larger hydrogen tank (8,572 kg / 286 MWh).

Table 4.3: CAPEX, OPEX, and total cost breakdown of the cheapest feasible hydrogen-based congestion mitigation configurations.

Scenario C (PV-only H_2)					
Component	**CAPEX (€)**	**% CAPEX**	**OPEX (€)**	**% OPEX**	*Total (€)*
Battery	120,000	17.2%	4,000	35.9%	124,000
Electrolyzer	70,000	10.1%	2,000	17.9%	72,000
Fuel Cell	150,000	21.5%	4,500	40.4%	154,500
H_2 Storage	322,000	46.2%	644	5.8%	322,644
Transformer	34,002	4.9%	–	–	34,002
Total	**696,002**	**100%**	**11,144**	**100%**	**707,146**
Scenario D (Grid-powered H_2)					
Component	**CAPEX (€)**	**% CAPEX**	**OPEX (€)**	**% OPEX**	*Total (€)*
Battery	60,000	1.3%	2,000	11.7%	62,000
Electrolyzer	70,000	1.5%	2,000	11.7%	72,000
Fuel Cell	150,000	3.3%	4,500	26.4%	154,500
H_2 Storage	4,286,000	93.2%	8,572	50.2%	4,294,572
Transformer	34,002	0.7%	–	–	34,002
Total	**4,600,002**	**100%**	**17,072**	**100%**	**4,617,074**

A direct cost comparison between the two feasible energy hub designs shows that both eliminate congestion, but differ in cost. **Scenario D (grid-powered hydrogen) is the more expensive option**, with a total system cost of approximately 4.6M. **Scenario C (PV-only hydrogen) has lower cost of** 707**k**, achieving the same level of congestion mitigation. A component-level cost breakdown is provided in Table 4.3, including CAPEX and OPEX.

Table 4.4: Performance and cost comparison of the optimal configurations for transformer congestion mitigation.[1]

Metric	**Baseline 2050**	**Grid Reinforcement**	**Scenario C[1] (PV-only H_2)**	**Scenario D[1] (Grid-powered H_2)**
System Design				
Transformer	250 kVA	630 kVA	400 kVA	400 kVA
Battery	–	–	800 kWh	400 kWh
Electrolyzer	–	–	100 kW	100 kW
Fuel Cell	–	–	150 kW	150 kW
Tanks	–	–	644 kg/21.5 MWh	8572 kg/286 MWh
System Performance				
Peak Violations	67.9 MWh	0 kWh	0 kWh	0 kWh
H_2 Balance	–	–	+8.3 MWh/year	+273 MWh/year
Grid Import (MWh/year)	1110 + 67.2[*]	1,177	1,106	1,510
Grid Export (MWh/year)	149.7 + 0.7 [*]	150.4	37.6	41.2
Cost (CAPEX + OPEX)				
Total Cost	€0	**€34k**	**€707K**	**€4.6M**

[*]Import exceeding the transformer limit, which means infeasible under 2050 conditions.
[1]Lowest-cost configuration within each scenario after feasibility filtering.

To place the energy hub in a decision context, these two configurations are compared not only with

each other, but also with the baseline case and the classical alternative of grid reinforcement. This comparison metrics are summarized in Table 4.4.

4.4.3. Configuration Performance under Baseline and Grid Reinforcement

Figure 4.13 visualizes both grid exchange and cost composition for the four cases. For each case, the left horizontal bar along the x-axis shows the annual grid exchange in MWh: red segments represent grid import up to the transformer rating, dark red indicates import above the transformer limit (congestion), and blue represents grid export. The light-red shaded background in the baseline row highlights this congestion effect. On the right side of each row, the stacked horizontal bar shows the total system cost in euros, decomposed into CAPEX categories (battery, electrolyzer, fuel cell, hydrogen storage, transformer upgrade) and OPEX, as indicated in the legend.

The baseline case (250 kVA) shows 67.9 MWh of import above the transformer rating, which is visualized as the dark-red segment. Grid reinforcement (630 kVA) removes this congestion while maintaining similar import (1,177 MWh) and export (150.4 MWh) magnitudes, consistent with Table 4.4. Scenarios C and D also eliminate congestion but display higher total system costs; in Scenario D the hydrogen-storage CAPEX segment is dominant. Scenario C and D shows reduced annual export relative to reinforcement, while Scenario D exhibits higher import (1,510 MWh).

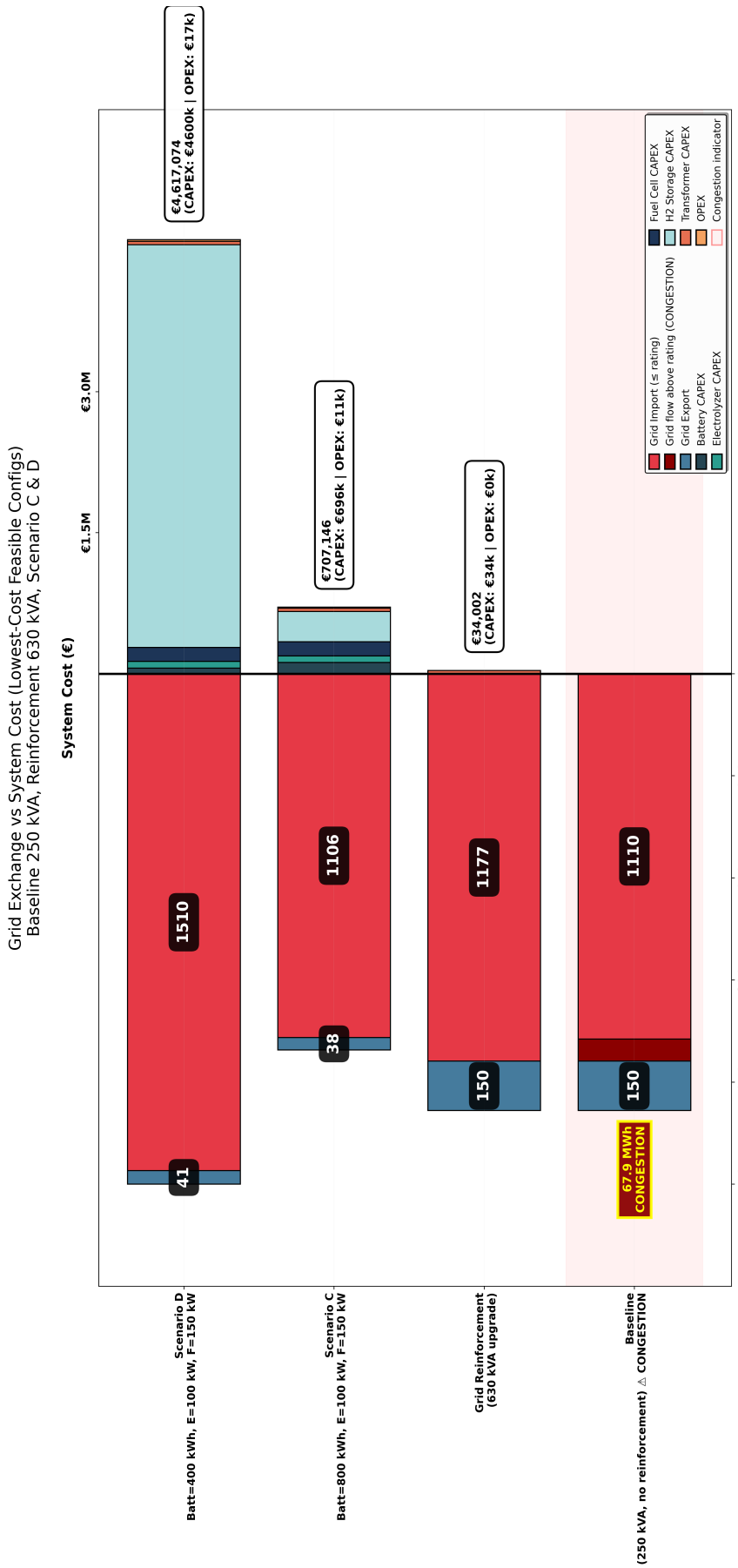

Figure 4.13: Annual grid exchange (left axis) and total system cost (right axis) for the baseline, grid reinforcement, and energy hub scenarios C and D. The horizontal bars show import and export magnitudes, as well as CAPEX and OPEX contributions

5

Discussion

This chapter describes the key findings of the techno-economic assessment and reflects on their implications for mitigating transformer congestion through decentralized hydrogen storage. It reviews the research objectives and sub-questions introduced in Chapter 1 and evaluates how each finding contributes to closing the knowledge gaps identified in Table 2.4. The discussion first reflects on the projected future energy landscape (Objective 1), then interprets the case study results and techno-economic feasibility of the energy hub configurations (Objective 2), and finally evaluates the applicability and credibility of the developed model (Objective 3). The chapter concludes with recommendations for DSOs, followed by the limitations, and translates this into recommendations for future work. Throughout this chapter, bold statements directly answer the sub-questions.

5.1. Assessment of the Future Energy Landscape

Objective 1 is to examine how expected developments toward 2050 shape both the need for and suitability of hydrogen-based energy hubs, thereby addressing the *scale and future-horizon gap*. This objective is explored through two sub-questions.

SQ1: Which built environment archetype is suitable for implementing the energy hub concept, and how transferable is the approach?
Archetype 3 is found to be a suitable and representative context for the energy hub concept, as it has high similarity to Dutch neighborhoods of archetype 3 and represents the largest share of the national neighborhood types (Figure 5.1). While absolute component sizes will differ between locations (number of houses), **the relative sizing logic, system interaction behavior, and configuration principles are transferable**. As long as PV, EV and HP penetration rates are comparable, proportional design rules derived in this study can be applied elsewhere.

In practice, applying the methodology to another neighborhood requires (i) updated load and PV generation profiles reflecting local electrification trends, and (ii) re-scaling component sizes accordingly. If these conditions are satisfied, **similar congestion-mitigation performance can be expected across comparable archetypes.**

SQ2: How do projected changes in consumption and generation affect the potential of the energy hub to mitigate congestion by 2050?
The baseline analysis shows that the low-voltage grid remains reliable until 2030, but transformer overloads become structural by 2050, with 67.9 MWh exceeding capacity (67.2 MWh import and 0.7 MWh export) for the case study of 155 households. These violations result from winter import peaks driven by electrification and heating demand and summer export peaks originating from high PV output. **This seasonal imbalance highlights the need for seasonal mitigation strategies.**

The operational capabilities of the energy hub align with these dynamics: the fuel cell can support winter import peaks, the electrolyzer converts summer surpluses to hydrogen, and the battery provides short-term balancing. Thus, **the future energy landscape creates the congestion challenge and**

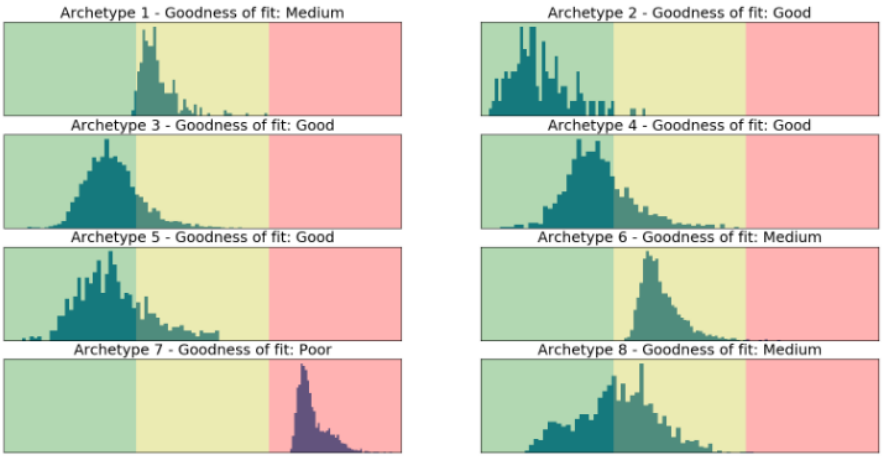

Figure 5.1: Goodness of fit of the eight Dutch neighborhood archetypes used for load profiling. Archetype 3, applied in this case study, shows a high fit with comparable neighborhoods, supporting transferability of the energy hub configuration approach.

the conditions under which the energy hub becomes functionally relevant. Following the observed trajectory, transformer overload risks are expected to reach unsustainable levels around 2035, reinforcing the urgency for flexible mitigation solutions.

5.2. Case-Study Evaluation and Techno-Economic Feasibility

Objective 2 is to test the applicability and performance of the energy hub concept in a realistic neighborhood setting, addressing the *performance-evaluation gap*. This objective is answered through four sub-questions.

SQ3: How does the existing energy management system (EMS) interact with the energy hub?
Scaling the autonomous 24/7 Energy Hub to neighborhood level, consisting of 155 households, shows that full grid independence is technically achievable but only under extreme over sizing and an unsustainable hydrogen imbalance (41:1 consumption–production ratio). This dependence on external hydrogen contradicts the autonomy goal and makes such a configuration **infeasible for real neighborhoods**. Consequently, **the EMS must shift from autonomy-oriented control to congestion-oriented dispatch**. This is consistent with [33], who show that autonomy on small scale requires disproportionately large hydrogen storage and fuel cell capacity, leading to high costs.

SQ4: How should the battery, electrolyzer and fuel cell be dimensioned to operate within transformer limits?
Hydrogen production scales with electrolyzer activation, thus operating hours and electrolyzer power, while fuel cell power determines congestion-relief capability. A comparison with the assumed base sizing reveals that feasible fuel cell ratings just below or at the base value, which confirms that the fuel cell capacity is tightly coupled to the congestion constraint: over sizing prevents transformer violations but induces hydrogen shortages, whereas under sizing prolongs congestion.

The battery plays a supporting role: in winter the low PV availability limits charging; in summer, a smaller battery accelerates electrolyzer activation, increasing hydrogen production. This reflects the model outcome where feasible battery capacities converged below the base assumption (when charging from the grid is not allowed). The smaller battery behavior aligns with [30], who show that smaller batteries paired with larger hydrogen systems produce more hydrogen.

Unlike the autonomous case, where operation minimizes imports and exports, **the congestion-mitigation case prioritizes respecting transformer limits** even if that increases seasonal exchange. Ultimately, **only 56 of 320 evaluated configurations satisfy both feasibility criteria: zero transformer violations and a positive annual hydrogen balance.**

SQ5: Under what production and grid conditions is seasonal hydrogen storage feasible for congestion mitigation?

- **Seasonal hydrogen buffering is infeasible at original 250 kVA transformer capacity.** Scenarios A and B show that storage cannot compensate for insufficient capacity because hydrogen consumption outpaces production.
- **A 400 kVA transformer enables a feasible design space.** Scenario C demonstrates congestion mitigation while maintaining hydrogen self-sufficiency and reducing summer exports, indicating that hydrogen storage becomes reasonable once minimal reinforcement is applied.
- Scenario D reveals that **grid-powered hydrogen production introduces flexibility but results in large import volumes and over sizing demands under the current rule-based control and over sizing of the electrolyzer**. This behavior suggests that charging with grid electricity is more effectively using batteries, given their significantly higher round-trip efficiency. A short test confirmed this: with an 11 MWh battery and a 250 kVA transformer, no congestion was observed for the case study.

SQ6: What are the investment and operational costs of the energy hub compared with grid reinforcement?
For the case study of 155 households supplied by an original 250 kVA transformer, the following costs were evaluated **Reinforcing the transformer to 630 kVA is the lowest-cost option (€34 k).** Scenario C mitigates congestion and substantially reduces annual exchange, but at an annual cost, including CAPEX and OPEX of €707 k. **Scenario D exhibits the highest cost (€4.6 M), dominated by hydrogen storage CAPEX of 93.2% of the total CAPEX (€4.3 M)**, which could be reduced through better control/optimization. However, **both feasible scenarios require a fuel cell investment (€150 k), which alone exceeds the cost of reinforcement**, making conventional upgrading the most economical solution under current cost assumptions. While future price reductions could alter this balance, today reinforcement remains more cost-effective, whereas energy hubs primarily provide strategic value by supporting local balancing and reducing curtailment risk.

5.3. Model Development: Validation and Applicability

Objective 3 is to develop a scalable model of the 24/7 Energy Hub suitable for neighborhood-level use, addressing the *system-integration gap*. This is answered via the final sub-question.

SQ7: How can the 24/7 Energy Hub be modeled as a reliable plug-and-play concept suitable for large-scale implementation in residential areas to mitigate grid congestion?
The energy hub model, based on household-level demand, PV generation and hydrogen conversion, successfully captures transformer congestion dynamics at a 15-minute resolution. This resolution reflects relevant LV dynamics: PV variability, EV charging ramps and heat pumps responses occur over minutes rather than seconds or hours. It also supports realistic control behavior by accurately representing electrolyzer activation, fuel cell dispatch and short-term storage interactions. Finally, it aligns with emerging operational practices, including the renewable-oriented 15-minute electricity market [19] and industry conventions such as EN 50160, which evaluates slow voltage variations over 10-minute windows [54].

Despite simplifications, including constant conversion efficiencies and simplifying the fuel cell ramping dynamics, the validation using The Green Village dataset confirms that the model reproduces realistic operation of the battery, electrolyzer and fuel cell.

Across all subsystems, the developed model shows the following accuracy relative to measured 24/7 Energy Hub data:

- PV generation remains within an energy error of 8.35% and peak-power error with a mean of 10% and a median of 6%.
- Electrolyzer energy consumption differs by 1.1–4.8%.
- Fuel cell hydrogen consumption deviates by 4% and AC output deviate by approximately 1.8%.
- Hydrogen storage is accurately reproduced in both winter and summer.

- Battery SOC follows realistic charge/discharge patterns, however with deviations due to synthetic demand and controller activation thresholds.

The detailed validation insights per subsystem are discussed below.

PV model Minor differences can be attributed to system-level factors such as soiling, panel degradation, and localized shading not captured in the weather model. Both metrics (energy and daily peak power error) are particularly relevant: energy error determines storage requirements; daily peak power is critical for control decisions, such as electrolyzer activation or identifying grid congestion events. Despite data input and sensor uncertainties, the validation confirms that the model accurately represents system behavior.

Electrolyzer These inaccuracies can be attributed to several factors, including measurement uncertainties and the use of a constant average efficiency for all production rates in the model, whereas actual system efficiency may vary slightly with load. Given the small magnitude of these differences, the model is considered to represent the real-system performance.

Hydrogen Although a gap in the measured data appears at the exact moment of depletion, the preceding trend supports the model's accuracy. This validation implicitly includes the fuel cell and controller behavior, confirming correct hydrogen consumption and timely activation.

In contrast, the August validation (Figure 4.5b) reflects summer conditions with increased PV input and more frequent charge-discharge cycles. While short-term oscillations in the measured data (caused by thermal transients, which is explained below) are not captured by the isothermal model, the long-term SOC trajectory is well reproduced. This indicates accurate representation of hydrogen balance and net production on operationally relevant timescales.

Thermal Transient Effects on Measured SOC The sawtooth oscillations in the measured SOC data (Figure 4.5b) result from thermal transients not captured by the isothermal model. During hydrogen charging, gas is compressed to 272 bar at elevated temperatures. However, after injection, the gas cools gradually toward ambient conditions, causing a pressure drop due to Gay-Lussac's Law ($P_1/T_1 = P_2/T_2$).

Since the sensor measures SOC from pressure (rather than mass, which establishes the SOC in the model), this cooling leads to a SOC decrease, despite constant hydrogen mass, creating the observed behavior. This pattern is evident in summer data (August 2024), while winter discharge-only periods (January) show no such behavior, confirming that the effect is specific to charging, during summer period.

Battery Validating the battery system is more challenging than for hydrogen storage due to the use of a synthetic load profile (2,200 kWh) in the simulation (Data protection). The battery responds to short-term load fluctuations, making it difficult to match long-term trends seen in real measurements. In contrast, hydrogen storage exhibits slower dynamics and allows for more meaningful monthly-scale comparisons.

Further uncertainty arises from limited insight into the EMS behavior during the measurement period. In the winter case, the modeled SOC does not drop below 40%, as the controller activates the fuel cell before 13:00 when SOC falls below a threshold. The synthetic load could trigger this condition, whereas the real load might not, resulting in deeper battery discharge. It is also difficult to verify whether the EMS was actively operating at specific moments during the measurement period.

In general, the validation confirms that the model is reliable, reproduces the behavior of the real-system, and is suitable for assessing congestion on a scale.

5.4. Recommendations for DSOs

The results show that DSOs are not deciding between "reinforcement *or* flexibility", but between "reinforcement only" and "reinforcement complemented with flexibility". Using power-to-hydrogen-to-power

only for congestion mitigation in the built environment of 2050 is inefficient; however, storage can reduce PV export. If a 630 kVA grid reinforcement is not feasible, scenario C demonstrates that an energy hub can be a viable congestion mitigation strategy for archetype 3 neighborhoods with a 400 kVA transformer. Scenario D indicates a promising direction: charging during off-peak winter hours. This strategy likely becomes more attractive when applied to batteries rather than hydrogen storage due to high conversion efficiency and high hydrogen storage prices. In the current setup, this scenario leads to considerable hydrogen overproduction, implying that a simple rule-based controller is insufficient; a more advanced strategy, would be required to balance production and consumption. Overall, Scenario D demonstrates the potential of using the grid during low-demand periods to generate additional storable electricity for later use. **In conclusion, grid reinforcement is the preferable option for DSOs compared to implementing this specific energy hub in the case study.**

5.5. Limitations and Future Work

This thesis includes several methodological, modeling, and contextual limitations that should be considered when interpreting the results.

5.5.1. Modeling Simplifications

- PV capacity was assumed constant and uniform in orientation; shading, rooftop diversity, degradation effects and soiling influences were not modeled, although these may be relevant in dense built environments.
- Heat pump adoption was assumed to be fully electric; in practice, mixed heating systems could alter demand peaks and seasonal patterns.
- Component degradation, efficiency decline and lifetime constraints were excluded; efficiencies were treated as constant despite their variation over time.
- Dynamic electricity prices, and market participation were not taken into account to maintain neutrality, even though they would significantly affect import flows, especially in Scenario D.
- No optimization was applied; consequently, feasible, but not necessarily optimal, component sizes were identified.

5.5.2. Technology Modeling and Validation Limitations

- PV modeling did not capture shading losses or real-world diversity in tilt, azimuth and rooftop configurations.
- In the model, the fuel cell output was kept constant because the real system at The Green Village operates at fixed power, and its efficiency at partial load was not experimentally validated. However, allowing variable output could reduce hydrogen consumption by operating only at the required power level.
- Compressor behavior could not be validated because the 24/7 Energy Hub uses an electrochemical compressor; For large-scale, a mechanical compressor model was applied instead, due to lower energy consumption.
- Balance-of-plant loads and auxiliary consumption were only included for the fuel cell; other subsystems were assumed ideal, without losses.

5.5.3. Scenario and Data Representation Limitations

- Only two forecast horizons (2030 and 2050) were investigated, meaning that the exact point at which congestion emerges remains uncertain. Due to lack of data of other years.
- Forecasted penetration levels for PV, EVs and heat pumps may evolve differently in practice; demand behavior and adoption uncertainty were not explicitly modeled.
- Only one neighborhood archetype was analyzed; while transferability was argued, applicability to other archetypes should be validated.
- Only one load and PV profile set was used, without sensitivity analysis, limiting representation of behavioral diversity.

- PV and load data represented a single historic year rather than multiple years, reducing the capture of inter-annual variability.

5.5.4. Economic and Environmental Assumptions

- Lifecycle and operational CO_2 emissions of storage components were excluded. The study adopts the perspective that energy hubs enable renewable integration and thereby supports sustainability, but the emissions of system installation and operation remain unaddressed.
- Component cost and process efficiencies were treated as static. No sensitivity analysis was conducted on future cost reductions, even though such parameters are highly uncertain (for example, hydrogen storage costs could decrease by an order of magnitude). Moreover, component technologies could improve over time, resulting in higher efficiencies.
- Transformer operational expenditure was not taken into account due to the investment-focused scope, although its inclusion could influence trade-offs under the alternative objectives.

5.5.5. System Boundary and Validation Constraints

- The study assumes no congestion at MV and HV levels, whereas upstream grid flows affects LV behavior.
- The selected neighborhood currently (2023 and 2030) does not show congestion, which reduces immediate urgency; this reflects data availability limitations.
- Model validation was constrained by uncertainty surrounding the exact EMS control logic at The Green Village at specific times, due to test periods and the use of synthetic household demand profiles, which limited alignment between measured and simulated behavior.

This thesis explores the extent to which energy hubs hold *potential* for mitigating transformer congestion. The identified limitations therefore serve as a pathway toward future work, where this potential can be further refined into more detailed and optimized outcomes. These limitations do not discourage the validity of the main findings, but they indicate where modeling assumptions, data constraints and system boundaries may influence outcomes. They also highlight directions in which the energy hub concept, the modeling framework and its techno-economic interpretation can be further researched. In this way, the limitations motivate several aspects for future work.

Future work should therefore focus on two promising directions. First, Scenario D shows that controlled charging during off-peak periods could help manage congestion, yet round-trip inefficiencies and high investment cost make hydrogen less suitable for this role. Research should therefore explore applying the same principle to batteries, with their higher efficiency and fast response, they could provide grid-supporting flexibility more effectively. Second, the seasonal imbalance, largely driven by heating during the winter, is observed in the case study suggests that power-to-heat storage may represent a more suitable seasonal buffering route than hydrogen. Investigate its performance relative to hydrogen could conclude whether thermal storage offers a more scalable and cost-effective alternative for residential congestion mitigation.

Based on the answers to SQ1–SQ7 based on objectives and driven by knowledge gaps, the discussion has formed the components necessary to answer the main research question. The following chapter integrates these findings into a concise concluding answer.

6

Conclusion

This thesis investigated whether an energy hub combining battery and hydrogen storage can mitigate transformer congestion in the residential built environment by 2050 at low-voltage transformer level.

A scalable plug-and-play energy hub model was derived from the 24/7 Energy Hub at The Green Village. In this configuration, the battery provides short-term balancing, the electrolyzer converts summer PV surplus into hydrogen, and the fuel cell supports winter peak demand. Validation showed that this rule-based model reproduces realistic operational patterns and can therefore be scaled to neighborhood level by adapting component capacities to local load and PV conditions.

To answer the main research question:

> *To what extent can decentralized hydrogen storage mitigate grid congestion at low-voltage distribution transformers within the existing built environment by 2050?*

Under projected 2050 electrification and PV penetration, transformer congestion becomes structural. The energy hub configurations evaluated in this study eliminated congestion while maintaining a positive annual hydrogen balance, meaning it produces more hydrogen then consumed, demonstrating that hydrogen-based seasonal storage can technically resolve transformer violations and reduce seasonal imbalance at neighborhood scale.

However, achieving this performance requires substantial capital expenditure (€0.7–€4.6 M for the 155-household case study with a 250 kVA transformer), far exceeding the cost of traditional reinforcement (€34 k). Moreover, seasonal hydrogen storage becomes feasible only after a minimum structural upgrade from 250 kVA to 400 kVA is in place; without this reinforcement, hydrogen self-sufficiency and congestion relief are not attainable.

Therefore, decentralized hydrogen storage can technically mitigate transformer congestion and reduce seasonal energy imbalances, but only as a complement to moderate grid reinforcement and not as a cost-effective replacement for conventional upgrading under current techno-economic conditions. Energy hubs provide strategic value through enhanced self-consumption, reduced export peaks and avoided curtailment, but their present efficiency and cost position them as a flexibility enhancement rather than a substitute for reinforcement. To build on these findings, future research should investigate whether controlled winter charging of batteries during off-peak periods can deliver congestion relief more efficiently than hydrogen-based pathways, given their higher round-trip efficiency and lower infrastructure requirements. In parallel, power-to-heat concepts such as thermal buffering or hybrid heat storage should be assessed as alternative seasonal flexibility options, as they may achieve similar system-level relief with lower cost and conversion losses than hydrogen-to-power cycles.

References

[1] *Aan de slag met het Stimuleringsprogramma Energiehubs*. RVO.nl. URL: https://www.rvo.nl/onderwerpen/energiehubs/stimuleringsprogramma-energiehubs (visited on 11/15/2025).

[2] *Alpiq installs the core component of the world's first energy self-sufficient apartment house*. Alpiq. URL: https://www.alpiq.com/alpiq-group/media-relations/media-releases/media-release-detail/alpiq-installs-the-core-component-of-the-worlds-first-energy-self-sufficient-apartment-house (visited on 05/16/2025).

[3] Mohammad Taufiqul Arif, Amanullah M. T. Oo, and A. B. M. Shawkat Ali. "Role of Energy Storage on Distribution Transformer Loading in Low Voltage Distribution Network". In: *Smart Grid and Renewable Energy* 4.2 (May 27, 2013). Number: 2 Publisher: Scientific Research Publishing, pp. 236–251. DOI: 10.4236/sgre.2013.42029. URL: https://www.scirp.org/journal/paperinformation?paperid=32197 (visited on 04/09/2025).

[4] Thomas Bauwens. "Analyzing the determinants of the size of investments by community renewable energy members: Findings and policy implications from Flanders". In: *Energy Policy* 129 (June 2019), pp. 841–852. ISSN: 03014215. DOI: 10.1016/j.enpol.2019.02.067. URL: https://linkinghub.elsevier.com/retrieve/pii/S0301421519301570 (visited on 05/19/2025).

[5] Manu Bracke, Niels de Smet, and Rosalie van der Ende. *Studie opschaling seasonal storage system*. Eindverslag. Sept. 2025.

[6] *Capaciteitskaart invoeding elektriciteitsnet*. URL: https://capaciteitskaart.netbeheernederland.nl (visited on 03/28/2025).

[7] Pure Energie. *Wat is de ideale hoek voor mijn zonnepanelen?* Pure Energie. URL: https://pure-energie.nl/kennisbank/de-ideale-hoek-voor-zonnepanelen/ (visited on 11/17/2025).

[8] *Energieagenda - Naar een CO2-arme energievoorziening*.

[9] *Experiment met Buurtbatterij in Rijsenhout*. URL: https://www.lente-akkoord.nl/nieuws/experiment-met-buurtbatterij-in-rijsenhout (visited on 05/16/2025).

[10] *Free Open-Source Weather API | Open-Meteo.com*. URL: https://open-meteo.com/ (visited on 07/18/2025).

[11] A. Fu. "Self-organizing voltage regulation in the distribution networks: Insights into planning, operation and validation". PhD thesis. Delft University of Technology, 2024. DOI: 10.4233/UUID:0CD87B4B-EC59-4FCC-83AA-FBDDA205F95D. URL: http://resolver.tudelft.nl/uuid:0cd87b4b-ec59-4fcc-83aa-fbdda205f95d (visited on 03/24/2025).

[12] Erwin Geurts. *Innovatief zonne-waterstof woonhuis in Berlijn zet overtollige zonne-energie om in waterstof*. Alles over Waterstof. July 26, 2023. URL: https://allesoverwaterstof.nl/innovatief-zonne-waterstof-woonhuis-in-berlijn-zet-overtollige-zonne-energie-om-in-waterstof/ (visited on 05/16/2025).

[13] Erwin Geurts. *Warmtenet in Stad aan 't Haringvliet met zonne-energie en waterstof via InnovaHub*. Alles over Waterstof. May 30, 2024. URL: https://allesoverwaterstof.nl/warmtenet-in-stad-aan-t-haringvliet-met-zonne-energie-en-waterstof-via-innovahub/ (visited on 05/16/2025).

[14] *GO-e – Projectsite*. URL: https://www.projectgo-e.nl/ (visited on 11/15/2025).

[15] Ron de Graaf et al. *De Families van Energy Hubs in Nederland*.

[16] *Grid congestion is posing challenges for energy security and transitions – Analysis*. IEA. Mar. 25, 2025. URL: https://www.iea.org/commentaries/grid-congestion-is-posing-challenges-for-energy-security-and-transitions (visited on 05/16/2025).

[17] Ministerie van Klimaat en Groene Groei. *Tweede Voortgangsrapportage Landelijk Actieprogramma Netcongestie - Rapport - Rijksoverheid.nl*. Last Modified: 2025-03-25T12:35 Publisher: Ministerie van Algemene Zaken. Mar. 24, 2025. URL: https://www.rijksoverheid.nl/documenten/rapporten/2025/03/24/landelijk-actieprogramma-netcongestie-tweede-voortgangsrapportgage (visited on 11/15/2025).

[18] Mazaher Haji Bashi et al. "A review and mapping exercise of energy community regulatory challenges in European member states based on a survey of collective energy actors". In: *Renewable and Sustainable Energy Reviews* 172 (Feb. 2023), p. 113055. ISSN: 13640321. DOI: 10.1016/j.rser.2022.113055. URL: https://linkinghub.elsevier.com/retrieve/pii/S1364032122009364 (visited on 05/19/2025).

[19] *Handel per 15 minuten sluit beter aan bij duurzame elektriciteit*. TenneT. URL: https://www.tennet.eu/nl/nieuws/handel-15-minuten-sluit-beter-aan-bij-duurzame-elektriciteit (visited on 12/08/2025).

[20] A. N. M. M. Haque et al. "Demand response for real-time congestion management incorporating dynamic thermal overloading cost". In: *Sustainable Energy, Grids and Networks* 10 (June 1, 2017), pp. 65–74. ISSN: 2352-4677. DOI: 10.1016/j.segan.2017.03.002. URL: https://www.sciencedirect.com/science/article/pii/S2352467716302296 (visited on 11/15/2025).

[21] *Hernieuwbare energie bij ingrijpende renovatie*. RVO.nl. URL: https://www.rvo.nl/onderwerpen/wetten-en-regels-gebouwen/energieprestatie-eisen-verbouw-renovatie/hernieuwbare-energie (visited on 04/29/2025).

[22] *Het elektrisch vermogen*. Sibelga. URL: https://www.sibelga.be/nl/aansluitingen-meters/mijn-aansluiting/elektrisch-vermogen (visited on 11/17/2025).

[23] *Illuminator documentation — Illuminator 1.0.0 documentation*. URL: https://illuminator-team.github.io/website/ (visited on 12/06/2025).

[24] *Innovahub Hylife inauguration in Holland May 21 2024 | Giacomini*. URL: https://www.giacomini.com/news/inauguration-innovahub-hylife-holland-21may2024 (visited on 05/16/2025).

[25] Binod Prasad Koirala et al. "Trust, awareness, and independence: Insights from a socio-psychological factor analysis of citizen knowledge and participation in community energy systems". In: *Energy Research & Social Science* 38 (Apr. 2018), pp. 33–40. ISSN: 22146296. DOI: 10.1016/j.erss.2018.01.009. URL: https://linkinghub.elsevier.com/retrieve/pii/S2214629618300641 (visited on 05/19/2025).

[26] *Kosten van energie en water*. Nibud. URL: https://www.nibud.nl/onderwerpen/uitgaven/kosten-energie-water/ (visited on 10/26/2025).

[27] Robèrt Kroonen. "Een veilig seizoensgebonden energieopslagsysteem op basis van waterstof voor de gebouwde omgeving". In: ().

[28] Jennifer Kurtz, Kevin Harrison, and Mansih Mohanpurkar. *Dynamic Modeling and Validation of Electrolyzers in Real Time Grid Simulation*. National Renewable Energy Laboratory: Idaho Naitional Laboratory, Aug. 6, 2017. (Visited on 11/16/2025).

[29] Ionel Lepadat et al. "Impact of Distributed Generation on voltage profile and power losses in a test power grid". In: *2017 International Conference on Optimization of Electrical and Electronic Equipment (OPTIM) & 2017 Intl Aegean Conference on Electrical Machines and Power Electronics (ACEMP)*. 2017 International Conference on Optimization of Electrical and Electronic Equipment (OPTIM) & 2017 Intl Aegean Conference on Electrical Machines and Power Electronics (ACEMP). Brasov, Romania: IEEE, May 2017, pp. 128–133. ISBN: 978-1-5090-4489-4. DOI: 10.1109/OPTIM.2017.7974959. URL: http://ieeexplore.ieee.org/document/7974959/ (visited on 03/24/2025).

[30] Na Li, Zofia Lukszo, and John Schmitz. "An approach for sizing a PV–battery–electrolyzer–fuel cell energy system: A case study at a field lab". In: *Renewable and Sustainable Energy Reviews* 181 (July 2023), p. 113308. ISSN: 13640321. DOI: 10.1016/j.rser.2023.113308. URL: https://linkinghub.elsevier.com/retrieve/pii/S1364032123001648 (visited on 04/04/2025).

[31] Na Li et al. "Evaluating the Impact of New Technology Deployment on Future Congestion of LV Distribution Grids". In: *2024* ().

[32] Paolo Marocco et al. “An MILP approach for the optimal design of renewable battery-hydrogen energy systems for off-grid insular communities”. In: *Energy Conversion and Management* 245 (Oct. 1, 2021), p. 114564. ISSN: 0196-8904. DOI: 10.1016/j.enconman.2021.114564. URL: https://www.sciencedirect.com/science/article/pii/S0196890421007408 (visited on 11/16/2025).

[33] Riccardo Maselli. “Multi-Objective Optimization of a grid-connected PV-Battery-Electrolyzer Fuel Cell Energy System”. In: ().

[34] *Modeling Guide*. PV Performance Modeling Collaborative (PVPMC). URL: https://pvpmc.sandia.gov/modeling-guide/ (visited on 07/18/2025).

[35] Awsan Mohammed et al. “A multi-objective optimization model based on mixed integer linear programming for sizing a hybrid PV-hydrogen storage system”. In: *International Journal of Hydrogen Energy* 48.26 (Mar. 26, 2023), pp. 9748–9761. ISSN: 0360-3199. DOI: 10.1016/j.ijhydene.2022.12.060. URL: https://www.sciencedirect.com/science/article/pii/S0360319922057779 (visited on 11/16/2025).

[36] United Nations. *Net Zero Coalition*. United Nations. Publisher: United Nations. URL: https://www.un.org/en/climatechange/net-zero-coalition (visited on 03/28/2025).

[37] *NOCT Cell Temperature*. PV Performance Modeling Collaborative (PVPMC). URL: https://pvpmc.sandia.gov/modeling-guide/2-dc-module-iv/cell-temperature/noct-cell-temperature/ (visited on 07/18/2025).

[38] None None. “Effect of Dynamic Pricing on the Low-voltage Grid”. In: (2024). URL: https://repository.tudelft.nl/record/uuid:bb5c444e-c499-4059-83e1-7b8452fbf42a (visited on 11/17/2025).

[39] None None. “Grid Impact of Different Types of Heat Pumps”. In: (2025). URL: https://repository.tudelft.nl/record/uuid:7e773dbb-3dac-4185-b27b-7c3f547960b4 (visited on 11/17/2025).

[40] None None. “H2 Integration Into a Residential Energy Hub”. In: (2025). URL: https://repository.tudelft.nl/record/uuid:960f6142-738f-401a-8fe0-883903449736 (visited on 10/12/2025).

[41] None None. “Stochastic water demand modelling for a better understanding of hydraulics in water distribution networks”. In: (2010). URL: https://repository.tudelft.nl/record/uuid:82f6a988-2cef-4eba-aef2-d9790e283f95 (visited on 11/17/2025).

[42] *Phase to Phase – Netten voor distributie van elektriciteit, hoofdstuk 13*. URL: https://www.phasetophase.nl/boek/boek_3_13.html#_13.2.1 (visited on 03/25/2025).

[43] *Regel uw aansluiting*. Stedin. URL: https://www.stedin.net/aansluiting (visited on 04/02/2025).

[44] *Report - 1.2 System analysis and hardware optimization of hydrogen storage systems v1.0*.

[45] *Report - 1.4 System-wide analysis focused on balance and efficiency v1.0*. v1.0.

[46] *Sandia PV Array Performance Model*. PV Performance Modeling Collaborative (PVPMC). URL: https://pvpmc.sandia.gov/modeling-guide/2-dc-module-iv/point-value-models/sandia-pv-array-performance-model/?utm_source=chatgpt.com (visited on 07/18/2025).

[47] *Schipper Bosch*. URL: https://schipperbosch.nl/innovatieproject-met-waterstof-openhofkerk-in-wolfheze-in-bouwend-nederland/ (visited on 05/16/2025).

[48] *Schipper Bosch*. URL: https://schipperbosch.nl/openhofkerk/ (visited on 05/16/2025).

[49] Martijn Siemes. *Laadprofielengenerator geeft inzicht in lokale impact laden elektrische auto’s op het stroomnet*. ElaadNL. Apr. 8, 2024. URL: https://elaad.nl/laadprofielengenerator-geeft-inzicht-in-lokale-impact-laden-elektrische-autos-op-het-stroomnet/ (visited on 10/26/2025).

[50] Gabriel Marinho Silva. *Sizing and Modeling of a Microgrid for Integrated Production of Hydrogen*. 2021. URL: https://urn.kb.se/resolve?urn=urn:nbn:se:kth:diva-304623 (visited on 11/16/2025).

[51] *SoCalGas' H2 Hydrogen Home Named a Fast Company 2021 World-Changing Idea*. Sempra. URL: https://www.sempra.com/socalgas-h2-hydrogen-home-named-fast-company-2021-world-changing-idea (visited on 05/16/2025).

[52] Krzysztof Sornek et al. "Power-to-Heat and Seasonal Thermal Energy Storage: Pathways Toward a Low-Carbon Future for District Heating". In: *Energies* 18.21 (Jan. 2025). Publisher: Multidisciplinary Digital Publishing Institute, p. 5577. ISSN: 1996-1073. DOI: 10.3390/en18215577. URL: https://www.mdpi.com/1996-1073/18/21/5577 (visited on 11/18/2025).

[53] *Spanningskwaliteit | Netbeheer Nederland*. URL: https://www.netbeheernederland.nl/veiligheid-en-infrastructuur/spanningskwaliteit (visited on 04/15/2025).

[54] *Standard EN 50160 – Voltage Characteristics of Public Distribution Systems*. Power Quality Blog. July 22, 2021. URL: https://powerquality.blog/2021/07/22/standard-en-50160-voltage-characteristics-of-public-distribution-systems/ (visited on 03/25/2025).

[55] Marco Stecca et al. "A Comprehensive Review of the Integration of Battery Energy Storage Systems Into Distribution Networks". In: *IEEE Open Journal of the Industrial Electronics Society* 1 (2020), pp. 46–65. ISSN: 2644-1284. DOI: 10.1109/OJIES.2020.2981832. URL: https://ieeexplore.ieee.org/document/9040552/ (visited on 04/08/2025).

[56] Cornelius Steinbrink et al. "CPES Testing with mosaik: Co-Simulation Planning, Execution and Analysis". In: *Applied Sciences* 9.5 (Mar. 5, 2019), p. 923. ISSN: 2076-3417. DOI: 10.3390/app9050923. URL: https://www.mdpi.com/2076-3417/9/5/923 (visited on 12/08/2025).

[57] *Studie opschaling seasonal storage systeem*.

[58] *Tarieven Stedin | Stedin*. Stedin.net. URL: https://www.stedin.net/zakelijk/betalingen-en-facturen/tarieven (visited on 11/12/2025).

[59] Simon Tindemans. *Low Carbon London smart meter data (refactored)*. In collab. with UK Power Networks, Imperial College London (Data Collection And Release) and Delft University Of Technology (Refactoring). Version 1. Sept. 12, 2023. DOI: 10.4121/FBBE775B-48D8-469F-A39B-B64488BFD6FD. URL: https://data.4tu.nl/datasets/fbbe775b-48d8-469f-a39b-b64488bfd6fd (visited on 11/17/2025).

[60] Reinaldo Tonkoski, Dave Turcotte, and Tarek H. M. EL-Fouly. "Impact of High PV Penetration on Voltage Profiles in Residential Neighborhoods". In: *IEEE Transactions on Sustainable Energy* 3.3 (July 2012), pp. 518–527. ISSN: 1949-3037. DOI: 10.1109/TSTE.2012.2191425. URL: https://ieeexplore.ieee.org/document/6194986/ (visited on 04/19/2025).

[61] *Wat doet Stedin*. Stedin. URL: https://www.stedin.net/over-stedin/wat-doet-stedin (visited on 04/02/2025).

[62] *Welke capaciteit thuisbatterij heb ik nodig? | Soly*. Soly.nl. URL: https://soly.nl/thuisbatterij/capaciteit-thuisbatterij/ (visited on 11/23/2025).

[63] Pagidela Yamuna and N. Visali. "Optimal placement of energy storage system in hybrid AC/DC microgrid to enhance stability". In: *International Journal of Power Electronics and Drive Systems (IJPEDS)* 16.1 (Mar. 1, 2025), p. 195. ISSN: 2722-256X, 2088-8694. DOI: 10.11591/ijpeds.v16.i1.pp195-203. URL: https://ijpeds.iaescore.com/index.php/IJPEDS/article/view/23509 (visited on 04/09/2025).

[64] Ministerie van Algemene Zaken. *Het energiesysteem van de toekomst: de II3050-scenario's - Rapport - Rijksoverheid.nl*. Last Modified: 2023-05-22T13:04 Publisher: Ministerie van Algemene Zaken. Apr. 6, 2023. URL: https://www.rijksoverheid.nl/documenten/rapporten/2023/04/06/het-energiesysteem-van-de-toekomst-de-ii3050-scenarios (visited on 11/17/2025).

[65] Ministerie van Algemene Zaken. *Hoe lang kan ik nog koken en stoken op gas? - Rijksoverheid.nl*. Last Modified: 2024-11-05T10:57 Publisher: Ministerie van Algemene Zaken. Apr. 5, 2017. URL: https://www.rijksoverheid.nl/onderwerpen/duurzame-energie/vraag-en-antwoord/onderwerpen/duurzame-energie/vraag-en-antwoord/hoe-lang-kan-ik-nog-koken-op-gas (visited on 04/29/2025).

[66] Ministerie van Algemene Zaken. *Salderingsregeling stopt in 2027 - Energie thuis - Rijksoverheid.nl*. Last Modified: 2025-04-01T14:45 Publisher: Ministerie van Algemene Zaken. Feb. 17, 2025. URL: https://www.rijksoverheid.nl/onderwerpen/energie-thuis/salderingsregeling (visited on 05/09/2025).

[67] *Zonnepanelen berekenen: benodigd aantal & jaarlijkse opbrengst*. Zonne-paneel.net. URL: https://www.zonne-paneel.net/zonnepanelen-berekenen/ (visited on 10/27/2025).

[68] E. T. H. Zurich. *Technology ready, but acceptance pending for distributed energy systems*. URL: https://phys.org/news/2017-12-technology-ready-pending-energy.html (visited on 05/16/2025).

7

Appendix

Supplementary content.

7.1. Low-Voltage Grid: Case Study

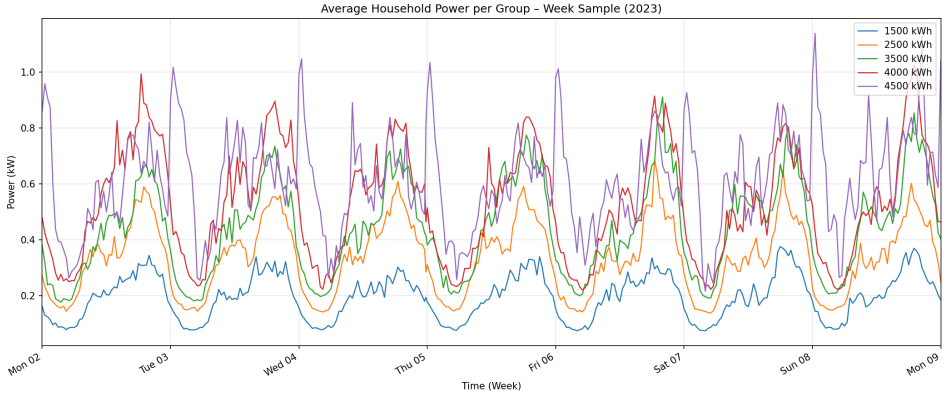

Figure 7.1: Average electricity demand across household groups over a representative week. Each curve represents the total load from all households in a specific consumption category (1,500–4,500 kWh/year).

7.2. Thermal Demand Model Equations

The model simulates both space heating and domestic hot water (DHW) requirements and was adapted from the thermal framework developed by [39].

The thermal demand model integrates water heating demands with space heating requirements to simulate total heating needs. Outdoor temperature data from KNMI (De Bilt station) is used to drive thermal losses.

Heat Loss Through Conduction

$$\dot{Q}_{\text{loss}} = U \cdot A \cdot (T_{\text{in}} - T_{\text{out}}) \tag{7.1}$$

where U [W/m^{2}K] is the overall heat transfer coefficient, A [m^2] the surface area, and T_{in} and T_{out} [°C] the indoor and outdoor temperatures.

Heat Loss Due to Infiltration and Ventilation

$$\dot{Q}_{\text{inf+vent}} = -c_{\text{air}} \cdot \rho_{\text{air}} \cdot (\dot{V}_{\text{inf}} + \dot{V}_{\text{vent}}) \cdot (T_{\text{in}} - T_{\text{out}}) \tag{7.2}$$

where c_{air} [J/kgK] is the specific heat of air, ρ_{air} [kg/m^3] the air density, and $\dot{V}_{\text{inf}}$, $\dot{V}_{\text{vent}}$ [m^3/s] are infiltration and ventilation flow rates.

Indoor Temperature Dynamics

$$T_{\text{in},t+\Delta t} = T_{\text{in},t} + \frac{\Delta t}{mc_p}\left(\dot{Q}_{\text{HP}} + \dot{Q}_{\text{TESS}} + \dot{Q}_{\text{SC}} + \dot{Q}_{\text{loss}}\right) \tag{7.3}$$

where mc_p [J/K] is the building's total thermal mass, and $\dot{Q}_{\text{HP}}$, $\dot{Q}_{\text{TESS}}$, and $\dot{Q}_{\text{SC}}$ [W] are heat flows from the heat pump, thermal storage system, and solar collector, respectively.

Coefficient of Performance (COP)

For the air-source heat pump:

$$\text{COP}_{\text{ASHP}} = 0.85 \cdot \left(6.08 - 0.09\Delta T + 0.0005\Delta T^2\right) \tag{7.4}$$

For completeness, the COP of a ground-source heat pump is also included:

$$\text{COP}_{\text{GSHP}} = 0.85 \cdot \left(10.29 - 0.21\Delta T + 0.0012\Delta T^2\right) \tag{7.5}$$

where $\Delta T = T_{\text{sink}} - T_{\text{source}}$ [K].

Domestic Hot Water (DHW) Tank Temperature

$$T_{\text{tank,new}} = \frac{(V_{\text{tank}}c_w + V_{\text{used}}c_w)T_{\text{tap}} - U_{\text{tank}}A_{\text{tank}}(T_{\text{tank}} - T_{\text{in}})\Delta t + \dot{Q}_{\text{HP}}\Delta t}{V_{\text{tank}}c_w + 0.5V_{\text{used}}c_w} \tag{7.6}$$

where V_{tank} [m^3] is the DHW tank volume, A_{tank} [m^2] is its surface area, U_{tank} [W/m^{2}K] the tank's heat loss coefficient, c_w [J/kgK] the specific heat of water, and $\dot{Q}_{\text{HP}}$ the heat input from the ASHP.

7.3. Model Development 24/7 Energy Hub

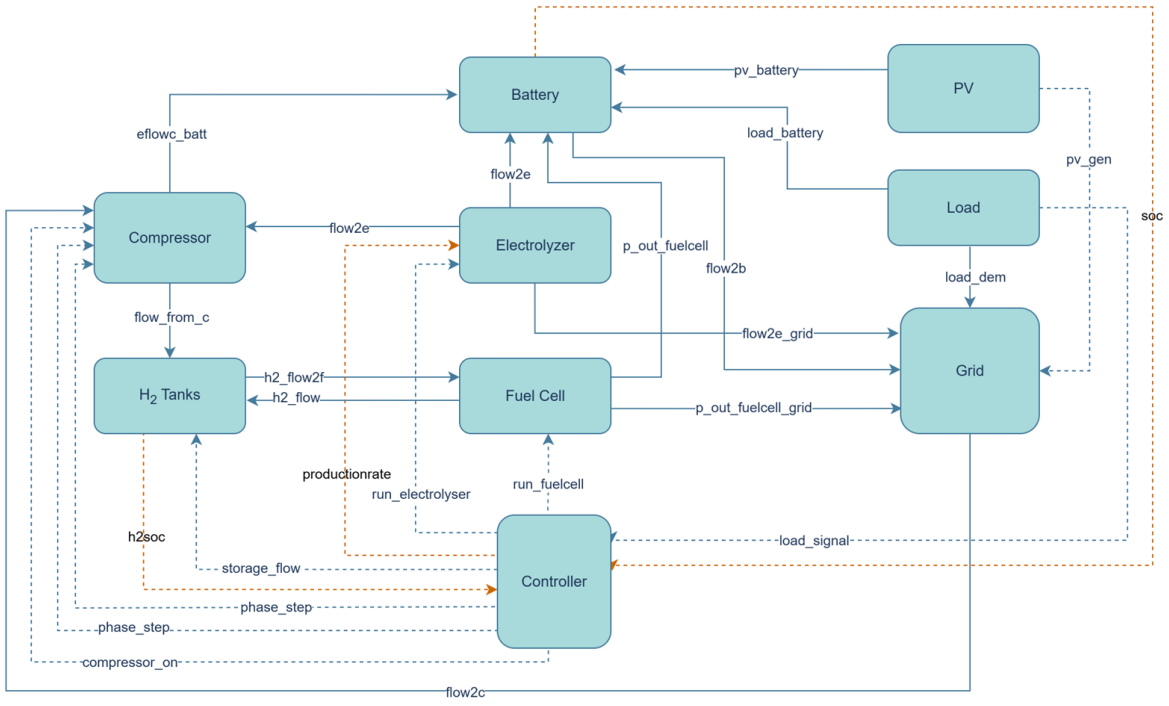

Figure 7.2: Model implementation of 24/7 Energy Hub

7.4. Electrolyzer Efficiency

The system efficiency η_{el} is derived from manufacturer test data of the 24/7 Energy Hub unit, which operates on AC input with integrated power electronics. Hydrogen flow, measured in NL/h and converted

to kg/h using $\rho_{H_2} = 0.00008988$ kg/NL, was compared with the theoretical hydrogen production based on the lower heating value (LHV) of hydrogen, as shown in Table 7.2:

$$H_2^{\text{theoretical}} = \frac{P_{\text{el}}}{\text{LHV}_{H_2}}$$

Table 7.1: Measured electrolyzer performance at various production rates (based on manufacturer testing) [44].

Production Rate (%)	Electrical Power (W)	Hydrogen Flow (NL/h)
60	1412	306
72	1714	367
80	1920	408
92	2240	470
100	2450	510

Table 7.2: Measured and calculated electrolyzer performance at various production rates (based on manufacturer testing) [44].

Production Rate (%)	Electrical Power (W)	H_2 Real (kg/h)	H_2 Theoretical (kg/h)	Efficiency (%)
60	1412	0.0275	0.0424	64.9
72	1714	0.0330	0.0514	64.1
80	1920	0.0367	0.0576	63.7
92	2240	0.0422	0.0672	62.9
100	2450	0.0458	0.0735	62.4

Across operating points between 60–100% load, the measured efficiency ranged from 62.4% to 64.9%. Given this narrow variation, a constant value of

$$\eta_{\text{el}} = 63.6\%$$

is applied in the model, representing the overall system efficiency including BoP and DC–AC conversion losses.

7.5. Fuel Cell Efficiency

At the stack level, the fuel cell produced 2.37 kW of DC power with a hydrogen-to-electricity conversion efficiency of approximately 58%. Table 7.3 summarizes the measured parameters. The hydrogen input flow rate of 22.7 NL/min corresponds to an energy input of about 4.08 kW based on the hydrogen LHV.

Table 7.3: Fuel cell stack performance and hydrogen inflow characteristics.

Parameter	Value
Hydrogen inlet flow rate	22.7 NL/min
Hydrogen mass flow	0.00204 kg/min
Hydrogen energy flow	4080 W
Fuel cell output voltage	33.8 V
Fuel cell output current	70.0 A
Stack DC power output	**2366 W**
Stack efficiency	**57.99%**

From the stack power, conversion steps and auxiliary loads reduce the available net power. The air blower, responsible for supplying oxygen to the stack, consumes around 213 W of DC power. Power is converted through a two-stage conversion system: DC/DC and DC/AC converters, with efficiencies of

97.1% and 85.6%. Additional AC loads include programmable logic controllers (PLC), cooling pumps, and hydrogen circulation systems. These auxiliary components collectively account for roughly 138 W of consumption.

The complete power flow and efficiency chain is presented in Table 7.4. Accounting for all conversion and auxiliary losses, the measured net AC output was 1.62 kW, corresponding to a total system efficiency of 39.8%. This value is used in the model to represent the overall fuel cell-to-grid conversion efficiency under normal operating conditions.

Table 7.4: Measured power conversion and auxiliary losses in the fuel cell system.

Component	**Value**
Air blower DC power	213 W
DC/DC conversion efficiency	97.12%
DC/AC conversion efficiency	85.57%
AC auxiliary loads (PLC, cooling, H_2 pump)	138 W
Net AC output power	**1623 W**
Total system efficiency	**39.8%**

7.6. PV Validation

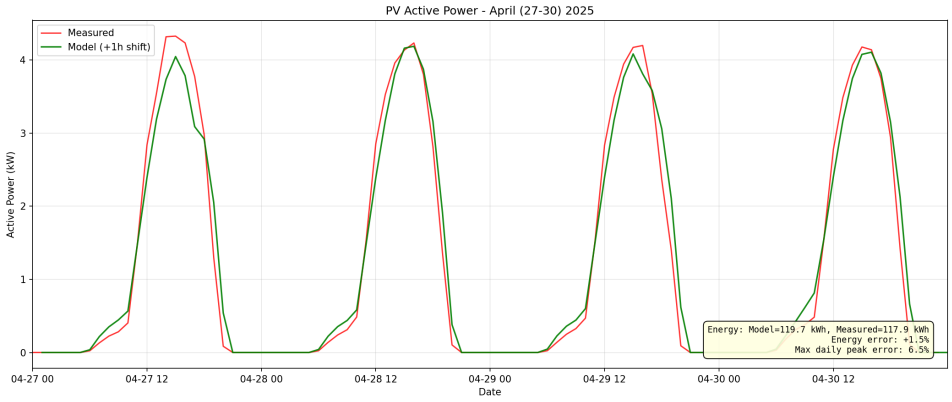

(a) Comparison of modeled and measured PV active power (kW); April 27-30.

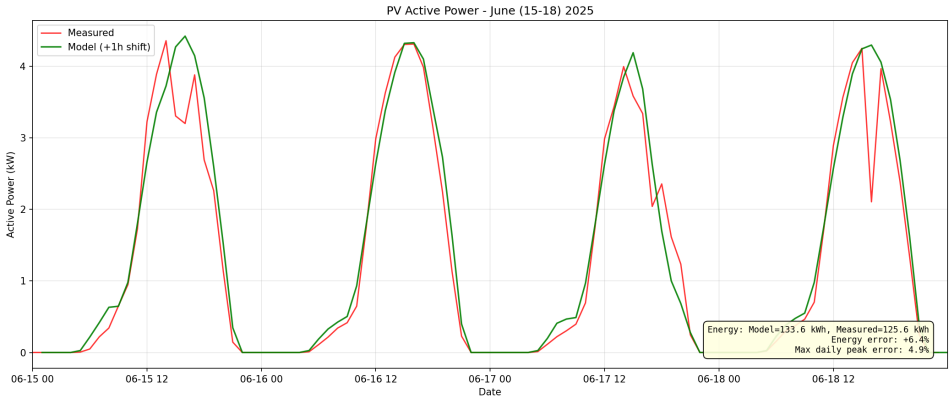

(b) Comparison of modeled and measured PV active power (kW); June 15-18.

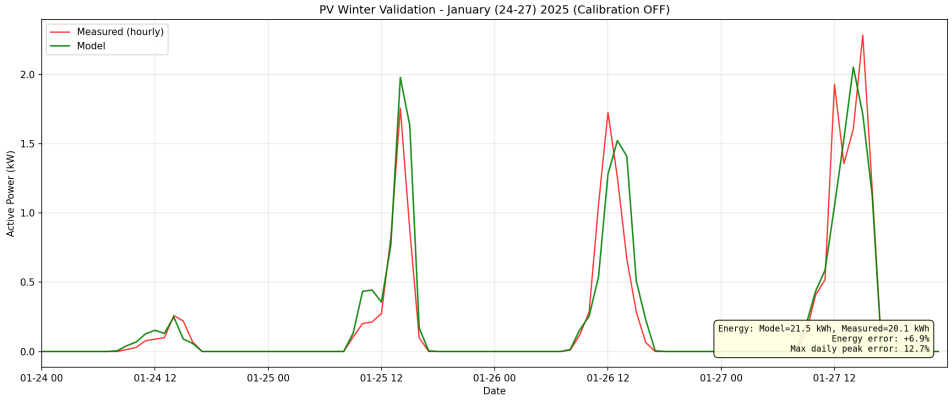

(c) Comparison of modeled and measured PV active power (kW); January 24-27.

Figure 7.3: Validation of the PV model: comparison of modeled and measured resulting PV active power output over a winter and summer period.

7.7. Baseline 2050

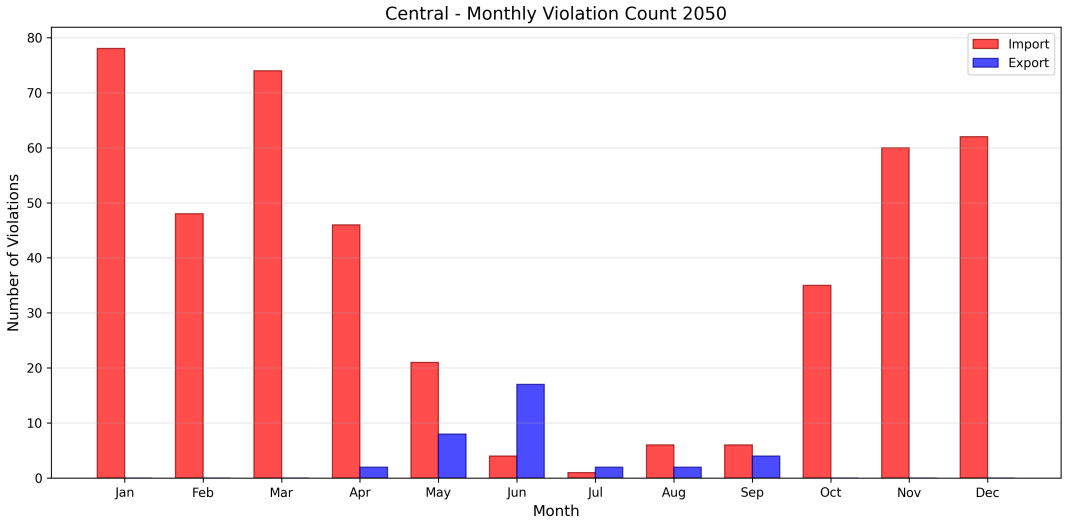

Figure 7.4: Monthly count of transformer limit violations in 2050, showing import dominance during winter months and occasional export violations in summer.

7.8. Autonomous Operation Analysis

The detailed results of the autonomous energy hub scenarios.

7.8.1. Annual Grid Flow

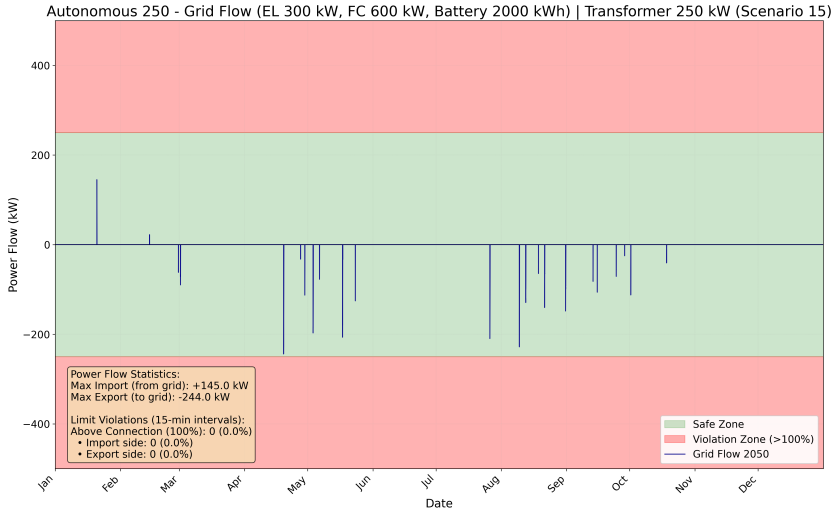

Figure 7.5: Annual grid flow for a 250 kVA transformer (with energy hub); Autonomous reference case (Battery = 2,000 kWh, Electrolyzer = 300 kW, Fuel Cell = 600 kW)

7.8.2. System Component Dimensioning

This section summarizes the component sizing logic used for generating the autonomous reference configuration and performing sensitivity analysis. Full methodological justification is provided in section .

For completeness, the table above lists the base sizing values (shown in bold) together with under- and over-sizing variants:
– Battery sizing reflects aggregated household installations (5, 10, 15 kWh per household with PV).

Table 7.5: Discrete component sizes used in the simulation study. Combining all variants yields 80 configurations ($5 \times 4 \times 4$).

Component	Simulated Values
Battery capacity	400, 800, **1,200**, 1,600, 2,000 kWh
Fuel cell rating	200, 400, 600, **780** kW
Electrolyzer rating	100, **150**, 200, **300** kW

– The fuel cell range represents peak required capacity.
– The electrolyzer range captures average to maximum surplus summer PV production.

7.8.3. Simulation Results

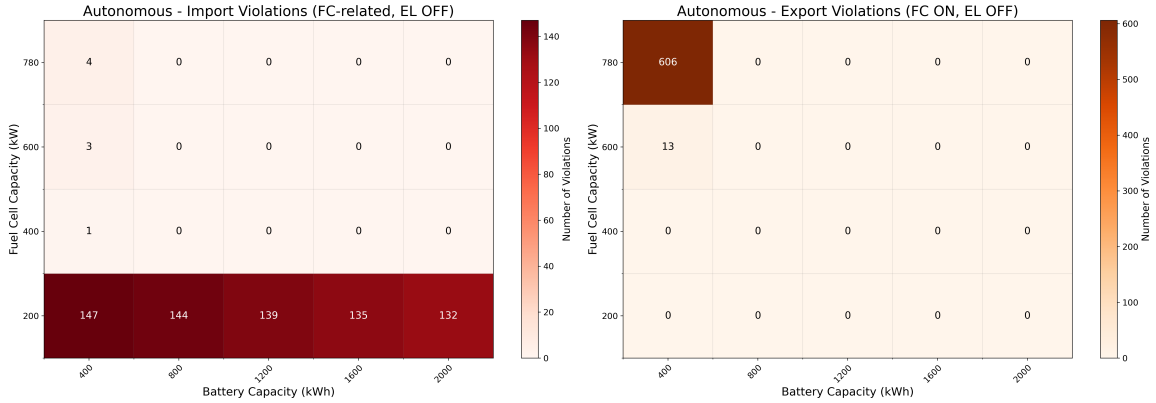

Figure 7.6: Import violations due to fuel cell under sizing (left), and export violations due to over sizing (right).

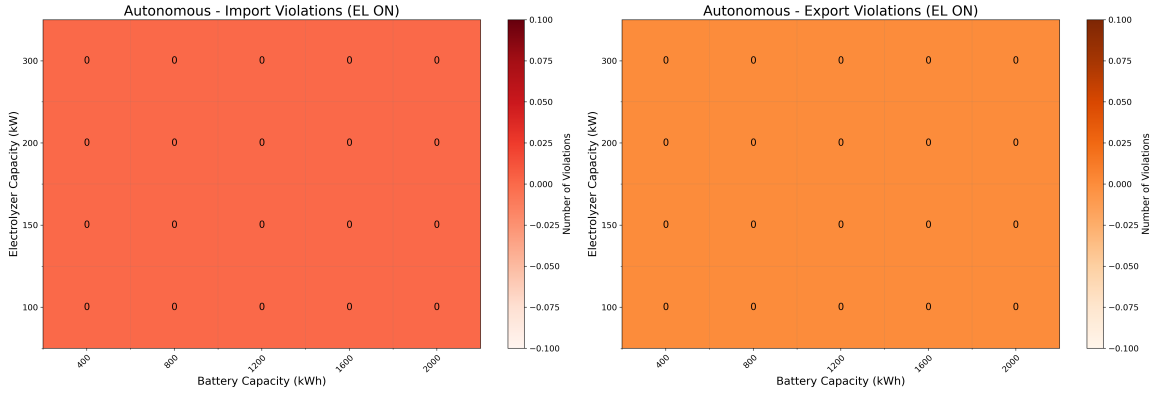

Figure 7.7: Electrolyzer operation causes no import or export violations across all configurations.

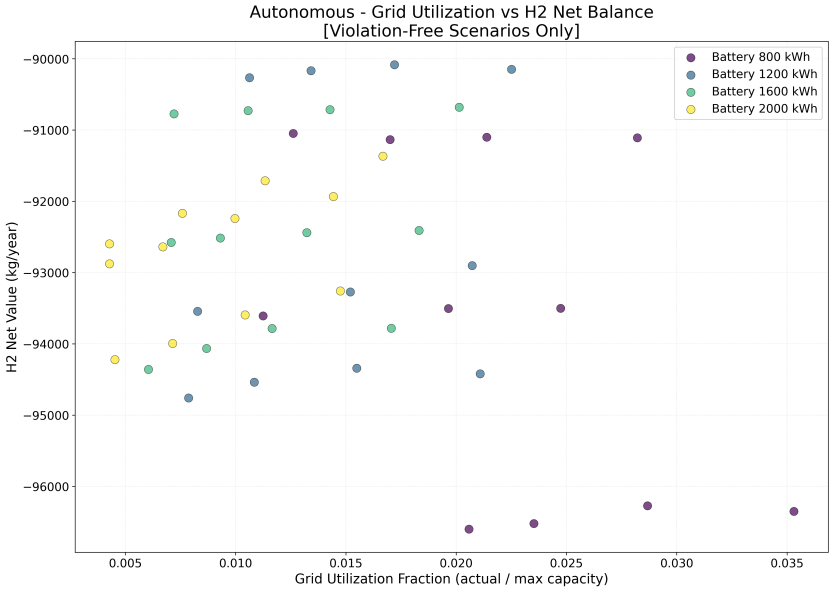

Figure 7.8: All violation-free scenarios result in negative net hydrogen balance.

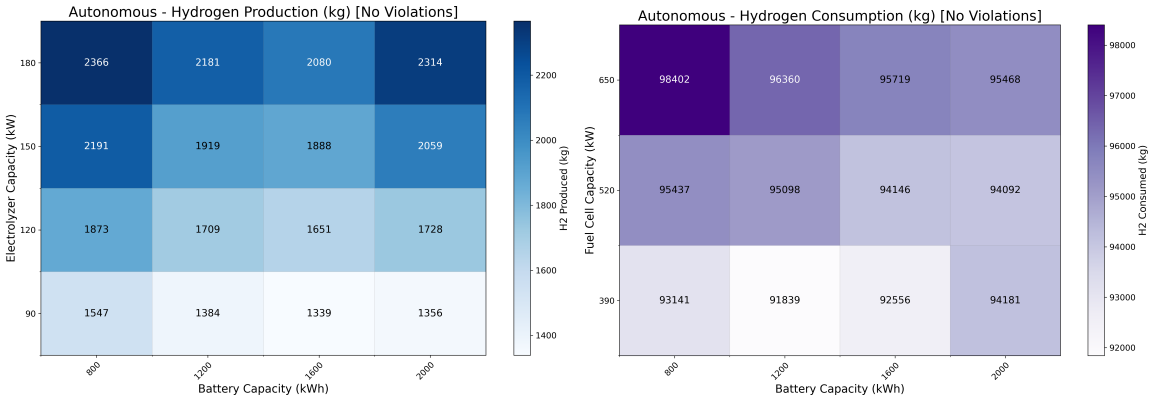

Figure 7.9: Hydrogen production (left) versus consumption (right). Production is approximately 40 times lower.

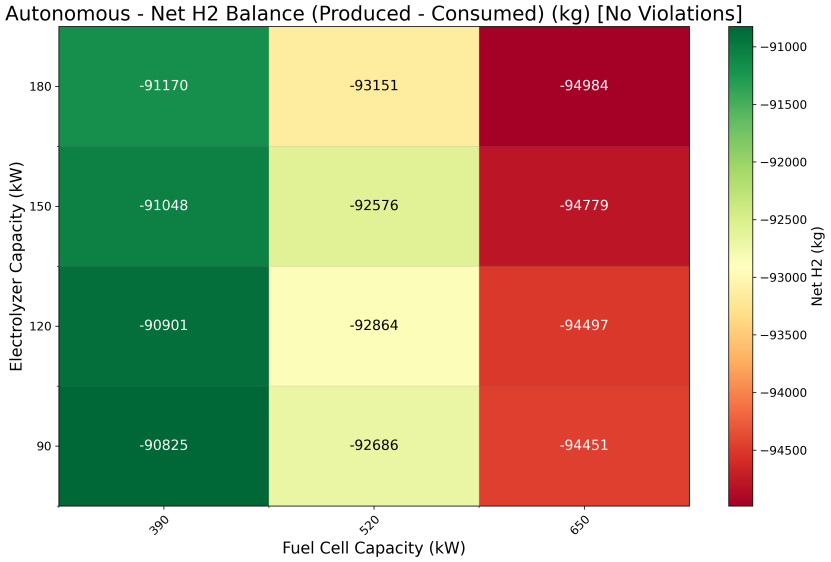

Figure 7.10: Net hydrogen balance remains negative across all configurations.

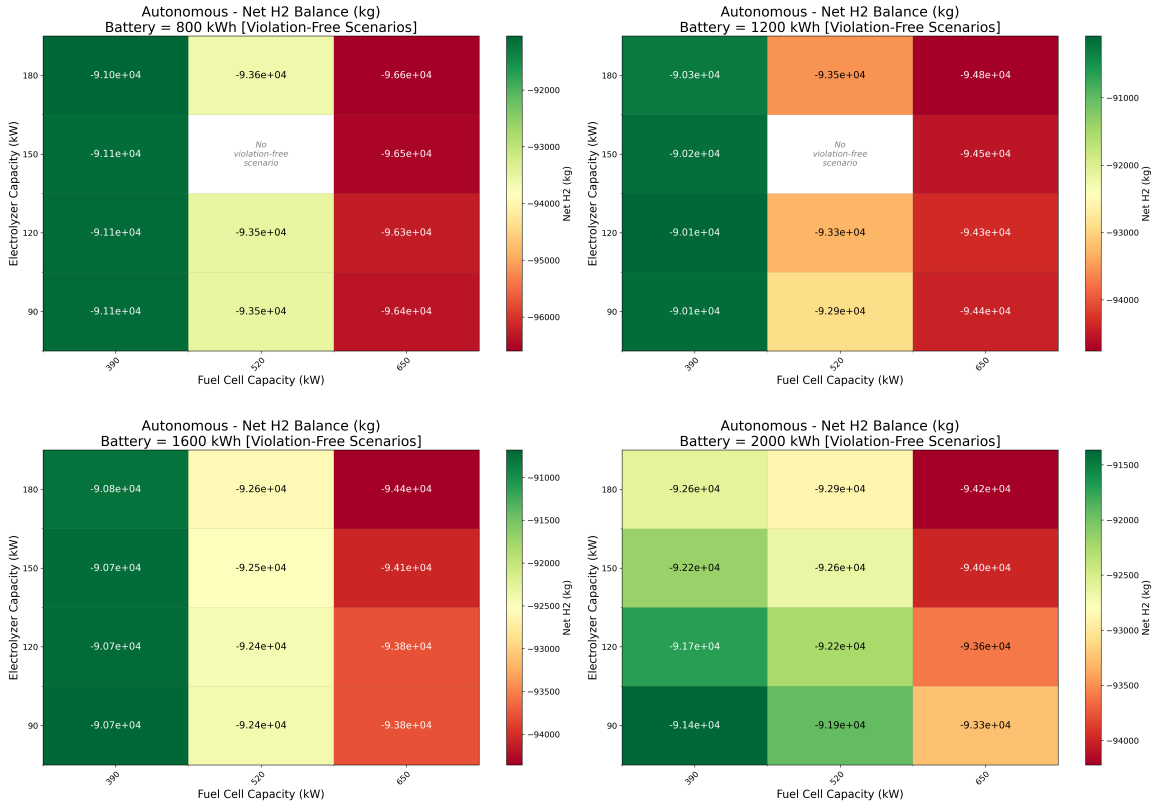

Figure 7.11: Net hydrogen balance for all battery sizes. No improvement with increasing storage.